Experimental study and modelling of the size effect associate to the stress gradient in contact fatigue

Barbara Ferry

NNT : 2017SACLN041

Study of the Stress Gradient Effect and the Size Effect in Fretting Fatigue.

Thèse de doctorat de l'Université Paris-Saclay
préparée à l'école normale supérieure Paris Saclay en cotutelle avec l'université de Brasilia

École doctorale n°579 Sciences mécaniques et énergétiques, matériaux et géosciences (SMEMAG)

Thèse présentée et soutenue à Poitiers, le 26/09/2017, par

Barbara Ferry

Composition du Jury

Thierry Palin-Luc Professeur, ENSAM	Président
Yves Nadot Professeur ENSMA	Rapporteur
Thierry Palin-Luc Professeur, ENSAM	Rapporteur
José Alexander Araújo Professeur, Universidade de Brasilia	Co-Directeur de thèse
Sylvie Pommier Professeure, ENS Cachan	Directeur de thèse
Claudio Montebello Ingénieur Mécanique, Safran Aircraft Engines	Invité
Quentin Pujol Ingénieur Mécanique, Safran Aircraft Engines	Invité

Thèse de doctorat

Remerciements – Agradecimentos

Je souhaite tout d'abord remercier Alex Araújo et Sylvie Pommier pour avoir suivi et dirigé ma thèse en France et au Brésil. Un grand merci à Alex pour l'aide qu'il m'a apporté lors de la rédaction qui n'a pas été une période facile. Je remercie également Jean Mériaux, Nathalie Serres, Claudio Montebello et Karim Demmou qui m'ont encadré d'un point de vue industriel. Merci pour tous les conseils que vous avez pu me donner et les bons moments passés ensemble à Brasilia ! Je tiens à remercier les membres de mon jury, Yves Nadot et Thierry Palin-Luc qui ont également été les relecteurs de ma thèse. Merci pour la rapidité avec laquelle vous avez corrigé ce manuscrit et pour la justesse de vos remarques et questions. Finalement, je tiens à remercier l'ANRT et Safran Aircraft Engines pour le co-financement de ma thèse.

D'un point de vue personnel, je tiens à remercier toutes les personnes avec qui j'ai passé ma première année de thèse à Paris : Sylvère, Werty, MF, Héléna, Thibault, Maxime, Morgan, Zouzou, Pierre…. Et tous ceux que j'oublierai de citer. J'appréhendais le début de cette thèse et grâce à vous j'ai passé une année formidable.

Eu me arriscarei em português para agradecer todas as pessoas incriveis que eu encontrei em Brasilia. Obrigada aos agregados bebâdos: Beca, Pedro, Vinicius, Solon, Julio, Dave, Dan, Carioca, Gabriel, Julia, Zech, Loli, Douglas, Jessica, José… e todos os outros. Obrigada as pessoas do laboraotio Vitor, Mauricio, José, Thomas… Quero agradecer particularmente Miguel quem me ajudou muito na minha integração no laboratorio e com meus testes. Agradeço aos professores professores do ENM e aos estudantes de mestrado por terem me ajudado diverzas vezes.

A mon grand père,

List of Figures

List of Tables

Nomenclature.

A	Composite compliance
A_{13}^{D}, A_{8}^{D}	Damaged area under the slip zone for the width of 13mm and 8mm respectively
A_{th}^{D}	Theoretical damaged area in mm²
A_{m}^{D}	Measured damaged area in mm²
a	Semi-width of the contact
a_{th}	Theoretical semi-width of the contact
a_{m}	Measured semi-width of the contact
a_8, a_{13}	Semi-width of the contact for the specimen of 8mm and 13mm respectively
$a_1(\varphi)$ and $a_2(\varphi)$	Halves size of the sides of a rectangular hull
B	Tensile force
c	Semi-width of the stick zone
c_{th}	Theoretical semi-width of the stick zone
c_{m}	Measured semi-width of the stick zone
c_8, c_{13}	Semi-width of the stick zone for the specimen of 8mm and 13 mm respectively
$\boldsymbol{d^a}$	Antisymmetric spatial reference field
$\boldsymbol{d^c}$	Complementary spatial reference field
$\boldsymbol{d^s}$	Symmetric spatial reference field
E	Young modulus
E^*	Equivalent Young modulus
f	Friction coefficient
f_O	Initial coefficient of friction
f_m	Average coefficient of friction
f_s	Friction coefficient within the slip zones
$f(r)$	Radial evolution of the spatial reference field
G	Modulus of rigidity
$\boldsymbol{g}(\theta)$	Tangential evolution of the spatial reference field
I^a	Antisymmetric part of the nonlocal intensity factor
I_{max}^{a}	Maximum of the antisymmetric part of the nonlocal intensity factor
I^s	Symmetric part of the nonlocal intensity factor
I^c	Complementary part of the nonlocal intensity factor
I_{MWCM}	Multiaxial Fatigue Index in terms of Modified Wölher Curve Method

I_{max}	Maximum value of the multiaxial fatigue index
I_{13}, I_8	Multiaxial Fatigue Index in terms of the Modified Wöhler Curve Method at x=-a for the width of 13mm and 8mm respectively
K	Simplified Stress Intensity Factor
K_I	Stress Intensity Factor in mode I
K_{II}	Stress Intensity Factor in mode II
K_{III}	Stress Intensity Factor in mode III
L	Critical distance
l_{PM}	Critical distance in the sense of the Point Method
m	Material parameter of the Weibull's theory
M	Number of nodes in the circular region delimited by Ω in the finite element model
M_P	Number of nodes of each part of the crack analogue model simulation
N	Number of cycles to failure
P	Normal Force
P_8, P_{13}	Normal force for the specimen's widths of 8mm and 13mm respectively
$p(x)$	Distribution of the normal traction
p_o	Peak pressure
$P_R(\sigma)$	Probability of failure of a material submitted to a stress σ
Q	Total tangential load
Q_8, Q_{13}	Tangential load applied to the specimen's widths of 8mm and 13mm respectively
$Q(t)$	Fretting/tangential load at instant t
Q_{max}	Maximum value of the tangential force
Q_a	Amplitude of the tangential load
$q(x)$	Distribution of the shear traction
$q'(x)$	Perturbation of the shear stress's distribution
R	Radius of the pad
R_σ	Stress ratio
$R_{po.2}$	Yield stress
R_B, R_Q	Load ratios of the bulk force and the tangential force respectively
S_M	Mesh size of the crack analogue model simulation
T_8, T_{13}	Thickness of the specimens of 8mm and 13mm respectively
u	Strain tensor

$\boldsymbol{v}(\boldsymbol{x}, t)$	Approximate velocity field expressed in the reference frame attached to the contact edge
V_8, V_{13}	Stressed volume of the specimens of 8mm and 13mm respectively
V_{eff}	Effective volume
V_W	Sub volume used to compute the Weibull's probabilities
W	Width of the pad and specimen
W_8, W_{13}	Width of the pad and specimen of 8mm and 13mm respectively
$Z(z)$	Exact solution for the stress field in an infinite plane containing a crack under an equibiaxial loading
β	Dundur's parameter
$\Delta K_{th,\ R=0,1}$	Threshold of the stress-intensity range for a stress ratio R_σ=0,1
$\Delta\sigma_o$	Fatigue limit of the material
ε_{rr} and $\varepsilon_{\theta\theta}$	Components of the displacement tensor in parametric coordinates
λ and κ	Material parameters of the MWCM
υ	Poisson's ratio
$\Phi(r, \theta)$	Airy function solution of the bi-harmonic equation
σ_o	Fatigue limit on traction for R_σ=0
$\sigma_{o,1}$	Fatigue limit on traction for R_σ=0,1
σ_{-1}	Fatigue limit on traction for R_σ=-1
σ_B	Tensile stress
σ_B^8 and σ_B^{13}	Bulk load applied to the specimen's width of 8mm and 13mm respectively
σ_{fa}	Maximum fatigue stress amplitude
$\sigma_{n,max}$	Maximum normal stress in the critical plane
σ_{rr} and $\sigma_{\theta\theta}$	Components of the stress tensor in parametric coordinates
σ_{xx}, σ_{yy}, σ_{zz}, τ_{xy}, τ_{xz} and τ_{yz}	Components of the stress tensor in Cartesian Coordinates
σ_u	Ultimate tensile stress
σ_W	Nominal stress of the Weibull's theory
τ_a	Amplitude of the equivalent shear stress
τ_a^{max}	Maximum amplitude of the equivalent shear stress

Contents

Chapter 1. Introduction

1.1. Context of the study

Fretting fatigue is a particular case of fatigue. It appears when the contact between two solids is submitted to micro-displacements and at least one of these solids experiences a bulk fatigue load. The interfacial damage caused by fretting wear and the high concentration of stresses under the contact may speed up the initiation of micro-cracks, which can lead to a premature fatigue failure of the structural components. This type of failure is a major concern for safety-critical applications such as the ones found in the aerospace, automotive or nuclear power generation industries.

In the aeronautical industry, the contact between fan blades and disk presents one of the major issues for the researchers (Papanikos et al., 1994). The characteristics of the multiaxial fretting fatigue loadings encountered with this particular configuration are not well known and lead to complex and time consuming computations. However, experimental campaigns have shown that this phenomenon presents a negative effect on the fatigue limit (Lindley, 1997) and it became important for the aeroengine industry to develop new simplest models to take it into account.

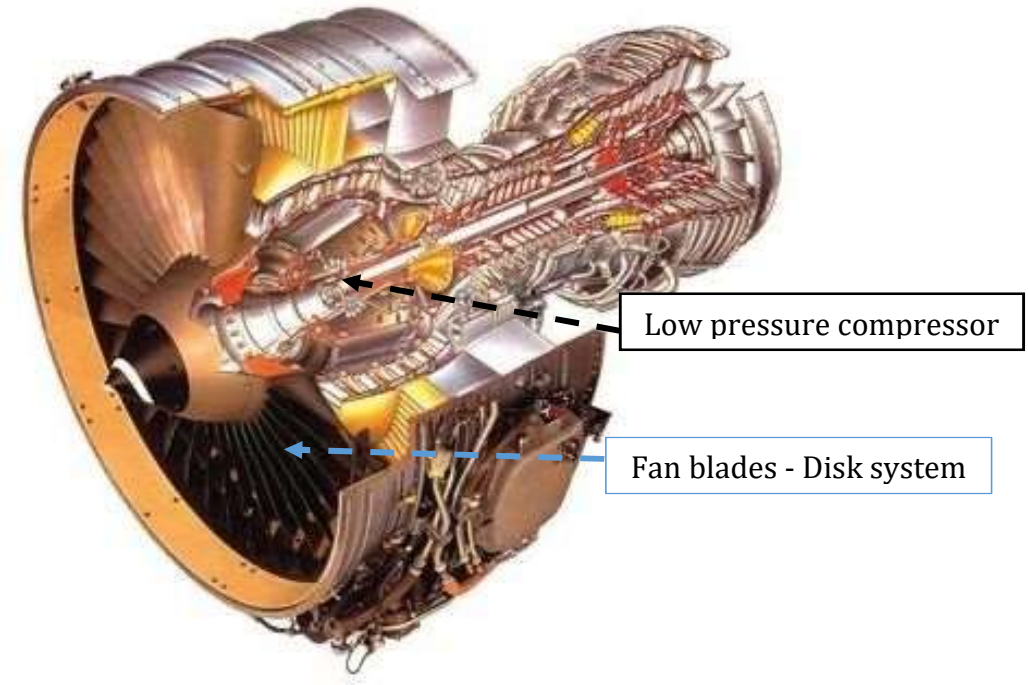

Figure 1-1: Cut view of the CFM56-5B Turbofan Engine.

On the low pressure stages of rotating compressors (Figure 1-1), dovetail roots (Figure 1-2(a)) are used to fix the fan blades in the disk. The type of loads present in this assembly is complex (Figure 1-2(b)). Indeed, during flights, the rotation of the compressor induces centrifugal forces in the blades which press them against the disk. Hence, a normal force is generated which creates the contact between each blade and the disk of the turbine. Moreover, the air flow on the blades engenders high-frequency vibrational loads. These vibrations induce a relative motion at the blade/disk interface, causing fretting wear/load.

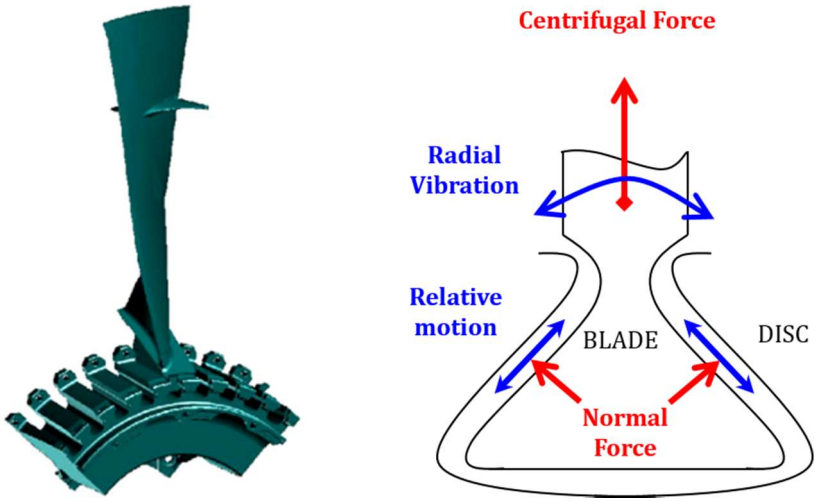

Figure 1-2: (a) schematic diagram of the dovetail fixing and (b) load configuration (adapted from (Mériaux, 2010)).

This configuration is today reliable and fully operational mainly because of a systematic oversizing and numerous maintenance operations. Moreover, the casing of the engine is designed to contain a possible failure of the blade. Hence, the rupture of a blade generally provokes severe damages of the engine but does not endanger the integrity of the airplane. However, uncontained fan blades failure may still happened, as that occurred in 2016 in the left hand CFM56-7B of the Southwest Airline's Boeing 737-700. Such failure occurred during cruise. The engine inlet was lost (Figure 1-3 (a)) and metal debris hit the fuselage, wing and empennage, causing severe damage (Figure 1-3 (b)). Fortunately, the aircraft was able to land safely. The National Transportation Safety Board (NTSB) reported that the fracture surface of the titanium alloy fan blade showed evidence of a fatigue crack.

(a) (b)

Figure 1-3: Photographs of an aircraft (a) engine and (b) fuselage damage in a Southwest Airline's Boeing 737-700 in August, 27th 2016 near Pensacola (Photo: Peter Lemme).

However, failure of the disk may lead to much more critical accidents. For example, in 2010, a Sun Way IL76 suffered an uncontained disk failure leading to the crash of the aircraft (Figure 1-4). All 6 crew members and 2 support engineers on board as well as 3 people on the ground were killed. The Pakistan's Safety Investigation Board (SIB) reported that they found evidence of fatigue fracture on the second stage disk of the low-pressure compressor.

Figure 1-4: Photographs of the recovered low pressure compressor 2nd stage disk (Photo: SIB).

Safran Aircraft Engines, a French aeroengine manufacturer, has special interest on the enhancement of their design methodologies against fretting fatigue. In this setting, it has funded a research project denominated COGNAC (Competition between the Gradient effect and the scale effect in Notch fatigue and Contact fatigue). This project has not only the objective to improve the understanding of fretting fatigue, particularly the role of the gradient and the size effects on the phenomenon, but also to promote the scientific cooperation between the

Fatigue, Fracture and Materials Research Group of the University of Brasília, the Laboratory of Mechanic and Technology of the Paris-Saclay University and the Department of Physics and Mechanics of Materials of the Institut P Prime.

1.2. Review of the state of the art

The first observations of fretting were reported by Eden et al. (1911). While doing experiments on rotating beams he observed the formation of oxides debris on the steel grips of the testing machine and the specimen. He concluded that this corrosion was due to the varying stress between the test-specimen and its holder. However, it is only in 1927 that Tomlinson (1927) developed the first fretting apparatus, a machine which generated small relative relation between two rings. His work (Tomlinson et al., 1939) introduced also some fundamental concepts for the fretting studies. In particular, he showed that the corrosion has mechanical origin and in order to observe it some surface alternating slip is necessary. These results were confirmed by McDowell (1953) who demonstrated that the pressure and the amplitude of motion between surfaces have an impact on the presence of oxides debris and on the severity of the fretting.

The effect of the fretting corrosion on the fatigue strength of materials was first shown by Warlow-Davies et al. (1941). He carried out fatigue experiments on specimens with fretting damages and he observed a reduction of 13% to 18% for the fatigue strength in comparison with unfretted specimens. Later, Horger (1953) pointed that, in presence of fretting, cracks initiate at very low stresses, which are not sufficient to lead to crack propagation once the environment producing fretting is removed. Moreover, he found that the necessary level to prevent crack initiation depends on the number of stress cycles considered. Similar results were obtained by Fenner and Field (1958) who proved that fretting has a great importance for the crack initiation process. Indeed, they suggested that this reduction in the fatigue strength was linked to the slip amplitude.

In the last 60 years, fretting-fatigue has become a subject of great interest to researchers and important advancements in the discipline were made. A rapid search in a scientific data base such as Science Direct using the term fretting fatigue between 1960 and 2017 provided 7099 results. Much of the work from the sixties to the nineties was achieved in material science departments to provide data about the resistance of materials to fretting fatigue. A reasonable amount of data and analysis was also produced on the quantification of propagation stage of a fretting crack. A good review of some of the most promising results obtained in this period was organised by Waterhouse (1992). In 1994 arises one of the few and most important books on fretting fatigue, by Hills & Nowell (1994). This book contains a summary of the substantial research work produced by the Oxford team. It presents the

fundamentals to model and to solve the contact problem of two dimensional elastic contacts under partial slip regime. The effect of the presence of a varying bulk load is also approached as the tools to compute stress intensity factors and propagation life under fretting fatigue. Little attention was paid to crack initiation.

From the middle end of the nineties most of the attention of the fretting community seems to have turned to the crack initiation mechanisms. To the author's best knowledge, the first attempt to use a multiaxial fatigue criterion to predict the crack initiation was done by Petiot et al. (1995). They used a numerical simulation to determine the stress field within the contact and then they applied the Dang Van multiaxial fatigue criterion (Dang Van et al., 1989) to predict whether or not the crack initiation can occur. Following this methodology, they obtained good predictions for the crack nucleation. Thereafter, Szolwinski and Farris (1996) applied a modified Smith Watson Topper criterion to take into account the effect of the mean stress in order to predict both the initiation site and life of fretting-fatigue cracks.

These methods, based on the critical plane model, allowed not only to determine the crack initiation site, but also the angle of propagation. Comparative studies were done by Araújo (2000) for the Smith, Watson and Topper parameter (Smith et al., 1970) and the Fatemi Socie criterion (Fatemi and Socie, 1988). While comparing estimated crack initiation lives to the experimental ones, he obtained overly conservative predictions for smaller contacts and satisfactory predictions for larger ones. He concluded that such a phenomenon occurred mainly because of the stress gradient, which is stronger for smaller contacts. This suggested that multiaxial fatigue criteria do not take into account the gradient effect encountered in fretting-fatigue and so new methodologies had to be developed.

Methodologies to take into account the gradient effect on fretting-fatigue

Different methodologies were identified in the literature to cope with the gradient effect. Araújo (2000, 2002) has proposed two methodologies to take the gradient effect into account. First, he proposed to average multiaxial fatigue parameters over a characteristic depth on the critical plane and secondly to average the stresses over a characteristic element of volume (Figure 1-5). This first methodology takes advantages of the critical plane method (Findley, 1959, Brown and Miller, 1973, Socie, 1987, Fatemi and Socie, 1988, and McDiarmid, 1991) to perform a two-dimensional analysis on the plane where the crack is expected to initiate. He applied the first methodology by averaging two multiaxial fatigue parameters, the Smith Watson Topper and the Fatemi and Socie parameters, along different characteristic depths. The second method consisted in averaging stresses over a characteristic rectangular element of volume under the contact. The fatigue parameters were evaluated at different planes for each

element of volume so that one could find their global maximum value. This procedure provided then the location of crack initiation and the "average" critical plane orientation (Figure 1-6). The numerical results were compared with experimental fretting fatigue experiments carried out with a cylinder/plane contact configuration for Ti-6Al-4V alloy and for an aluminium alloy. Both methodologies gave satisfactory life estimations by using a constant critical depth of 20μm for the aluminium alloy and of 10μm for the Ti-6Al-4V. Finally, he observed that although it was not possible to firmly conclude about the physical nature of the critical length (i.e. whether it was a material parameter or a stress gradient dependent quantity). The best fitting values of this length appeared to be of a similar magnitude as the grain size for both materials.

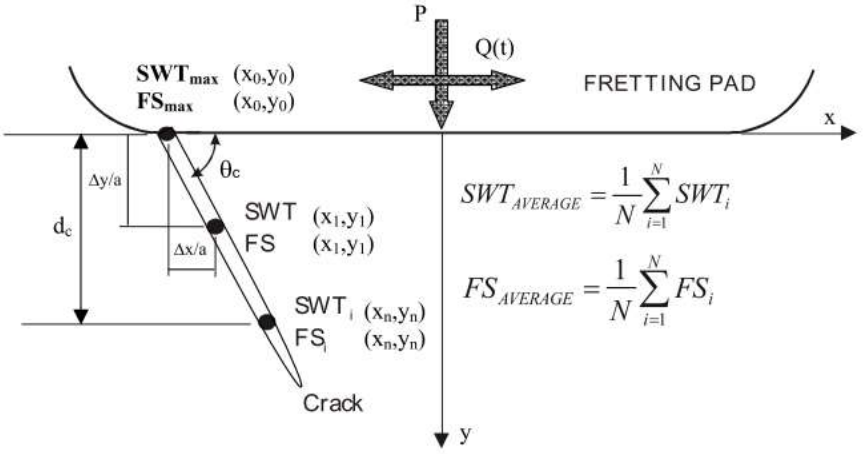

Figure 1-5: Schematic description of the methodology 1 (Araújo, 2000)

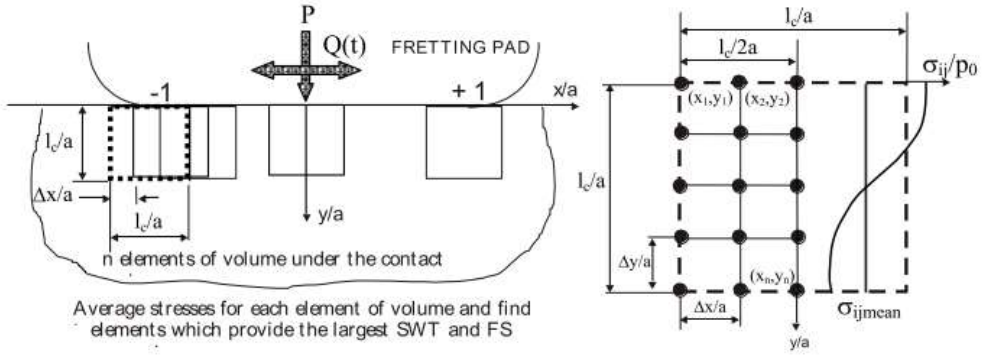

Figure 1-6: Schematic description of the methodology 2 (Araújo, 2000)

Following this idea, Fouvry (2000) has suggested that it is possible to predict the crack nucleation by averaging the loading state over a critical elementary volume, whose characteristic length is more related to a physical constant dimension characteristic of the microstructure than to the contact size. Later, he has shown that, for steel, the micro-volume

identified to find the experimental loading leading to the fretting initiation may be linked to a characteristically dimension of the microstructure, as the grain size (Fouvry, 2002). This aspect was discussed by Naboulsi and Mall (2003) by using finite elements computation for three different multiaxial criteria: the Shear Stress Range (MSR), the modified Smith Watson Topper parameter (SWT) and the Findley parameters. They used two approaches to average the multiaxial parameters. First, they averaged the values of each parameter at different points of a specified rectangular volume. Secondly, they averaged the values of stress and strain over a specified radial volume and then computed the different parameters from these average states of stress and strain. To investigate the effect of the stress gradient two radii of cylindrical pads were considered: one of 50,8 mm and the other of 5,08mm. They observed good predictions for the angle of crack initiation for both methods and both pad radii. However, it exists a huge dependence of the size of the process zone on the average parameters, and this dependence increases for higher stress gradients.

Another axis of research that has been followed to model fretting fatigue in the last twenty years is the so called crack analogy method. By taking advantage of the similarities between the singular stress and strain fields for sharp-edged contacts (Gladwell, 1980, Johnson, 1985 and Hills, 1993) and for cracked bodies (Kanninen, 1985 and Anderson, 1995), Giannakopoulos et al. (1998) suggested that there is a quantitative equivalence between a fretting-fatigue and a cracked body under cyclic loadings. To perform the analysis of this analogy, they first established a geometrical analogy between the radius of the contact zone and the cracked specimen. Then, they found the stress and strain evolutions for both configuration. They considered a cracked body subjected to a normal compressive load whose magnitude is the same as the one used to press the punch on the flat specimen in the contact configuration. Next, they expressed the stress fields of the contact configuration in terms of K_I and K_{II} and then determined the expression of these two stress intensity factors for the cracked body. Finally, they demonstrated the stress intensity factors computed previously are identical in both cases. They established this analogy for two contact configurations: a two-dimensional contact by considering a rectangular rigid punch pressed against a flat surface; a three-dimensional contact with a cylinder pressed against a flat specimen. Then they considered the limited case of complete stick under the contact. The pads considered are pressed against the specimen by a fixed pressure P and submitted to a fluctuating tangential force Q. The specimens are submitted to a uniform cyclic stress. The proof of the analogy between contact and crack configuration allowed them to apply a prediction model for fretting-fatigue based on this crack analogy. Comparing their numerical results with experimental results from literature they found good predictions for the crack initiation angle and growth. For the crack initiation angle they assumed initial direction given when the amplitude of K_{II} is null at the maximum

value of the loading (complete stick condition). For crack's growth they used a long-crack threshold expressed in terms of the bulk stress.

Looking at these encouraging results Giannakopoulos et al. (2000) extended the previous crack analogue model to a notch analogue model for two-dimensional contacts. In this work they developed a new analytical solution for a rounded corner punch pressed against a substrate submitted to a fretting-fatigue loading by using an analogy with fatigue crack initiation at the notch tip. This methodology has shown to provide a direct connection between this configuration of fretting-fatigue and the plain fatigue crack initiation of a smooth specimen of the same material by considering the bulk stress of the fretting-fatigue loading as a stress intensity factor. Indeed, the stress field induced by the contact appeared to be very similar to the square-root singular stress field around an external crack and the bulk stress to the T-stress in fracture mechanics terminology. The reduction factor between the two configurations was predicted by deriving the analytical results. They carried out an experimental validation of this model by using the results of Hutson et al. (1999, 2000) obtained with a Ti-6Al-4V alloy. The average predictions for the maximum bulk stress have shown a difference of 10% for a loading ratio R=0.1 and of 4% for R=0.5. They concluded that crack initiation in fretting-fatigue for a bi-dimensional contact (flat on flat) can be predicted using the so called "notch analogue model".

Later Conner (2004) took advantages of the crack-analogue model, proposed by Giannakopoulos (1998), to predict the total fatigue lives by computing the stress intensity factors proposed on the model and by applying the Paris' law. The results obtained with this approach match the experimental results with an accuracy of ±30%. Based on these results Chambon (2006) carried out an analysis of the model to assess its potential for futures researches, but also its limitations in order to determine the improvement that can be made. To do so he proposed a phenomenological model to describe each stage of crack propagation based on the crack-analogue approach used to describe the contact problem through fracture mechanics "tools". He conclude that if such a description brings good qualitative and quantitative predictions, some aspects of the fretting-fatigue already have to be incorporated in the model, such as the residual stresses that may be presented because of the mechanical treatment of the surface.

A first attempt to complete the original crack analogue model proposed by Giannakopoulos (1998) was done by Ciavarella et al. (2003a) They observed that in the first crack analogue model proposed, the bulk stress is only considered for the crack growth condition. In order to improve the determination of the crack initiation condition, they considered this stress also for the computation of the stress intensity factors K_I and K_{II}. Lately, Ciavarella et al. (2017) provided a new estimation of the stress intensity factors used in this model for the case of varying normal load. However, the whole demonstration for the

determination of these new stress intensity factors is based on the assumption that the equation for full stick condition of a square-ended punch is still valid.

Another way to take advantage of the crack analogy was proposed by Dini (Dini et al., 2006). He considered the classical analysis of notches based on critically stressed regions approaches, such as point, line and area methods (Taylor, 1999, Lazzarin, 1997) and applied them to fretting-fatigue. These analyses are constructed on the assumption that, in order for failure to occur, the average stress must exceed the fatigue limit over some critical volume surrounding the stress raiser. Thus, he formalised the idea developed by Araújo (2000, 2002) and Fouvry (2000, 2002) of using a characteristic length to average the stresses under the contact along a line or over a volume. This critical length is here well defined as a material parameter, and its value is fixed by the El Haddad's length parameter (El Haddad et al., 1979). Moreover, the simplest approach of the Point Method may be applied, where it is assumed that the value of the fatigue limit has to be calculated so that the total stress range at the critical length equals the fatigue limit. This method was compared to experimental results performed on aluminium alloys with different cylinder pad radii but by maintaining a constant peak pressure. Such a set of experiments allows to highlight the gradient effect. Good predictions of fretting-fatigue threshold were obtained, however, there are criticisms with respect to the use of the El Haddad parameter as a material property (Castro et al., 2009).

A proposition to express this fatigue limit in the case of the fretting-fatigue was done by Araújo et al. (2007). They studied the application of the Modified Wöhler Curve Method (MWCM) (Susmel and Taylor, 2003) in conjunction with the Theory of Critical Distance (TCD). The MWCM assumes that fatigue damage depends on two parameters: the shear stress amplitude, τ_a, computed with the Minimum Circumscribed Circle (Dang Van, 1973, Papadopoulos, 1998) and the maximum normal stress, $\sigma_{n,max}$, on the critical plane of the material, and is expressed in terms of τ_a, ρ and two material parameters: κ and λ. According to this method, a threshold condition for crack initiation may be extracted from the expression of the criterion at the critical distance of the material. In order to evaluate the accuracy of the methodology, they proposed an experimental campaign for a cylinder/plane contact configuration on AL4%Cu. The error index proposed by Papadopoulos (1995) was adopted to evaluate the accuracy of the methodology. This error index is expressed in terms of τ_a, $\sigma_{n,max}$, κ and λ, and if a negative value is obtained it means that fatigue failure should not occur up to the number of cycles considered to compute the material parameters. Finally, this proposed method was able to predict failure within an error interval of ±20%. An improvement of this method was given recently by Araújo et al. (2017). First, to compute the shear stress amplitude the Maximum Rectangular Hull (MRH) method (Mamiya et al., 2002, 2009 and 2014, Araújo et al., 2011 and 2014, Carpinteri et al., 2014) was used instead of the Minimum Circumscribed Circle (MCC) (Papadopoulos, 1998). This modification was motivated because the MRH

showed to be able to provide more accurate endurance limit estimates when used in conjunction with multiaxial models for some complex loading paths test programs. Moreover, the critical distance was no longer consider as a material parameter as it was defined for the Point Method by Taylor (Taylor, 1999). Indeed, some recent developments (Susmel and Taylor, 2007 and 2008) have demonstrated that to correctly estimate the static strength under fatigue loading, the critical distance should be calculated as a function of the number of cycles to failure. While the first version of this methodology allowed only to predict the fretting-fatigue limit, this new version could be used to estimate the fatigue lives for fretting-fatigue tests within a factor of 2. Finally, it should be noted that this methodology was applied to validate the analogy proposed between fretting and notch fatigue (Araújo et al., 2016).

Returning to the description of the fretting-fatigue mechanisms by means of stress intensity factors, a new model has been recently proposed by Montebello et al. (2016). This model is based on the description of an approximate velocity field extracted at the proximity of the contact edge with a Finite Element Analysis. The nonlocal intensity factors are computed by a decomposition of this "velocity field", and are used to build a crack initiation map. One of the main advantages of this method is that it proved to be geometrically independent, i.e. when the crack initiation map is expressed in terms of nonlocal stress intensity factors, the gradient effect is taken into account and there is only one crack initiation frontier for all geometries studied, for a particular material. In order to predict the location of the crack initiation frontier by using only materials data, several multiaxial fatigue criteria were coupled to the nonlocal stress intensity factors description. In particular, The MWCM previously described was applied, and the comparison with experimental data of the literature has shown a good prediction of the crack initiation frontier (Montebello, 2015). However, the major part of the experimental validation was conducted with fretting results and no study about the effect of the normal stress on the crack initiation frontier has been achieved.

It is interesting to note the effort made by Montebello et al. (2015) to develop a geometrical independent crack initiation map. This has been motivated by the industrial need to transpose the results obtained on laboratory to real-scale industrial components. This aspect highlights another issue encountered in fretting-fatigue problems, the possible size effect that may exist between the laboratory contact configuration and industrial components.

The size effect on fretting-fatigue

A number of authors have reported a size effect where a significant number of fatigue lives are achieved below a contact zone (Hills et al., 1988, Bramhall, 1973). However, this phenomenon has been investigated by Araújo et al. (1999) and appeared to be a stress gradient issue, as the

stress under the contact will decrease faster when smaller pad configurations are used. Since this observation, very little work has been done to define properly the contact size effects.

A recent work of Fouvry et al. (2013) tried to address this problem with a tribological approach. His objective was to describe the influence of the contact size on the friction and the wear rate. To do so he carried out numerous fretting tests with different contacts and loads configurations. First, he conducted tests with sphere-plane contact and then tests with spherical-plane contact, with different pad radii. To change the size of the contact area, he studied different contact pressure for the sphere-plane configuration. The contact pressure of the cylinder-plane configuration has been maintained constant as the modification of the pad radii already change the size of the contact area. All the experiments were conducted on a reference AISI52100/AISI52100 interface. The results were analysed regarding the evolution of two different parameters: the mean coefficient of friction and the Archard wear rates (Archard, 1953). The results have shown that, for this particular material, the sliding amplitude and the contact pressure have little influence on the evolution of both parameters considered. Hence, it was assumed that the major role was played by the contact size. Indeed, it appears that with larger contact size there were a decrease of the mean coefficient of friction and an increase of the wear rate. Two explanations of this phenomena cropped up. First, it can be described by a tribological approach. Indeed, an increase of the contact size helps to trap the debris created by the fretting process and so leads to a thicker third body layer. This will easy the shear interface accommodation and provoke a reduction of the coefficient of friction and of the wear rates. Secondly, it is also reminded that a larger contact size means a softer stress gradient. The tribological approach was largely discussed in this work and a model was proposed, an offset power law between a tribological parameter, i.e. the mean friction coefficient or the Archard wear rates, and a contact size parameter, which describe well the tough decrease of the two parameters studied with small contact conditions and their quasi-constant evolution in larger contact domains. However, the way to use this model for an extrapolation of the laboratory to the industrial issues has not been yet proposed, and the influence of the gradient effect was not isolated.

Conclusion on the literature review and objective of the thesis

In recent decades, the gradient effect of the fretting fatigue has been often studied and different models to describe the problem were proposed, but only a few approaches were concerned to the extension of these design methodologies, usually validated under simple laboratory conditions, to the industrial needs. As it was previously discussed, the model proposed by Montebello (2015, 2016) seems appealing in this context, but it neither addressed in details the effect of the mean stress on the crack initiation boundary nor validated the model for a wider

range of metallic materials under fretting-fatigue conditions. One can also observe from our review of the state of the art that another issue which has clearly received little attention from the scientific community in fretting-fatigue is the size effect. The work presented in this thesis will therefore try to present new contributions to address these problems. New experimental data will be generated considering a Ti-6Al-4V alloy (used to produce fan blade and disks in aircraft engines) not only to further validate the crack analogue model, but also to try to isolate and identify the role of the size effect on fretting-fatigue.

1.3. Thesis scope

To answer the problematics of the thesis, both experimental and analytical work is necessary and will be described in this manuscript.

In Chapter 1 the context of the work has been defined as well as the review of the state of the art and the objectives of the thesis. In Chapter 2, the theoretical background on which the analytical work is based on will be detailed. It consists on (i) the modelling of two dimensional elastic contact mechanics under partial slip conditions and in the presence of bulk fatigue loads, (ii) the presentation of the theory of critical distances (TCD) and (iii) the fundamentals about the two models used on this work: The Multiaxial Wöhler Curve Method the Crack Analogue Model (using nonlocal Stress Intensity Factors), both used in conjunction with the TCD.

In Chapter 3, an overview of the material properties and of the experimental methodologies and facilities will be presented. This will allow to gain insight on the experimental results used in the following chapters as two groups of experimental tests will be carried out.

In Chapter 4, the first group of experimental results will be used to test the ability of the crack analogue model to deal with the gradient effect encountered on fretting-fatigue. The advantages of this model, specifically the savings on computational time, are of great interest for aeronautical companies. Indeed, if successful, this methodology could be implemented industrially to study more complex geometry encountering likewise issues of fretting fatigue.

In Chapter 5, the second group of tests results will be detailed and analysed to investigate the size effect. Indeed, it exists only a few study about this phenomenon and there is an increasing demand for its understanding. The nonlocal multiaxial fatigue criterion of the Multiaxial Wöhler Curve Method used in conjunction with the Critical Distance theory will be used to investigate the influence of the width size of the specimens and the size of the damage area on fretting-fatigue crack initiation.

Finally, in Chapter 6, general conclusions about this work and proposal for future work will be presented.

Chapter 2. Theory

2.1. Introduction

In order to analyse the experimental results, a theoretical background will be necessary.

The formulation of the stress state induced by fretting-fatigue loadings has been completely formalised on the book of Hills and Nowell, "Mechanics of Fretting Fatigue" (Hills and Nowell, 1994), and will be reproduced here for the experimental configuration chosen.

Two criteria will also be analysed and assessed. The Multiaxial Wöhler Curve Method in conjunction with the theory of the critical distance, as proposed by Araújo et al. (2007) and a crack analogue model based on nonlocal Stress Intensity Factor proposed by Montebello et al. (2015, 2016).

2.2. Basic contact mechanic

Usual experimental contact configurations

Industrial components and structures usually show complex geometry which can hardly be reproduced in laboratory. That's why different simplifications of the contacts have been developed to allow easier experiments (Figure 2-1). Three reference contacts are generally defined:

- Spherical fretting pads loaded against a plane specimen. This contact geometry is unidimensional and so does not require alignment (Kuno et al., 1989). Therefore it is easier to implement experimentally. However, the computation for this representation is more complicated because it is a 3 dimensional problem.
- Cylinder fretting pads loaded against a plane specimen. This two-dimensional contact is regularly used even if it requires a cautious alignment of the pad. Moreover, it is described by the Hertz theory (Hertz, 1981) and analytical solution already exists (Hills and Nowell, 1994).
- Flat fretting pads loaded against a plane specimen. This the three-dimensional configuration is the closest from the industrial configurations. However, it is scarcely used because of the difficulty encountered for the alignment. Moreover, this geometry is characterised by high discontinuities for the pressure and shearing's profiles at the bordering of the contact, nevertheless analytical solutions have been developed (Alexandrov et al. (2001), Ciavarella et al. (2003b)).

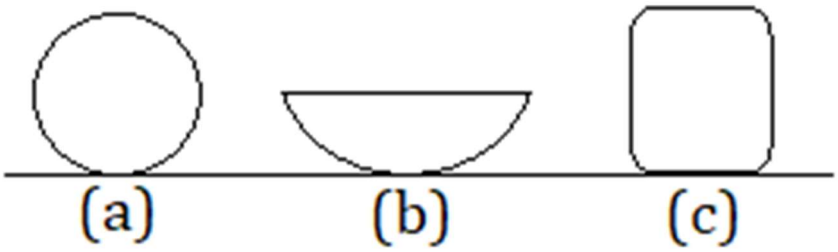

Figure 2-1: Geometries of the three reference contacts: (a) sphere/plane; (b) Cylindrical/plane; (c) Flat/plane contact.

The industrial contact involved for the COGNAC project is complex to model. However, the main objectives of this study are to improve the today knowledge about the gradient effect and the size effect. Hence, a simplified geometry can be considered. The one selected for this study is the cylinder/plane contact because its analytical solution is easy to implement and different gradient of stress can be encountered by modifying the radius of the pad. Thus, the methodology to obtain the subsurface stress field will be developed for this configuration.

Determination of the surface traction for a fretting-fatigue loading

The determination of the internal fields is divided into two stages. First, the contact pressure distribution has to be determined by solving the contact problem. Then, the internal stress, strain and displacement field is found using the expressions of the surface tractions deduced previously.

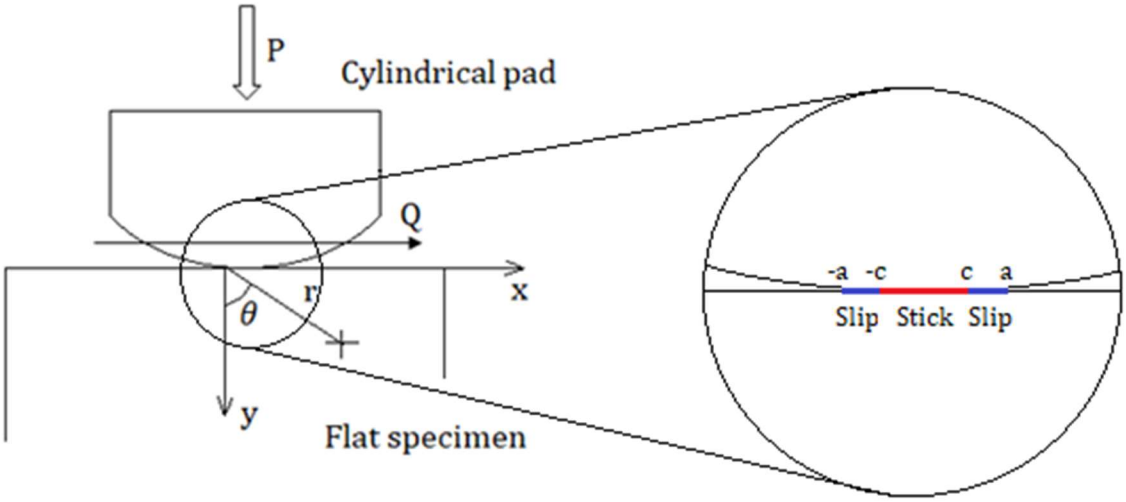

Figure 2-2: Cylinder-plane contact subject to normal and tangential forces.

Plane monotonically problem: Figure 2-2 shows a cylindrical pad loaded by a normal force P against a flat specimen. A tangential force, Q, is applied to the pad. The Hertz's theory (Hertz, 1881) can be used as it is a non-conformal contact. Then, by applying the hypothesis of plane strain, the stress state may be extracted with an Airy function solution of the bi-harmonic equation (Timoshenko and Goodier, 1951):

$$\Phi(r,\theta) = -\frac{r\theta}{\pi}(Psin\theta + Qcos\theta) \tag{2.1}$$

$$\frac{1}{r}\frac{\delta\Phi}{\delta r} + \frac{1}{r^2}\frac{\delta^2\Phi}{\delta r^2} = \sigma_{rr} = -\frac{2}{\pi r}(Pcos\theta - Qsin\theta) \tag{2.2}$$

$$\sigma_{\theta\theta} = \tau_{r\theta} = 0 \tag{2.3}$$

The stress field may be find by using the Hooke's law:

$$\boldsymbol{\varepsilon} = \frac{-\nu}{G} tr(\boldsymbol{\sigma})\boldsymbol{I} + \frac{1+\nu}{G}\boldsymbol{\sigma} \tag{2.4}$$

$$\begin{cases} \varepsilon_{rr} = \frac{1}{G}\{\sigma_{rr} - \nu\sigma_{\theta\theta}\} = \frac{\sigma_{rr}}{G} \\ \varepsilon_{\theta\theta} = \frac{1}{G}\{\sigma_{\theta\theta} - \nu\sigma_{rr}\} = \frac{-\nu\sigma_{rr}}{G} \\ \gamma_{r\theta} = \frac{(1+\nu)}{G}\tau_{r\theta} = 0 \end{cases} \tag{2.5}$$

with G the shear modulus and υ the Poisson's ratio. When the strain field is known and as $\varepsilon(i) = \frac{\partial u}{\partial i}$, the displacements can be found:

$$\begin{cases} \frac{\delta u}{\delta x} = \frac{1-2\nu}{2G}p(x) + \frac{1-\nu}{\pi G}q(x)\int\frac{q(\xi)d\xi}{x-\xi} & (2.6) \\ \frac{\delta v}{\delta x} = -\frac{1-2\nu}{2G}q(x) + \frac{1-\nu}{\pi G}q(x)\int\frac{p(\xi)d\xi}{x-\xi} & (2.7) \end{cases}$$

The derivatives of the surface displacements are given by the equation *(2.6)*. They are due to distributed direct traction, $p(\xi)$, and shear traction, $q(\xi)$, applied over the surface.

Considering now the relative displacement on the vertical axe because of the force occurring: $h(x) = v_1(x) - v_2(x)$, and the relative displacement of the contacting surface: $g(x) = u_1(x) - u_2(x)$, one will get:

$$\frac{1}{A}\frac{\delta h}{\delta x} = \frac{1}{\pi}\int \frac{p(\xi)d\xi}{x-\xi} - \beta q(x) \tag{2.8}$$

$$\frac{1}{A}\frac{\delta g}{\delta x} = \frac{1}{\pi}\int \frac{q(\xi)d\xi}{x-\xi} + \beta p(x) \tag{2.9}$$

with:

$$A = \frac{1-\nu_1}{G_1} + \frac{1-\nu_2}{G_2} \tag{2.10}$$

$$\beta = \frac{\Gamma(1-2\nu_1) - (1-2\nu_2)}{\Gamma(1-\nu_1) + (1-\nu_2)} \tag{2.11}$$

$$\Gamma = \frac{G_2}{G_1} \tag{2.12}$$

A being the composite compliance, β the Dundur's parameter (Dundur, 1969) and the subscripts 1 and 2 stand for body 1 (for instance the fretting pad) and body 2 (the flat specimen).

As two identical materials for the specimen are involved:

$$A = 2\left(\frac{1-\nu}{G}\right) \tag{2.13}$$

$$\beta = 0 \tag{2.14}$$

$$\Gamma = 1 \tag{2.15}$$

For the cylinder-plane contact problem, the Muskhelishvili's solution (Muskhelishvili, 1953) of the equation (2.7) is:

$$p(x) = p_0\sqrt{1-\left(\frac{x}{a}\right)^2} \tag{2.16}$$

where p_o is the peak pressure:

$$p_0 = \frac{2P}{\pi a} \tag{2.17}$$

and a is the semi width of contact:

$$a = \sqrt{\frac{4PR}{\pi E^*}} \tag{2.18}$$

where R is the equivalent radius:

$$R = \left(\frac{1}{R_1} + \frac{1}{R_2}\right)^{-1} \tag{2.19}$$

and E^* is the equivalent Young modulus:

$$E^* = \left(\frac{1-\nu_1^2}{E_1} + \frac{1-\nu_2^2}{E_2}\right)^{-1} \tag{2.20}$$

The subscripts 1 and 2 stand for body 1 (for instance the fretting pad) and body 2 (tensile specimen).

The tangential load is, for its part, the solution of the equation (2.8) and has been firstly described by Cattaneo (1938):

$$q(x) = f p_0 \sqrt{1 - \left(\frac{x}{a}\right)^2} + q'(x) \tag{2.21}$$

where the perturbation $q'(x)$ is zero in the slip zone ($c \leq |x| \leq a$). In the stick zone, $q'(x)$ can be found by noticing there is no variation of the relative displacement between corresponding points. Therefore, the complete solution for the cylinder-plane case has been find by Hills and Nowell (1993):

$$q'(x)/_{fp_0} = \begin{cases} 0 & if\ c \le |x| \le a \\ -\frac{c}{a}\sqrt{1-\left(\frac{x}{c}\right)^2} & if\ |x| < c \end{cases} \quad (2.22)$$

The size of the stick zone is found by enforcing tangential equilibrium:

$$\frac{c}{a} = \sqrt{1 - \left|\frac{Q}{fP}\right|} \quad (2.23)$$

Figure 2-3 shows the normalised distribution of pressure and shear stress for a typical loading configuration.

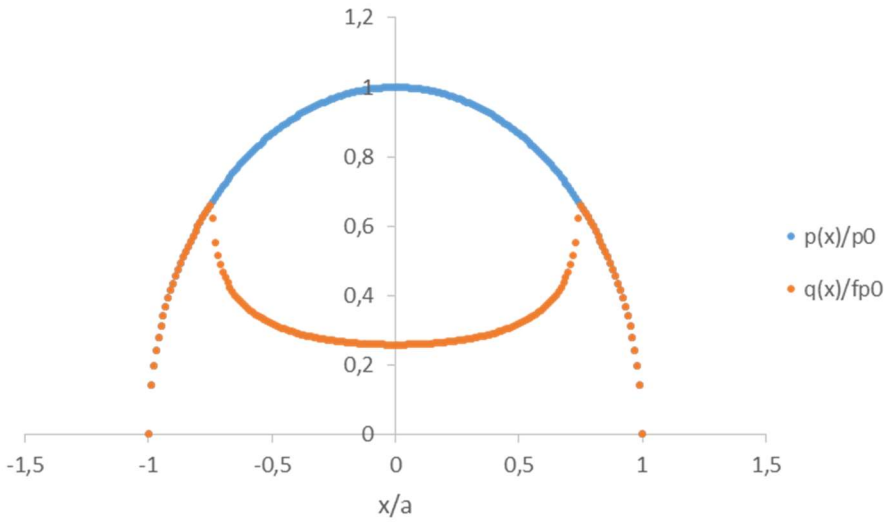

Figure 2-3: Normalised distribution of pressure and shear stress for Q/fP=0,45 and σ_B/fp_0=0.

Cyclic loading: Fretting experiments induce a cyclic tangential load between constant limits, $\pm Q_{max}$ (Figure 2-4). It follows that the expressions previously determined are validated only for the extreme values of the loading. The expressions of the surface tractions for whole parts of the loading will be given in this part.

The Amonton's law (Wolfram, 1983) gives the relation between the shear traction and the tangential load within the slip zone:

$$|q(x)| = -fp(x) \quad (2.24)$$

and the direction of the shear traction opposes the relative motion of the surfaces:

$$sgn\big(q(x)\big) = -sgn\left(\frac{\delta g}{\delta t}\right) \tag{2.25}$$

In the central region, where there is no relative slip between corresponding particles, the shear traction must be less or equal to the limiting frictional value:

$$|q(x)| \leq -fp(x) \tag{2.26}$$

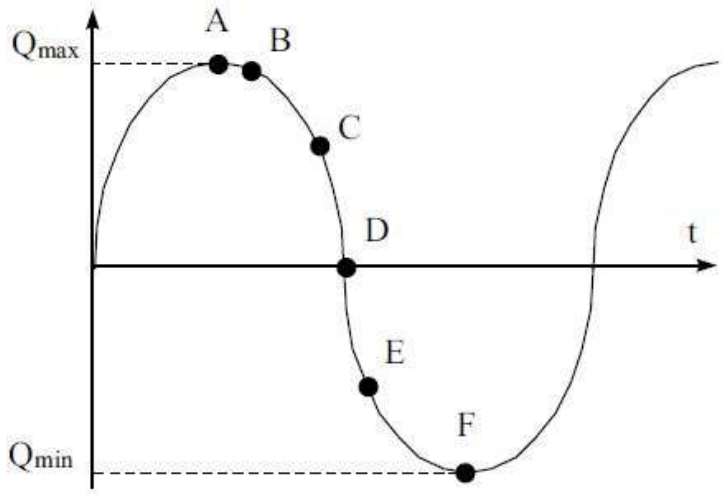

Figure 2-4: Variation of shear load Q with the time

Returning to the determination of the shear traction, Figure 2-4 depicts the variation of the tangential load among the time. When the load increases monotonically from 0 to Q_{max}, the maximum amplitude of the tangential force, the shear traction is defined as described by the equation (2.21) and (2.22)

Now consider that the load has been infinitesimally reduced from its maximum value, point A, to point B. Hence, it will have a change of sign in the rate of the tangential displacement $\partial g/\partial t$, so the equation (2.3) is no longer valid and instantaneous stick must occur over the entire contact.

If the fretting load is further reduced until the point C, a relative slip will appear at the contact edges. In these new slip zones ($d < |x| \leq a$), the shear traction will have changed from $fp(x)$ to $-fp(x)$. The corrective traction necessary to prevent this slip is:

$$q''(x) = +2fp_0 \frac{d}{a}\sqrt{1-\left(\frac{x}{d}\right)^2} \tag{2.27}$$

Then, the net shear traction can be written as:

$$q(x)\Big/_{fp_0} = \begin{cases} -\sqrt{1-\left(\frac{x}{a}\right)^2} & , \quad d < |x| \le a \\ -\sqrt{1-\left(\frac{x}{a}\right)^2} + 2\frac{d}{a}\sqrt{1-\left(\frac{x}{d}\right)^2} & , \quad c < |x| \le d \\ -\sqrt{1-\left(\frac{x}{a}\right)^2} + 2\frac{d}{a}\sqrt{1-\left(\frac{x}{d}\right)^2} - 2\frac{c}{a}\sqrt{1-\left(\frac{x}{c}\right)^2}, & \quad |x| \le c \end{cases} \tag{2.28}$$

As with the case of monotonic loading, the size of the new stick zone at the reversal of load is obtained from the overall equilibrium:

$$\frac{d}{a} = \sqrt{1-\left(\frac{Q_{max}-Q}{2fP}\right)} \tag{2.29}$$

Figure 2-5 depicts the variation of shear tractions at different values of Q, corresponding to points A, C, D, E and F of the fully reversed fretting cycle.

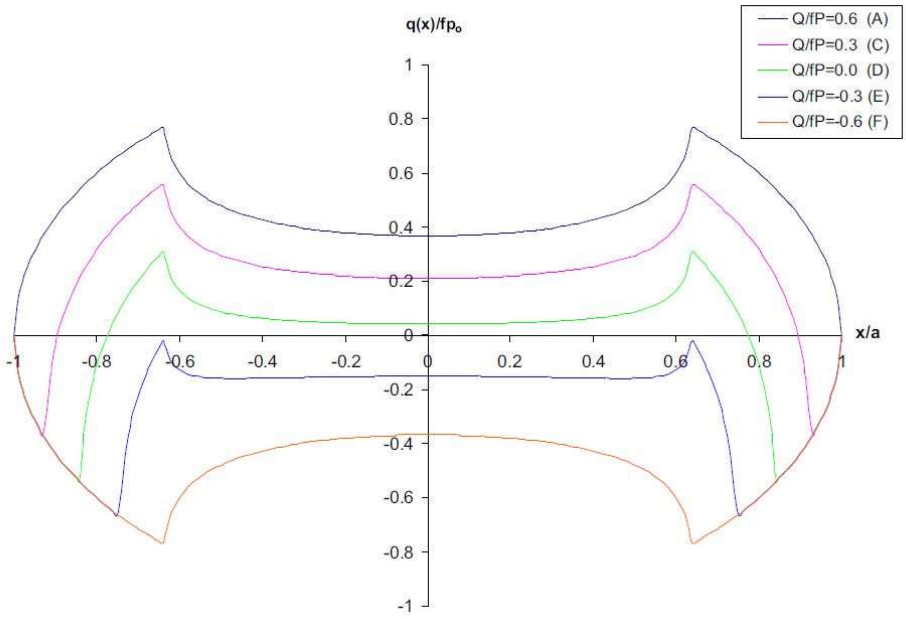

Figure 2-5: Variation of shear traction at different instants of the fully reversed fretting cycle. Q/fP varies from +0.6 to -0.6.

Effect of the bulk load: In the present work, a fretting-fatigue loading is considered and so the flat specimen is submitted to a bulk stress which modifies the classical Mindlin solution for the shear traction. This will be necessary as the bulk load will cause a strain in the specimen that is not present in the pads. This mismatch in strain caused an additional term in the tangential equation (2.8), and the resultant shear tractions will differ from those arising in pure fretting configuration. Nowell's experimental configuration is used to illustrate this situation (Figure 2-6).

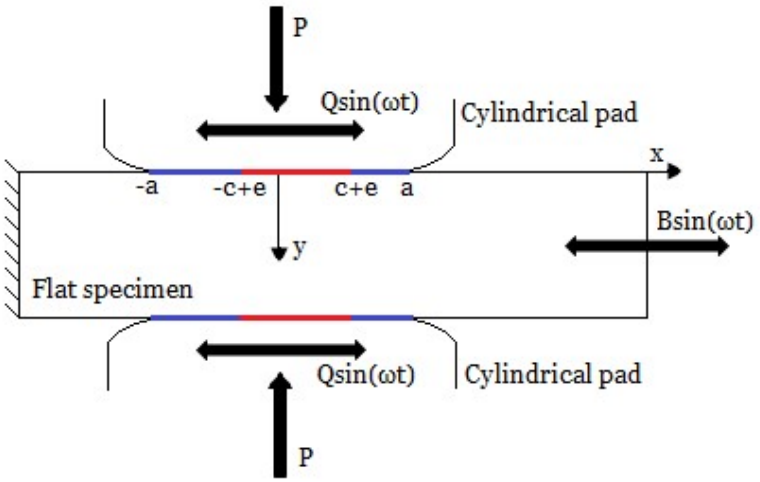

Figure 2-6: Schematic representation of the experimental contact configuration used by Nowell showing the coordinate system chosen for the analysis.

In this case, the partial derivative of the relative tangential displacement is no longer zero in the stick zones. The left hand side of the equation (2.8) can then be written in form of stress yields:

$$-\frac{\sigma_B}{4\pi} = \frac{1}{\pi}\int \frac{q(\xi)d\xi}{x-\xi} \tag{2.30}$$

The effect of the bulk stress, σ_B, is to offset the stick zone, which was centrally positioned in the absence of bulk stress. The domain of the perturbation in the full solution now becomes $|x-e| < c$ rather than the former symmetrical $|x| < c$, where e is the offset of the centre stick zone from the centre of the contact. Application of appropriate boundary conditions in and outside of the stick zone together with the integration of the equation (2.7) fix the value e:

$$e = \frac{\sigma_B a}{4 f p_0} \tag{2.31}$$

Thus the perturbation term for the shear traction becomes:

$$q'(x) = f p_0 \frac{c}{a}\sqrt{1-\left(\frac{x-e}{c}\right)^2} \qquad |x-e| < c \tag{2.32}$$

The solution developed above is satisfactory for moderate values of the bulk tension. If larger values of tension are applied, one edge of the stick zone will approach the edge of the contact. The current solution is therefore only valid for $e + c \leq a$.

Determination of the stress field for a fretting-fatigue loading

Once the surface traction has been determined, it is possible to evaluate the stresses in the specimen by superposing the effects of the normal pressure, the shear traction and the specimen bulk load using Muskhelishvili's potential theory (Muskhelishvili, 1953). For most of the stress components, it is possible to use a half-plane assumption in the computation of stresses due to the contact.

If the material remains elastic linear, the evaluation of the xx component of stress due to the normal load can be obtained with the superposition of the results for the elliptical tractions. Although, the shifted origins of the perturbations terms, *q'(x)* and *q"(x),* will have to be taken

into account. It is particularly worthy to note that four different combinations of superposition will be necessary to express the stress field at the maximum and minimum load, and during unloading and reloading. For instance, the normalised *xx* components of stress at each stages will be:

- At maximum load:

$$\frac{\sigma_{xx}(x,y)}{p_0} = \left(\frac{\sigma_{xx}^{n}\left(\frac{x}{a},\frac{y}{a}\right)}{p_0}\right) + f\left(\frac{\sigma_{xx}^{t}\left(\frac{x}{a},\frac{y}{a}\right)}{fp_0}\right) - f\frac{c}{a}\left(\frac{\sigma_{xx}^{t}\left(\frac{x-e}{c},\frac{y}{c}\right)}{fp_0}\right) + \sigma_B \qquad (2.33)$$

- During unloading:

$$\frac{\sigma_{xx}(x,y)}{p_0} = \left(\frac{\sigma_{xx}^{n}\left(\frac{x}{a},\frac{y}{a}\right)}{p_0}\right) - f\left(\frac{\sigma_{xx}^{t}\left(\frac{x}{a},\frac{y}{a}\right)}{fp_0}\right) + 2f\frac{d}{a}\left(\frac{\sigma_{xx}^{t}\left(\frac{x-e'}{d},\frac{y}{d}\right)}{fp_0}\right) - f\frac{c}{a}\left(\frac{\sigma_{xx}^{t}\left(\frac{x-e}{c},\frac{y}{c}\right)}{fp_0}\right) + \sigma_B \qquad (2.34)$$

- At minimum load:

$$\frac{\sigma_{xx}(x,y)}{p_0} = \left(\frac{\sigma_{xx}^{n}\left(\frac{x}{a},\frac{y}{a}\right)}{p_0}\right) - f\left(\frac{\sigma_{xx}^{t}\left(\frac{x}{a},\frac{y}{a}\right)}{fp_0}\right) + f\frac{c}{a}\left(\frac{\sigma_{xx}^{t}\left(\frac{x-e}{c},\frac{y}{c}\right)}{fp_0}\right) + \sigma_B \qquad (2.35)$$

- During reloading:

$$\frac{\sigma_{xx}(x,y)}{p_0} = \left(\frac{\sigma_{xx}^{n}\left(\frac{x}{a},\frac{y}{a}\right)}{p_0}\right) + f\left(\frac{\sigma_{xx}^{t}\left(\frac{x}{a},\frac{y}{a}\right)}{fp_0}\right) - 2f\frac{d}{a}\left(\frac{\sigma_{xx}^{t}\left(\frac{x-e'}{d},\frac{y}{d}\right)}{fp_0}\right) + f\frac{c}{a}\left(\frac{\sigma_{xx}^{t}\left(\frac{x-e}{c},\frac{y}{c}\right)}{fp_0}\right) + \sigma_B \qquad (2.36)$$

Where c is the half width of the stick zone, e is the offset of the centre of the stick zone from the centre of the contact, σ_{xx}^{n}, σ_{xx}^{t}, σ_B are the *xx* components of the stress due to the normal,

tangential and bulk loads respectively, and $\sigma_{xx}^{c}$is the stress correction for the finite thickness effect.

Similar formulations can be derived for the $\underline{yy}$ and xy components of stress at the same loading stages, and the zz components may be obtained from the other two direct stresses (plane strain condition). The function in brackets may be evaluated using Muskhelishvili's potentials (Muskhelishvili, 1953, Hills and Nowell, 1993).

Determination of the friction coefficient: Oxford's method

Previous study (Hills and Nowell, 1994) has shown that, due to the complexity of the loading for the fretting fatigue, the coefficient of friction is not constant under the contact surface. However, for this study a constant coefficient of friction will be assumed. One methodology used to determine the coefficient of friction is the method developed by Hills and Nowell (1994).

At the beginning of the experiment, the coefficient of friction, f_O, is uniform under the contact (Figure 2-7). It is the combination of stick and slip zone, which results from the fretting fatigue loading, which will raised a local coefficient of friction, f_s, within the slip zones (Figure 2-8).

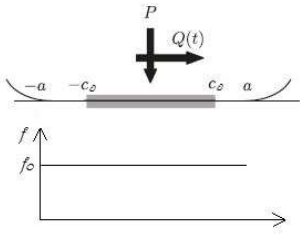

Figure 2-7: Coefficient of friction under the contact at the beginning of the experiment.

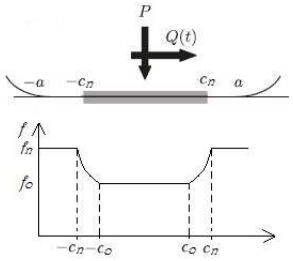

Figure 2-8: Coefficient of friction under the contact after n cycles.

It is assumed that the coefficient of friction $f(x)$ remains unknown in the interval $c_o \leq |x| \leq c_n$, but that it has to lie between f_o and f_s. The size of this stick zone is given by:

$$\frac{c_n}{a} = \sqrt{1 - \frac{Q}{f_s P}} \qquad (2.37)$$

When this step of the experiment is reached, the average coefficient of friction may be measured by stopping the fretting and increasing gradually the tangential force until sliding occurs. The value of the average coefficient of friction, f_m, is given by:

$$\frac{\pi a f_m}{4} = \int_0^{c_0} f_0 \sqrt{1-\left(\frac{x}{a}\right)^2}\,dx + \int_{c_0}^{c_n} f(x) \sqrt{1-\left(\frac{x}{a}\right)^2}\,dx + \int_{c_n}^{a} f_s \sqrt{1-\left(\frac{x}{a}\right)^2}\,dx \qquad (2.38)$$

which gives, after differentiation:

$$\frac{\pi a}{4}\frac{\partial f_m}{\partial n} = \frac{\partial f_s}{\partial n}\left[\frac{\pi}{4} - \frac{c_n}{2}\sqrt{1-\left(\frac{x}{a}\right)^2} - \frac{1}{2}sin^{-1}\left(\frac{c_n}{a}\right)\right] \qquad (2.39)$$

Then, the equation (2.38) may be rewrite as:

$$f_m = f_n - \frac{2}{\pi}\int_{f_0}^{f_s}\left[\frac{Q}{f_s P}\sqrt{1-\frac{Q}{f_n P}} + sin^{-1}\sqrt{1-\frac{Q}{f_s P}}\right]df_s \qquad (2.40)$$

In most fretting tests, the initial coefficient of friction is quite low. Hence, as the initial sliding may be anticipated, it may be assumed that $f_o = Q/P$ and the equation (2.40) becomes:

$$f_m = f_s - \frac{2Q}{\pi P}\left\{-2sin\alpha + 2ln\left[tan\left(\frac{\alpha}{2}+\frac{\pi}{4}\right)\right] + \frac{P f_s \alpha}{Q} - tan\alpha\right\} \qquad (2.41)$$

where:

$$\cos\alpha = \frac{Q}{f_s P} \qquad (2.42)$$

A graph of this function, with different value of Q/P is shown on the Figure 2-9. This graph may allow to determine the coefficient of friction of the material. However, it may be observed that for low value of Q/P, there is only a few difference of the value of the mean coefficient of friction, f_m, between two points. Then, it is better to use a coefficient Q/P > 0,2 to determine correctly f_s.

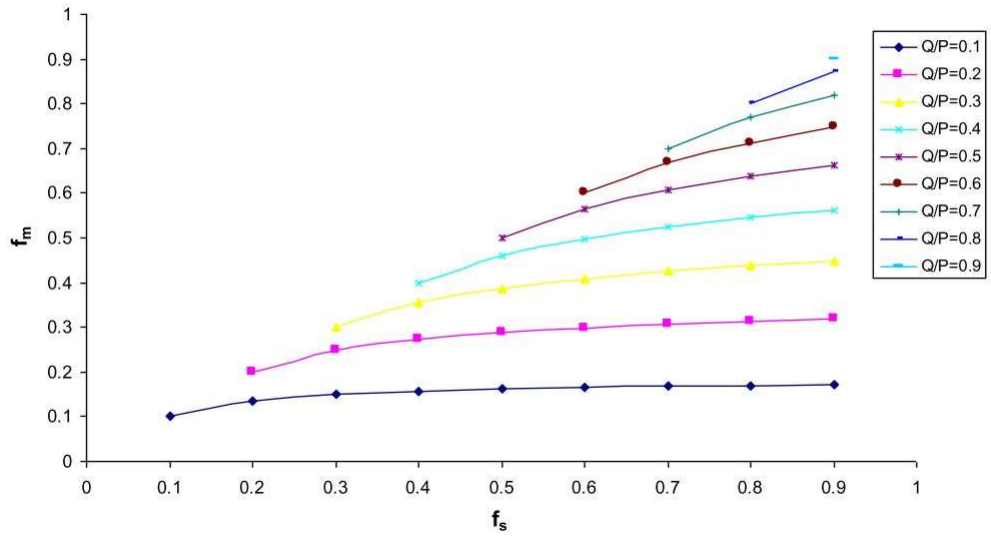

Figure 2-9: Prediction of the coefficient of friction within the slip zones measured from average values (Araújo, 2000).

For the sake of simplicity, a simplified contact geometry will be considered during this study: the cylinder-plane contact. For this kind of contact, an analytical formulation of the surface tractions exists and the stress field under the contact may be determined by using the Muskhelishvili potential's theory. This 2D analytical formulation of the contact problem will be coded using a Python script, after the determination of the coefficient of friction corresponding to our contact. This will allow a rapid computation of the stress field corresponding to the different experiments which will be realised.

2.3. Multiaxial fatigue

The fracture of materials under service conditions depends on many factors which will interact on each other's. Some of these parameters are listed below:

- Material properties and microstructure;
- Load frequency;
- Load amplitude;
- Loading ratio;
- Stress concentration;
- Stress multiaxiality;
- Scale of structural components;
- Environment;

- Temperature;
- Material defects;
- ...

Two regimes of fatigue can be observed: the Low Cycle Fatigue and the High Cycle Fatigue. In the first case, the structure experiences high levels of loads. Plastic deformations may be observed, due to that high level of forces, and the life is relatively short, under 10^5 cycles. In the other hand, for HCF, the level of solicitation stay low and elastic deformations are firstly observed. In that case, concepts of infinite life and fatigue limit stress may be defined. Usually, it will be considered that after 10^6 or 10^7 cycles the material will never break.

In order to deal with all the issues listed above, different criteria have been formulated. One of these criteria will be presented below, a criteria based on the critical plane.

The critical plane approach (Findley, 1959, Brown and Miller, 1973, Socie, 1987, Fatemi and Socie, 1988, and McDiarmid, 1991), to identify the fatigue strength estimated of a component, is really attractive from a mechanical point of view. This is because it will not only give the fatigue strength of the component, but it will also provide information about the location and the direction estimated for the crack initiation.

Cracks initiate in preferential material planes, usually associated with high shear stresses. However, the normal mean stress plays also a role on the mechanism. It will keep the crack faces open and makes easier their growth. The idea behind the critical plane method is therefore to find the plane which will experiencing the highest combination of some equivalent normal and shear stress. There are several method to compute the equivalents shear stress and normal stress. Dang Van (1973) and later Papadopoulos (1994) proposed that the equivalent shear stress is given by the radius of the minimum circle circumscribing the stress path. However, such a minimum circle does not exist for a non-convex polygonal stress path. Improvement of this method were proposed later, Li et al. (2000) considered the minimum ellipsoid enclosing the deviatoric stress path, but it may fails for some paths such as the rectangular ones, and Mamiya et al. (2002) proposed a new definition of the minimum ellipsoid based on its Frobenius norm and they observed that for elliptical paths this norm was easily computed from the axes of rectangular Hull. Based on this observation, Mamiya et al. (2009) proposed a new method: The Rectangular Hull.

Rectangular Hull Method

The Rectangular Hull Method, as proposed by Mamiya et al. (2009) in the deviatoric stress space and later by Araújo et al. (2011) on the material plane, is a method to compute the equivalent shear stress, τ_a, characterizing the fatigue damage under multiaxial loading. In the

first case, while working in the deviatoric space, some loading paths may need a rotation of the Hull around up to five axes, which will require an optimizing algorithm. This is no longer necessary if the Rectangular Hull Method is applied on the material planes. Indeed the rotation of the hull is done on the material plane and so a simple rotation in two dimensions is sufficient to calculate τ_a (Figure 2-10).

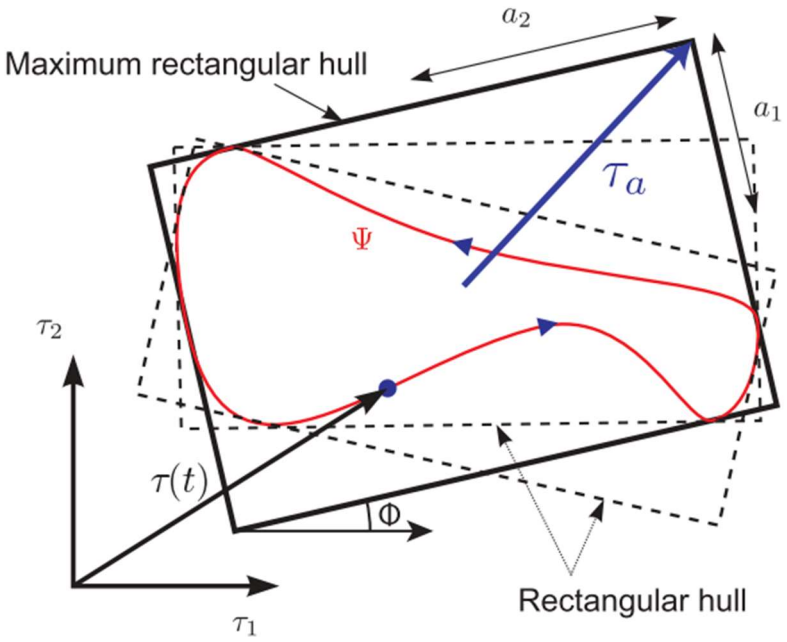

Figure 2-10: Stress path $\boldsymbol{\psi}$*, its convex hull and the identification of the characteristic lengths used to compute the shear stress amplitude in a material plane.*

Thus, the first step to find the equivalent shear stress amplitude on a material plane Δ is to compute the halves size of the sides of a rectangular hull $a_1(\varphi)$ and $a_2(\varphi)$:

$$a_i(\varphi) = \frac{1}{2}\left[\max_t \tau_i(\varphi, t) - \min_t \tau_i(\varphi, t)\right] \qquad i = 1,2 \qquad (2.43)$$

Then, for each φ-oriented rectangular hull, the amplitude of the equivalent shear stress may be defined as:

$$\tau_a(\varphi) = \sqrt{a_1^2(\varphi) + a_2^2(\varphi)} \qquad (2.44)$$

Finally, the equivalent shear stress which will be used is the one which maximises the equation (2.43):

$$\tau_a = \max_{\varphi} \sqrt{a_1^2(\varphi) + a_2^2(\varphi)} \qquad (2.45)$$

The Modified Wöhler Curve Method

This method developed by Susmel and Taylor (2003) is founded on the hypothesis that metallic materials have a linear, elastic, homogeneous isotropic behaviour. Then, damages due to the fatigue can be estimated with the modelling of the initiation and the propagation of the micro, or miso, cracks with the continuum mechanic.

Thus, the multiaxial High-Cycle Fatigue behaviour of metallic materials can be expressed with a relation between τ_a and $\sigma_{n,max}/\tau_a$. This MWCM can be formalised as follow:

$$I_{MWCM} = \tau_a(\phi^c, \theta^c) + \kappa \frac{\sigma_{n,max}}{\tau_a}(\phi^c, \theta^c) \leq \lambda \qquad (2.46)$$

where κ and λ are material constants. Susmel et al. (2005) proposed to obtain them using two fatigue strengths limits generated under different loading conditions. They are defined as:

$$\kappa = \frac{\sigma_{-1} - \sigma_0}{2} \qquad and \qquad \lambda = \sigma_{-1} - \frac{\sigma_0}{2} \qquad (2.47)$$

where σ_{-1} is the fatigue strength limit generated under fully reversed loading (R_σ=-1), and σ_0 is obtained under repeated uniaxial load (R_σ=0).

A proper procedure to define the critical plane is proposed by Araújo et al. (2011):

- Find the maximum shear stress amplitude among all material planes. As the cracks usually initiate at the boundaries of the contact, the computation will be made at the distance a (equation (2.18)) of the centre of the contact. Then, the stress tensor at this point should be extracted for all the time t of the period. This is usually made with a FEM computation. And finally, considering θ, the angle between a material plane and the normal to the surface. The method developed in the previous sub-section has to be applied to compute $\tau_a(\phi, \theta)$ on all the material planes. A double maximisation may then be carried out to get $\tau_a^{max}(\varphi, \theta)$:

$$\tau_a^{max} = \max_{\varphi,\theta}[\tau_a(\varphi, \theta)] \qquad (2.48)$$

- The candidates planes should be selected within a tolerance:

$$\tau_a^{max} - tol \leq \tau_a(\varphi, \theta) \leq \tau_a^{max} \tag{2.49}$$

- The critical plane is the plane among the candidates' planes where the maximum normal stress is maximized.

$$(\varphi^c, \theta^c) = \max_{\varphi^*, \theta^*} \left[\sigma_{n,max}(\varphi^*, \theta^*)\right] \tag{2.50}$$

As we have seen on the review of the state of the art, several multiaxial fatigue models exist on the literature, and may be divided into two main categories: the criteria based on stress invariants and the ones based on a critical plane approach. The non-linear nature of the friction at the contact interface make difficult the application of such models because the loading is likely to be non-proportional in the neighbourhood of the contact. Among all the critical plane approach, the one proposed by Susmel and Taylor (2003) presents the advantage to take into account the equivalent shear stress as well as the maximum normal stress for the determination of the critical plane, which is what motivated our decision to use this particular model.

2.4. Critical distance

There are three different ways to apply a force to allow a crack to propagate. Irwin (1958) proposed a classification corresponding to these situations, or fracture modes, represented in Figure 2-11. The mode I is connected to traction condition, with force normal to the crack plane. The mode II and III correspond to shearing type loading conditions. For the mode II, the shearing stress acts in parallel to the crack plane, while it acts in parallel to the crack tip for the mode III. Generally, a mixed mode situation can be observed, with a superposition of the modes. In the particular case of the cylinder/plane fretting fatigue configuration, cracks will propagate with a combination of mode I and II.

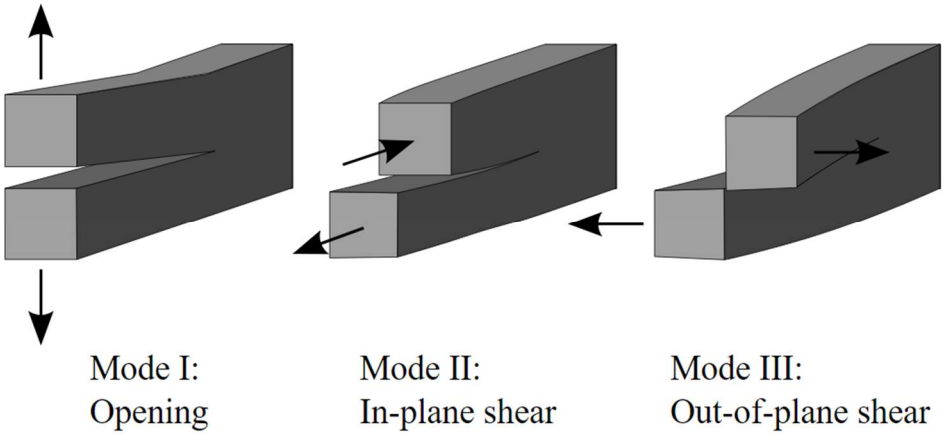

Figure 2-11: Illustration of the three propagation modes.

Stress Intensity Factor

Westergaard (1939) has found an Airy stress function that is the solution for the stress field in an infinite plane containing a crack under an equibiaxial loading (Figure 2-12). This exact solution, *Z(z)* is expressed as follow:

$$\frac{\partial Z^{\infty}}{\partial z} = S(z^2 - a^2)^{1/2} \tag{2.51}$$

where a is the semi-width of the crack.

Later, Irwin (1957) expressed this exact solution in local coordinate ($z = a + re^{i\theta}$) and gave the first order of the asymptotic expansion:

$$\sigma_{xx}(r,\theta) = \frac{S\sqrt{\pi a}}{\sqrt{2\pi r}} cos\frac{\theta}{2}\left(1 - sin\frac{\theta}{2}sin\frac{3\theta}{2}\right) \tag{2.52}$$

$$\sigma_{yy}(r,\theta) = \frac{S\sqrt{\pi a}}{\sqrt{2\pi r}} cos\frac{\theta}{2}\left(1 + sin\frac{\theta}{2}sin\frac{3\theta}{2}\right) \tag{2.53}$$

$$\tau_{xy}(r,\theta) = \frac{S\sqrt{\pi a}}{\sqrt{2\pi r}} cos\frac{\theta}{2}sin\frac{\theta}{2}cos\frac{3\theta}{2} \tag{2.54}$$

and he introduced the concept of the Stress Intensity Factor (SIF):

$$\begin{Bmatrix} K_I \\ K_{II} \\ K_{III} \end{Bmatrix} = \lim_{r\to 0} \sqrt{2\pi r} \begin{Bmatrix} \sigma_{xx}(r,0) \\ \tau_{yx}(r,0) \\ \tau_{yz}(r,0) \end{Bmatrix} \tag{2.55}$$

where σ_{xx}, τ_{yx} and τ_{yz} are the near crack tip stresses and K_I, K_{II} and K_{III} are associated with the three different crack opening modes (opening, shearing and tearing).

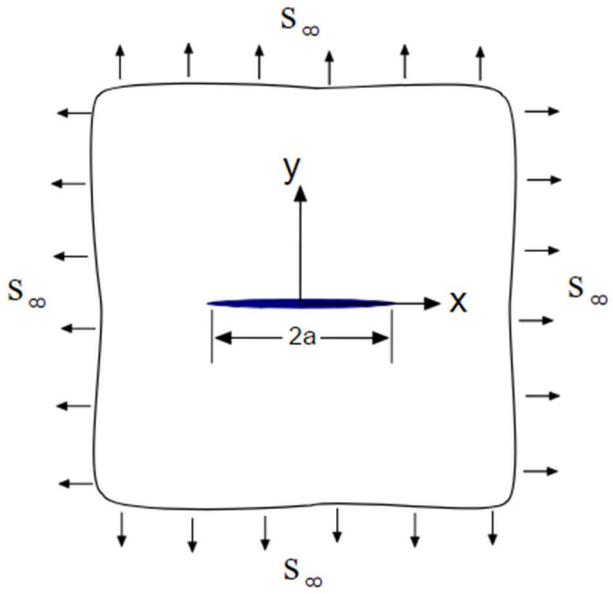

Figure 2-12: Crack in an infinite plane.

Critical distance theory

The first use of a critical distance theory was done by Neuber (1936, 1958) to predict the fatigue strength of notched components. He assumed that to represent the real stress damaging the fatigue process zone, the stress close to the stress raiser has to be an average of the stress distribution close to the stress concentration. He formalised this idea in terms of the so-called line method (LM) (Figure 2-13(b)). A few years later, Peterson (1959) suggested a simplify way to apply this theory by observing that it exists a reference stress which, while compared with the material plain fatigue limit, will indicate if the material would break or run out. The theory he proposed is that this reference stress may be computed at a given distance from the stress raiser. This distance being the critical distance computed with the point method (PM) (Figure 2-13(a)).

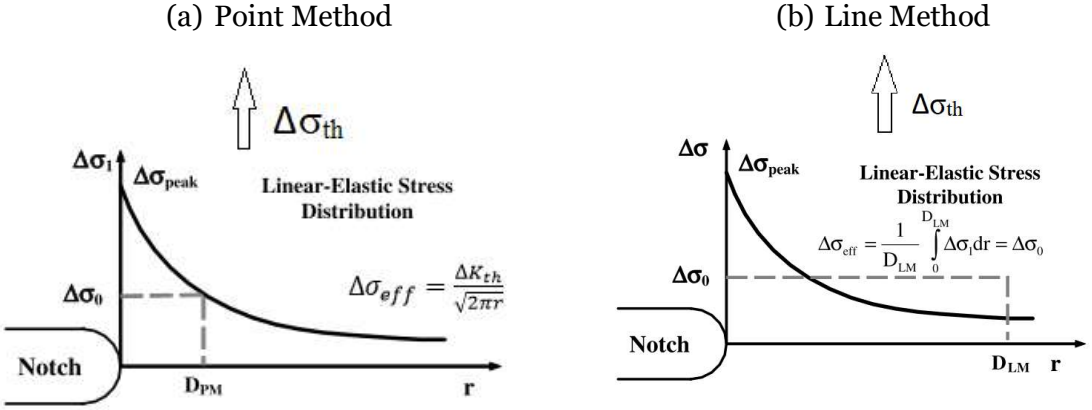

Figure 2-13: Schematic configuration of (a) the Point Method and (b) the Line Method [adapted from Susmel (2006)]

More recently, Taylor (1999) has generalised this theory for any kind of geometry with the Area Method, and expressed it as the Theory of Critical Distance (TCD). He formulated properly the idea developed by Peterson that the endurance occurs when the range of the maximum principal stress at the critical distance is inferior to the fatigue limit of the material, and he expressed this critical distance for fatigue problems as:

$$L = \frac{1}{\pi}\left(\frac{\Delta K_{th}}{\Delta\sigma_0}\right)^2 \qquad (2.56)$$

with ΔK_{th} the crack propagation threshold and $\Delta\sigma_0$ the fatigue limit of the material. Hence, under threshold conditions, a fracture mechanics test and a fatigue limit test can be used to extract the value of the critical distance for the considered material.

In the particular case of the PM, theoretical arguments (Taylor, 1999, Whitney and Nuismer, 1974, Tanaka, 1983) have shown that the critical distance l_{PM} is equal to $L/2$.

One of the most interesting aspect of the TCD is that it can be used in conjunction with any multiaxial fatigue criterion (Susmel and Taylor, 2006). However, as it has been demonstrated by Castro et al. (2009), the critical distance depends on the multiaxial fatigue model used.

The severity of the stress gradient for a fretting fatigue loading makes difficult the application of a local approach to predict the life of the samples. However, the use of the Point Method in conjunction with the MWCM have shown good prediction (Araújo et al., 2009) and is easy to be implemented. Hence it is the method which has been selected for this study.

2.5. Crack analogue

Non-conformal contact configurations submitted to fretting fatigue usually generate a strong stress gradient at the vicinity of the contact. Hence, the comparison between the crack tip and the contact's edge shows not only a geometric similarity (Figure 2-14), but also stress similarities as it has been demonstrated by Giannakopoulos (1998, 2000). Indeed, both configurations present a severe and located stress gradient. Consequently, it is possible to use a crack analogue model to study the fretting fatigue when the contact generates a stress singularity at the contact tip, but this analogy is limited to contact with limited friction zone, i.e. contact with sharp edges.

Based on this analogy and on the work of Pommier et al. (2007 and 2009) over the description of the mixed mode cyclic-elastic plastic behaviour at the crack tip, Montebello et al. (2016) take advantage of these similarities between crack and fretting fatigue to develop a nonlocal model which can be applied for non-negligible slip zone, as long as this slip zone is confined inside an elastic bulk.

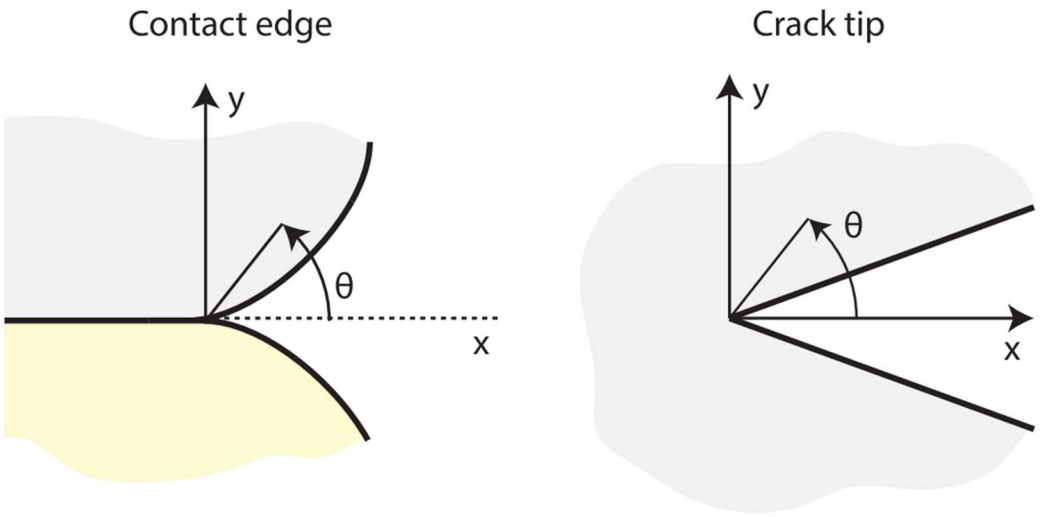

Figure 2-14: Geometrical similarities between the contact edge and the crack tip.

Representation of fretting fatigue characteristics.

The geometry that will be studied for this work is the classical cylinder against plane under partial slip conditions (Figure 2-15). The loading history is as follow: first a mean bulk load is applied to the specimen, then the cylindrical pad is pressed against it. Once the contact region is defined, the fretting and the bulk cyclic loads are applied in phase. Experimental evidences (Araújo et al., 2007 and 2012, Proudhon et al., 2007) have shown that, for this particular

configuration, cracks usually initiate at the vicinity of the contact edge. Moreover, a strong stress gradient occurs at this particular location. Consequently, the local geometry will impose the spatial distribution of the stress field and the macroscopic loads will induce the intensity of the mechanical field. To solve this problem, a "fracture mechanics" approach has been chosen through the decomposition of an approximate velocity field between reference fields and nonlocal intensity factors:

$$\boldsymbol{v}(\boldsymbol{x},t) \approx \underbrace{\dot{I}^{s}(t)\boldsymbol{d}^{\boldsymbol{s}}(\boldsymbol{x}) + \dot{I}^{a}(t)\boldsymbol{d}^{\boldsymbol{a}}(\boldsymbol{x})}_{\boldsymbol{v}^{e}} + \underbrace{\dot{I}^{c}(t)\boldsymbol{d}^{\boldsymbol{c}}(\boldsymbol{x})}_{\boldsymbol{v}^{c}} \tag{2.57}$$

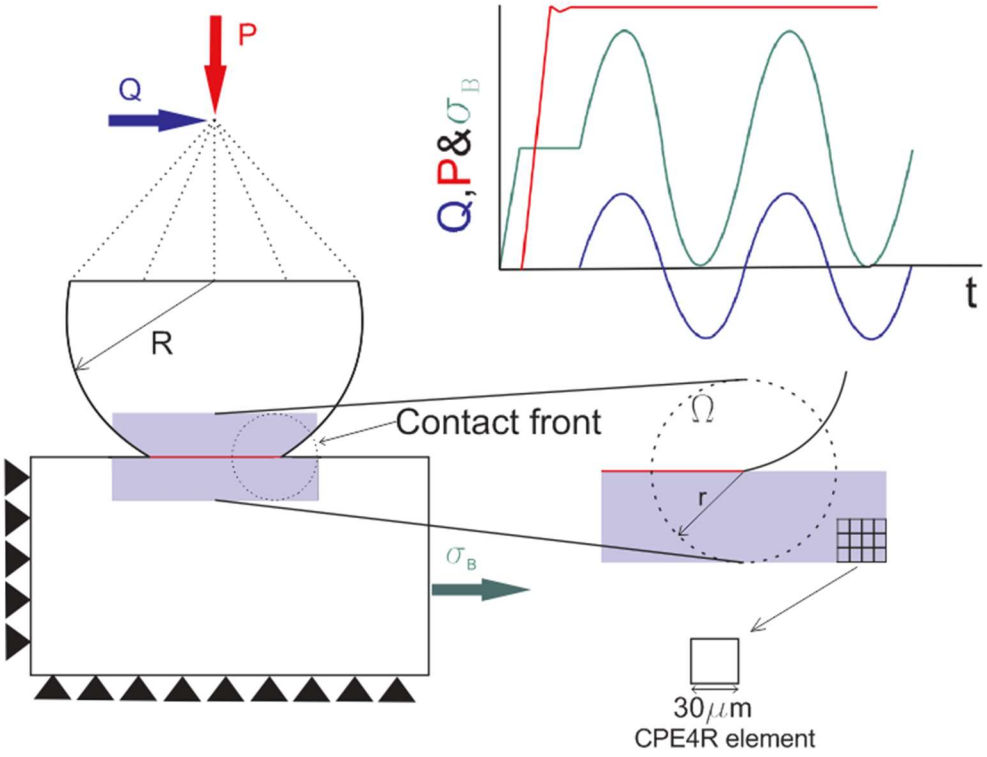

Figure 2-15: FEM details and loading evolution used.

This approximate velocity field is extracted with respect to a reference system attached to the crack tip (Figure 2-14). The first part of the equation, $\boldsymbol{v}^{e}$, corresponds to the linear elastic response of the material and the second part, $\boldsymbol{v}^{c}$ to the non-linear contributions due to friction. The reference fields, ($\mathbf{d}^{s}$, $\mathbf{d}^{a}$, $\mathbf{d}^{c}$), can also be identified, being $\mathbf{d}^{s}$, $\mathbf{d}^{a}$ and $\mathbf{d}^{c}$ their symmetrical, anti-symmetrical and complementary parts, respectively. It is defined by the local geometry and forms the orthonormal basis of the approximate velocity field. This is a moving reference

frame, which is attached to the contact front. The nonlocal intensity factors; I^s, I^a and I^c are independent variables, which are defined by the macroscopic loads.

The equivalent velocity field is extracted through a Finite Element Analysis (FEA). Only the nodes within the circular region, Ω, centred at the contact edge (Figure 2-15) are analysed. For the FEA, this circular region is defined by a radius r such that r/R < 0.1; being R the radius of the cylindrical pads. Close to the surface, the region is characterized by a mesh size (S_M in mm) which depends on the size of the contact and on the number of nodes (M_P) implemented for each part by the user:

$$S_M = \sqrt{\frac{0{,}5\pi a^2}{N_P}} \tag{2.58}$$

with CPE4R elements to describe the stress gradient evolution. The choice of this particular mesh allows to have a relatively fast implicit analysis with the software Abaqus. The contact has been modelled with the Lagrange multipliers technique and the Coulomb's friction law was employed to handle the relative slip. Among the techniques available in Abaqus^{tm}, these were the ones which proved to present the best correlation with the analytical solution for this configuration (Montebello et al., 2016).

Once the finite element computation has been concluded, the approximate velocity field can be extracted at each mesh node for all the simulation time steps. It has been observed that the bulk fatigue stress, σ_B, has an effect on both the symmetric field (corresponding to the mode I crack opening) (Figure 2-16(c)); and the anti-symmetric field (corresponding to the mode II crack opening) (Figure 2-16 (c)); while the normal load, P, only influenced the symmetric field and the fretting load, Q, the anti-symmetric one. Hence, it can be considered that the symmetric and anti-symmetric reference fields are generated by the normal and the fretting loads, P and Q respectively. Even if during the particular fretting fatigue load studied here the contact is mainly under stick-slip conditions, these fields should be extracted in the particular condition of complete stick. Indeed, during this particular condition, the two bodies behave as one, and the crack analogy may be applied. This also allows to separate the linear elastic response from the nonlinear contributions of the friction. An additional complementary term,$\boldsymbol{d^c}(\boldsymbol{x}, t)$, may be computed during the partial slip regime to take into account the non-linear contribution of the complete cycle of the loading. Montebello et al. (2016), have shown that this term decreases exponentially and can be neglected out of the friction area.

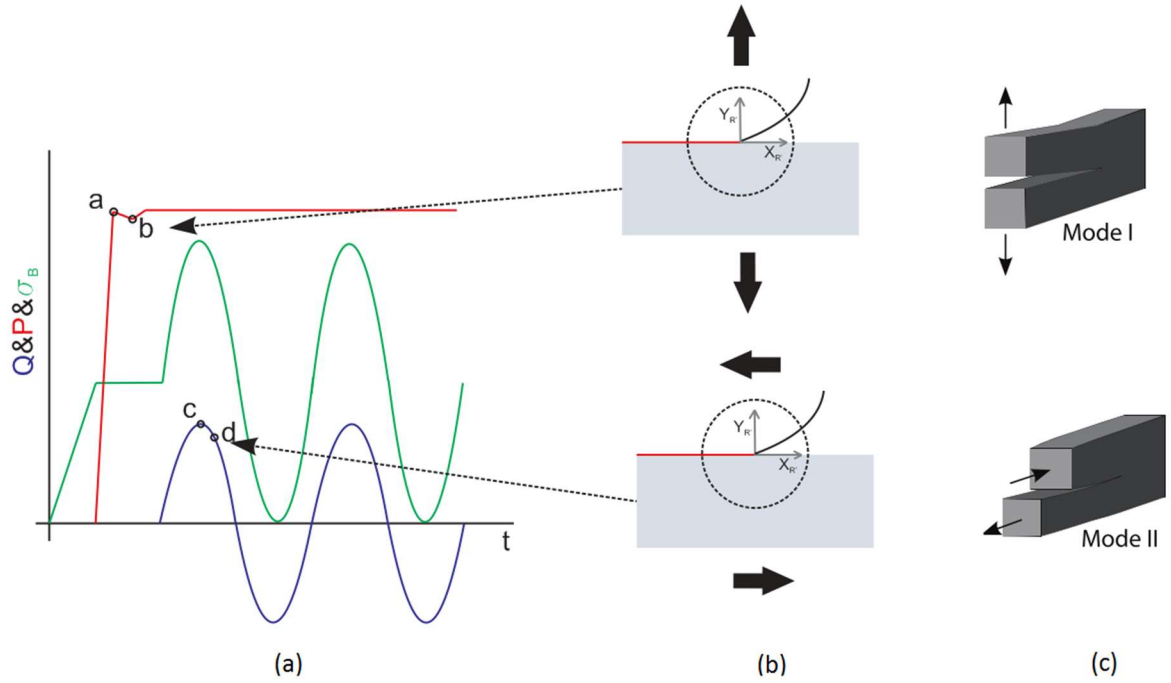

Figure 2-16: (a) Loading history, (b) Contact configuration, (c) schemes of modes I and II cracks.

Figure 2-16 (a) illustrates a typical loading path found in fretting fatigue tests. As the normal load is constant, in order to compute the symmetric velocity field, $\boldsymbol{d^s}$(equation (2.59)), associated with such a load, it is necessary to artificially generate a small variation, ΔP, on it from point a to point b in Figure 2-16 (a). Similarly, a variation ΔQ (from point c to point d) allow us to extract the anti-symmetric reference field $\boldsymbol{d^a}$ (equation (2.60)).

$$\boldsymbol{d^s}(\boldsymbol{x},t) = \frac{\boldsymbol{x}(t_b) - \boldsymbol{x}(t_a)}{t_b - t_a} \tag{2.59}$$

$$\boldsymbol{d^a}(\boldsymbol{x},t) = \frac{\boldsymbol{x}(t_d) - \boldsymbol{x}(t_c)}{t_d - t_c} \tag{2.60}$$

Where $\boldsymbol{x}(t_a)$, $\boldsymbol{x}(t_b)$, $\boldsymbol{x}(t_c)$ and $\boldsymbol{x}(t_d)$ are the positions of a node in the time instants t_a, t_b, t_c and t_d. Then, the reference fields are expressed in polar coordinates and a Karhunen-Loeve decomposition (Karhunen, 1946) gives an expression of the fields as a product of f(r) and g(θ). The comparison of the radial and tangential evolutions of $\mathbf{d^s(x)}$ and $\mathbf{d^a(x)}$ and the evolution of the displacement field at the crack tip (respectively for modes I and II) proved to correlate well (Montebello et al., 2016). This validates the crack-tip analogy.

$$\boldsymbol{d^s}(\boldsymbol{x},t) \rightarrow \boldsymbol{d^s}(r,\theta) \sim f^s(r)\boldsymbol{g^s}(\theta) \tag{2.61}$$

$$\boldsymbol{d^a}(\boldsymbol{x},t) \rightarrow \boldsymbol{d^a}(r,\theta) \sim f^a(r)\boldsymbol{g^a}(\theta) \tag{2.62}$$

Finally, the projection of the reference fields on the velocity field, **v**(**x**,t), gives the expression of the symmetric and anti-symmetric parts of the nonlocal parameters. Considering an analogy with the Linear Elastic Fracture Mechanics approach, I^s and I^a provide a measure of the magnitude of the velocity/displacement/stress field around the contact edge under normal and shear load modes (Figure 2-16 (b)), just as K_I and K_{II} do for Mode I and Mode II cracks (Figure 2-16 (c)).

$$\dot{I}^s(t) = \frac{\int_\Omega \boldsymbol{v}\boldsymbol{d}^s}{\int_\Omega \boldsymbol{d}^s\boldsymbol{d}^s} \rightarrow I_t^s = \frac{\sum_i^M \boldsymbol{v}_{i,t}\boldsymbol{d}_i^s}{\sum_i^M \boldsymbol{d}_i^s\boldsymbol{d}_i^s} \tag{2.63}$$

$$\dot{I}^a(t) = \frac{\int_\Omega \boldsymbol{v}\boldsymbol{d}^a}{\int_\Omega \boldsymbol{d}^a\boldsymbol{d}^a} \rightarrow I_t^s = \frac{\sum_i^M \boldsymbol{v}_{i,t}\boldsymbol{d}_i^a}{\sum_i^M \boldsymbol{d}_i^a\boldsymbol{d}_i^a} \tag{2.64}$$

Hence, the expression of the elastic part of the approximation of the velocity field is obtained:

$$\boldsymbol{v}^e(\boldsymbol{x},t) = \dot{I}^s(t)\boldsymbol{d}^s(\boldsymbol{x}) + \dot{I}^a(t)\boldsymbol{d}^a(\boldsymbol{x}) \tag{2.65}$$

In the following of this study, it is suggested the hypothesis that the elastic nonlocal intensity factors (I^s, I^a) are sufficient to characterize the contact edge because the nonlinearity is constrained inside an elastic bulk. Then, the methodology to obtain the complementary part of the approximation of the velocity field will not be explained.

Application of the model to a multiaxial criterion

To isolate the safe from the failure zone, it is interesting to apply a multiaxial fatigue criterion to the nonlocal parameters. A multiaxial fatigue model was chosen to take into account the particularity of the present loading. Moreover, a model which deals with the effect of the stress gradient and of the mean stress will yield better results. The methodology suggested by Araujo et al. (2007) seems to contain all those characteristics.

This model consists of an association between the Theory of Critical Distance with the Modified Wöhler Curve Method. It relies on the assumption that all the physical mechanisms which lead to crack initiation are confined into a so-called critical volume and the characteristic length of this volume, the critical distance, *L/2*, is independent of either the stress

concentration feature or the complexity of the stress field as it has been defined by Taylor (1999):

$$L = \frac{1}{\pi}\left(\frac{\Delta K_{th}}{\Delta \sigma_{-1}}\right)^2 \tag{2.66}$$

Considering this method, the principal mechanisms leading to the crack initiation are the equivalent shear stress amplitude, τ_a, and the maximum normal stress in the critical plane, $\sigma_{n,max}$:

$$I_{MWCM} = \tau_a + \kappa \frac{\sigma_{n,max}}{\tau_a} \leq \lambda \tag{2.67}$$

τ_a is determined using the Maximum Rectangular Hull Method (Figure 2-10), κ and λ are the material parameters:

$$\kappa = \tau_{-1} - \frac{\sigma_{-1}}{2} \qquad \lambda = \tau_{-1} \tag{2.68}$$

To apply this model to the nonlocal method, it is necessary to express the stress tensor in terms of nonlocal parameters. To do so, two observations can be made. Firstly, the stress field evolution may be split between the symmetric and the anti-symmetric parts:

$$\sigma_{i,j}(x,t) = I^a(t)\sigma^a_{i,j}(x) + I^s(t)\sigma^s_{i,j}(x) \tag{2.69}$$

Secondly, the crack analogy allows to express the stress tensor in terms of the stress intensity factor. For the sake of simplicity, in the equations that will follow $K = K_I = K_{II} = 1MPa\sqrt{m}$. The unitary value comes from the fact that the reference fields are normalized in order to correspond to the displacement field obtained at the crack tip during an elastic loading phase characterized by a stress intensity factor equal to 1.

$$\sigma(t) = -\frac{K}{4\sqrt{\pi r}}\begin{bmatrix} I^s + 3I^a_{max}\sin(\omega t) & -(I^s + I^a_{max}\sin(\omega t)) & 0 \\ -(I^s + I^a_{max}\sin(\omega t)) & I^s + 3I^a_{max}\sin(\omega t) & 0 \\ 0 & 0 & 4(I^s + I^a_{max}\sin(\omega t)) \end{bmatrix} \tag{2.70}$$

Once this expression is obtained, the Rectangular Hull Method (Figure 2-10) may be applied to calculate the equivalent shear stress amplitude and find the critical plane at the

critical distance; then, the maximum normal stress to this plane. In terms of nonlocal stress intensity factors, such variables can be expressed as:

$$\tau_a = \frac{I^a_{max} K}{2\sqrt{2\pi \frac{L}{2}}} \qquad \sigma_{n,max} = \mathrm{K}\frac{\left(-2+\sqrt{2}\right) I^s + 2I^a_{max}}{4\sqrt{\pi \frac{L}{2}}} \tag{2.71}$$

To find the boundary between the safe and the failure zone, the expression of I^a_{max} to get the equality of the equation (2.67) has to be found. There are two values of I^a_{max} which respect this condition:

$$I^a_{max,1} = 2\frac{\Delta K_{th}}{K}\frac{\tau_{-1} - \sqrt{2}\kappa + \sqrt{\left(\tau_{-1} - \sqrt{2}\kappa\right)^2 - 2\frac{K}{\Delta K_{th}}\sigma_{-1}\kappa(1-\sqrt{2})I_s}}{\sigma_{-1}}$$
$$I^a_{max,2} = 2\frac{\Delta K_{th}}{K}\frac{\tau_{-1} - \sqrt{2}\kappa - \sqrt{\left(\tau_{-1} - \sqrt{2}\kappa\right)^2 - 2\frac{K}{\Delta K_{th}}\sigma_{-1}\kappa(1-\sqrt{2})I_s}}{\sigma_{-1}} \tag{2.72}$$

However, the result obtained for $I^a_{max,2}$ is negative and so does not respect physical conditions for crack initiation. Then, the complete expression that defines the boundary between the safe and the failure zones corresponds to $I^a_{max,1}$.

In this study a shear stress based model was chosen because crack initiation in ductile materials is usually associated with the formation of persistent slip bands, hence the amplitude of the shear stress should play a major role in this process. The contribution of the maximum normal stress to the crack initiation process depends on material and loading conditions. In order to conduct a comparative study two scenarios will be considered. First, the expression which defines the boundary between the safe and the failure zone will be determined considering all the forces which happened during the fretting fatigue process (equation (2.72)). Then, the contribution of the maximum normal stress will be discarded (equation (2.73)), and so the contribution of the maximum normal stress for this specific study will be highlighted.

$$I^a_{max} = 2\frac{\Delta K_{th}}{K}\frac{\tau_{-1}}{\sigma_{-1}} \tag{2.73}$$

The nonlocal model proposed by Montebello (2015) is really interesting for an industrial point of view. Indeed, it is easy to be implemented in an Abaqus environment and allows fast computations for complex geometries. However, there is no fully validation of the model for fretting fatigue experiments, even not for simple geometry such as cylinder-plane contact.

Chapter 3. Material and methods

3.1. Introduction

The crack analogue model proposed by Montebello et al. (2016) to estimate crack initiation threshold under fretting fatigue conditions is, in principle, capable to deal with the stress gradient problem. However, to apply this kind of model to the aeronautical industry further assessment considering specific materials and loading conditions are necessary. For instance, in the fan blade root/disc assembly of aeroengines Ti-6Al-4V is the material to be considered. The load history in such an assembly involves not only normal and shear loads at the contact interface but also a remote fatigue load generated in the blade (by the centrifugal force) and in the disc (by the circumferential stress due to its rotation). One should notice that the validation of the crack analogue model for the Ti-6Al-4V data was essentially conducted for data under pure fretting loading conditions (Montebello et al. 2016), without the presence of a time varying bulk fatigue load. Therefore, one of the objectives of this experimental campaign is to study the accuracy of such model under this more realistic and challenging loading conditions. Additionally, to further exploit the capability of this model to deal with the stress gradient phenomenon a set of tests was designed with three different pad radii (20 mm, 50mm and 70mm). These tests were denominated Group I Tests.

A second set of tests, Group II Tests, was also proposed in this work to study aspects related to the size effect in fretting fatigue. As previously seen in the literature review, few works were carried out with this objective and most of these were either related to stress gradient problems (Bramhall, 1973, Nowell, 1988) or were applied to consider tribological issues (Fouvry et al., 2013) rather than mechanical ones. Thus, a new experimental protocol has been here designed to tackle this problem. The tests will focus on the effect of two size parameters on the fretting fatigue life/strength: the width of the specimens and the size of the slip area within the contact zone. As far as the width of the specimen is concerned, the hypothesis to be verified is whether the volume of material being stressed under the contact plays a role in the fretting fatigue resistance keeping all the other relevant test parameters constant. Similar hypothesis needs to be checked but varying now the size of the superficial damaged area within the slip zones from test to test, but with all the other tests parameters kept constant. Again, the material considered in these tests will be the Ti-6Al-4V alloy.

In this chapter the details on the common material and methods applied to conduct these two Groups of Tests will be provided. The specific loads applied for each configuration within Test Groups I and II and their resultant fretting lives will be reported in Chapters 4 and 5, respectively.

3.2. Titanium alloy

Titanium alloys are commonly used for aeronautical engineering because of their interesting properties (high mechanical properties to weight ratios, excellent corrosion resistance and seawater fatigue strength regarding to its low density). In this section, the specific characteristics of the titanium alloy used by Safran Aircraft Engines to manufacture the blades and disks of an aero engine will be studied. The fabrication process, which plays a major role for the characterisation of the microstructure and, hence, the fatigue properties of the Ti-6Al-4V, will also be detailed.

Generality on the titanium alloy used

The characteristics of the Ti-6Al-4V are due to the balance presence of α and β phases (Figure 3-1). The α-stabiliser, aluminium representing around 6% of the mass, allows to increase mechanical strength and creep resistance. The β-stabilizer, vanadium with around 4% of the mass, increases the ductility at low temperature but decreases the oxidation resistance. The composition of the Ti-6Al-4V used by Safran is listed in the Table 3-1. The presence of these phases are due to the particular process implemented to form the alloy.

Elements	Al (%)		V (%)		O (ppm)		H (ppm)	
	Min	Max	Min	Max	Min	Max	Min	Max
Specified	5.5	6.75	3.5	4.5	-	2000	-	100
measured								

Table 3-1: Principal elements of TI-6Al-4V alloys manufactured for the Safran Snecma fan disc and blade.

.

This manufacturing process starts with the melting of the purified titanium with the stabilizer, here the aluminium. For the discs and the blades of aeroengines, Ferré (2013) explains that the material is first submitted to a vacuum induction melting and then to three vacuum arc remelting. Those processes avoid the formation of oxides and ensure the homogeneity of the alloy.

Thermo-mechanical treatment is then applied to the Ti-6Al-4V. The first stage is usually a forge of the raw alloy in the β domain. In Safran this forge is operated at 940°C and allows to reduce the β grain size. Then, a hot isostatic pressing is applied in the α+β domain.

Another treatment is also applied to make appear the grain in phase α and a quenching to transform the β phase into a metastable α' phase. Finally, an annealing process around

700°C is conducted to transform the α' phase into a lamellar α+β grain, constituted of α_s platelets in a β matrix.

The β-transus temperature of the Ti-6Al-4V is around 1000°C and it can be noted that all the temperatures used during the manufacturing process are lower than this. It is this particularity which allows the control of the microstructure final part. As highlighted by Crupi et al. (2017), the microstructure obtained here, with α grains embedded in a matrix of α and β lamellae, has better mechanical properties and fatigue resistance than the microstructure obtained by considering temperature higher than the β-transus one for the Ti-6Al-4V. This has also been observed by other authors (e.g., Le Baviant et al. 2002).

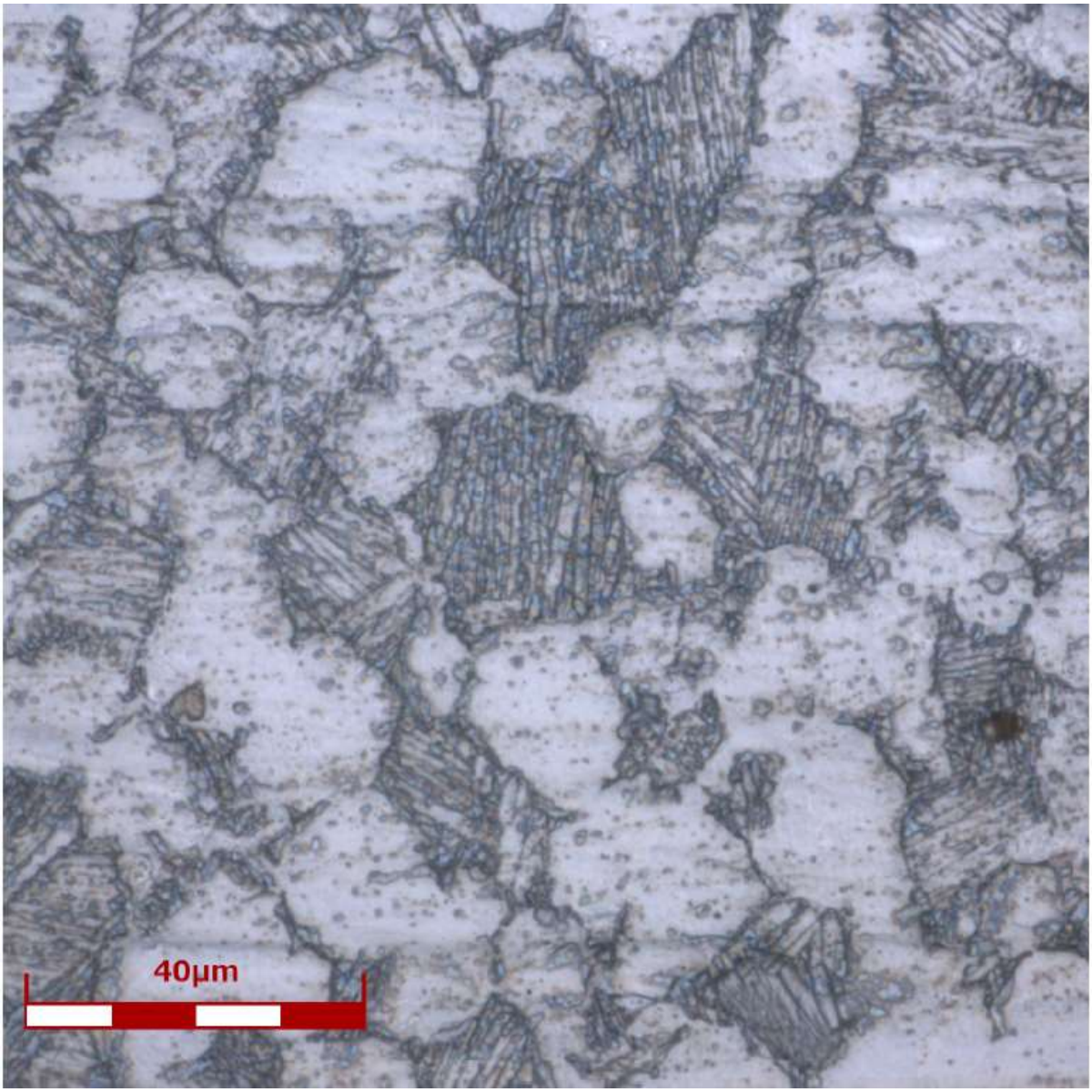

Figure 3-1: Microstructure of the Ti-6Al-4V alloy used.

Material properties observed in the literature

In most of the cases, the Ti-6Al-4V alloy used in industry presents the same bimodal microstructure, an equiaxed α_p and transformed β-grains. Table 3-2 reports some essential mechanical properties for such an alloy. This table provides values for the amplitude of the fatigue limit under fully reversed loading, σ_{-1}, amplitude of fatigue limit for stress ratio R_σ=0.1, $\sigma_{0,1}$, threshold stress intensity factor range, $\Delta K_{th,R=0,1}$, Young´s modulus, E, Poisson´s coefficient, υ, yield stress, $R_{p0.2}$, and ultimate tensile strength, σ_u. However, depending on the manufacturing parameters, such as the temperature, the pressure, cooling rate, surface treatment, etc, the microstructure and mechanical properties of this alloy may significantly vary (Oberwinkler et al., 2010, Stoschka et al., 2009, Wu et al., 2013). For instance, in Table 3-3 one can find values of the fatigue strength, in terms of maximum stress, $\sigma_{max} = \sigma_a + \sigma_m$, for different lives ($10^5$, 10^6, 10^7) and provided by different studies available in the literature. All the tests were performed at room temperature, in air and under uniaxial loading conditions with a sine wave on unnotched specimens.

Material	σ_{-1} (MPa)	$\sigma_{0,1}$ (MPa)	$\Delta K_{th,R=0,1}$ (MPa.m$^{1/2}$)	E (GPa)	υ	$R_{p0.2}$ (MPa)	σ_u (MPa)
Ti-6Al-4V	382 (10^6)	276 (10^6)	4.5	120	0.29	910	980

Table 3-2: Material properties of the Ti-6Al-4V studied.

Reference	Ratio of α_p-grain in %	Average size of α_p-grain in µm	Frequency in Hz	Stress ratio	HCF Fatigue limit σ_{max} (MPa)		
					10^5	10^6	10^7
Nalla et al. 2002	64	20	25	0.1	700	600	540
Zuo et al. 2008a.				0.5	850	780	640
Nagai et al. 1993	55	10	20 000	-1		546	518
		4	20	0 .01	800	720	640
		4			800	720	690
		2.8			800	740	720
				-1	588	547	539
Peters et al. 1984	6	80	-1	710	675	675	
Bellows 1999	60	13	60	-1	450	400	390
				0.1	667	611	556
				0.5	860	800	640
				0.8	950	920	900
Hines and Lutjering 1999	35	7.5	90	-1	545	470	445
Ivanova et al. 2002	60.5	8	30	0.1			467
	24.8	8.5			830 (3.10^4)	620 (2.10^6)	550
Nalla et al. 2003	64	20	5	-1	450		
ZUo et al. 2008b	55	10	25	-1	570	530	
Ivanova et al. 1999	60.5	8	30	-1	462	441	414
	24.8	8.5			455	421	407
	28.7	5.5			510	497	490
	60.5	8		0.1	720	582	491
	24.8	8.5			720	613	551
	28.7	5.5			798	751	720
Lanning et al. 2005				-1		482	
				0.1		591	
Araújo et al. 2007	65	5		0		596 ($1.4.10^6$)	
				-1		325 ($1.4.10^6$)	
Ferré 2013 ; Mériaux 2010	60	30		-1	593.97		
Delahaye 2014				-1	630 (2.10^5)	583 (2.10^6)	
Moshier et al. 2001	60	20					
Le Baviant et al. 2002	50	15					
Lee and Mall 2004a.	60	10					
Bantounas et al. 2010	80	15					

Table 3-3: Literature review of bimodal macrostructure parameters and HCF data of Ti-6Al-4V titanium alloy.

It exists a strong variation between the fatigue properties observed in the literature for the Ti-6Al-4V alloy. This may be explained by the variability of the microstructure resulting from the thermos-mechanical treatments. Moreover, test conditions and surface preparations of the pads and specimens also affect the fatigue limits. In this work, we will use the values determined by Bellecave (2015) which have shown a good correlation with the theory of the critical distance for the Ti-6Al-4V used. For a life of 106 cycles the fatigue limits adopted will be:

σ_{-1} = 382 MPa, $\sigma_{0,1}$ = 276 MPa.

3.3. Group Tests

Group I tests

As previously mentioned, the experimental work carried out during this thesis was divided into two groups. The first group of experiments has the objective to test the ability of the crack analogue model detailed in section 2.5 to deal with the gradient effect encountered in fretting-fatigue.

In order to generate different gradients, a variation of the pad radius will be considered. Indeed, when the peak pressure p_o, the ratio σ_{fa}/p_o and the ratio Q_a/fP are constant, the different radii of the pads will not affect the magnitude of the stress at the surface, but will produce different stress decays with distance from the surface (Figure 3-2). Indeed, from the equations (2.17) and (2.18), it follows that p_o is proportionate to $\sqrt{P/R}$ and a to $\sqrt{PR}$.

In the framework of the COGNAC's project, a previous experimental work with Ti-6Al-4V alloy was carried out, under fretting fatigue loading conditions, by Bellecave (2015) at the University of Brasilia. The configuration of his experimental campaign was based on cylindrical fretting pads, with radii of 20mm and 70mm, loaded against a flat specimen. Both pads and specimen had a width of 13mm. Experimental results of this work were obtained by maintaining the stress state constant at the surface while varying the pad radius. The aim of Bellecave's experimental work was essentially to validate a T-stress based methodology to estimate short crack arrest in fretting fatigue. Tests with the same stress magnitude at the surface but with different stress gradients would produce different fatigue lives. Therefore although these tests had the same severity at the surface some would break because a reasonable level of stress could be sustained for a certain distance, while others would last "forever" (Run-out conditions defined at 1 000 000 cycles) as short initiated cracks would rapidly grow into a zone of low stresses, due to the strong stress gradient, and hence become

dormant. Some of these experimental results were used for the present study, but the theoretical analysis conducted is totally different.

Indeed, another approach of the gradient effect was used. A variation of the pad radius was still considered, but among the experimental parameters, only the peak pressure p_o has been maintained constant. New ratios σ_{fa}/p_o and Q_a/fP have been sought in order to obtain the same magnitude of the multiaxial index, in the sense of the Modified Wöhler Curve Method (I_{MWCM}), at the critical distance, computed with the Point Method ($L/2$), for the different radii of the pads (Figure 3-3 (a)).

Then, according to the Modified Wöhler Curve Method (MWCM) applied in conjunction with the Theory of Critical Distance (TCD), if different experiments have the same magnitude of the multiaxial index at the critical distance, the same fretting fatigue life is expected (Figure 3-3 (b)).

Finally, the aim of the Group I Tests is to verify the ability of the crack analogue model presented in section 2.5 to take into account this gradient effect. To do so, the nonlocal stress intensity factors, I^s and I^a, are computed for all the loading and geometrical configurations and they are plotted in the I^s-I^a map. If this gradient effect is well incorporated by the model, the experimental results having similar lifetimes are supposed to be correlated in such a nonlocal map (Figure 3-3 (c)).

To achieve this objective, one took advantage of some experimental results carried out by Bellecave (2015). Indeed, in his work, experimental data obtained with the same Ti-6Al-4V are available for pad radii of 20mm and 70mm. Therefore, to validate the crack analogue model considered, complementary fretting fatigue tests were carried out using a cylindrical fretting pad with radius of 70mm, and new data were obtained with a pad radius of 50mm. Details about the strategy to determine the loads applied in these tests are provided in the section 4.2. The actual shape and dimensions of both specimen and pads used for this analysis are available in Figure 3-4 and Figure 3-5.

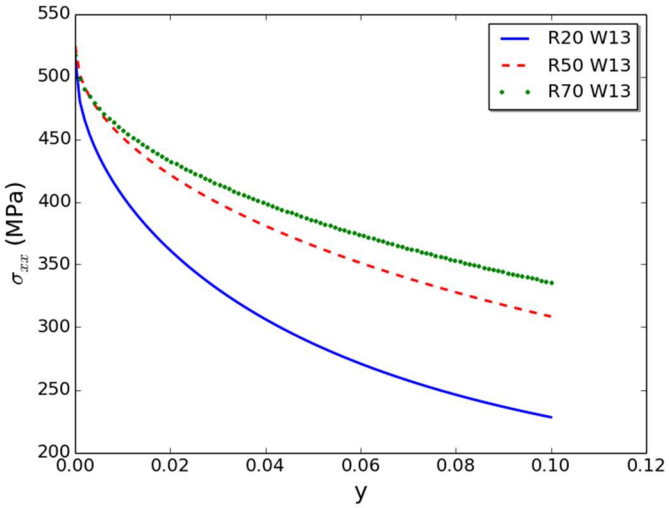

Figure 3-2: Illustration of the stress gradient: σ_{xx} for three pad radii (p0=500MPa, $\sigma_{B,max}$ = 300MPa ad Q/fP = 0,46).

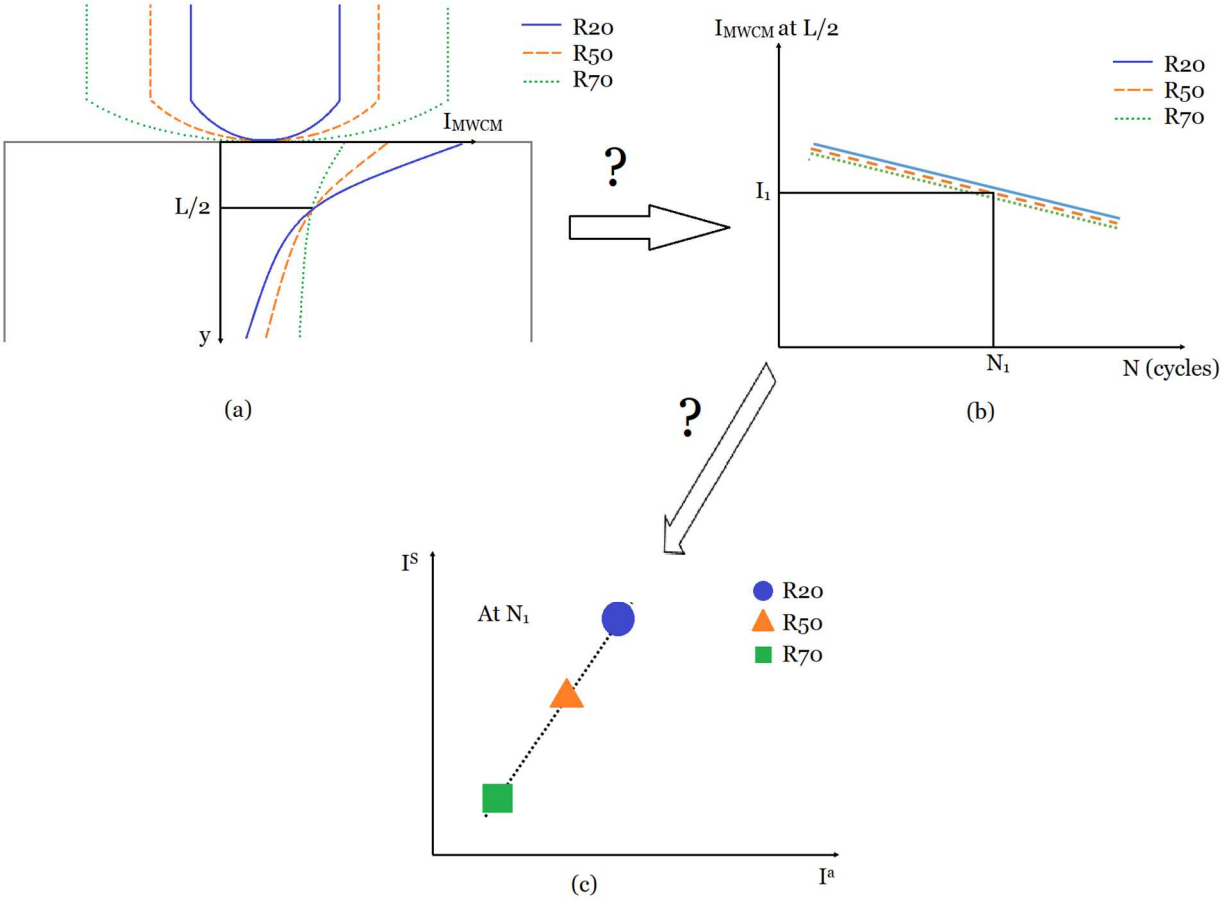

Figure 3-3: Methodology follows for the Group I Tests: (a) Illustration of the evolution of the Multiaxial Index gradient studied in this work, (b) Excepting results with the application of the Theory of Critical Distance and (c) Intended results after the application of the nonlocal criterion.

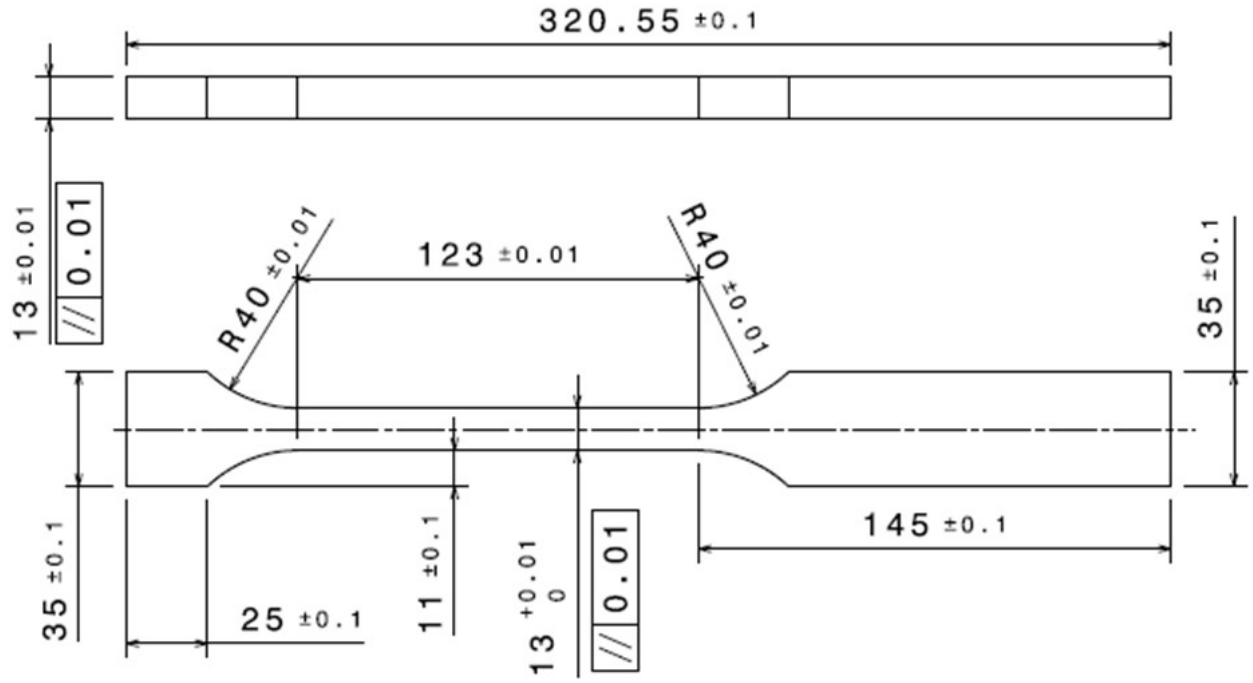

Figure 3-4: Fretting fatigue specimen of the first group of experiment (dimension in mm).

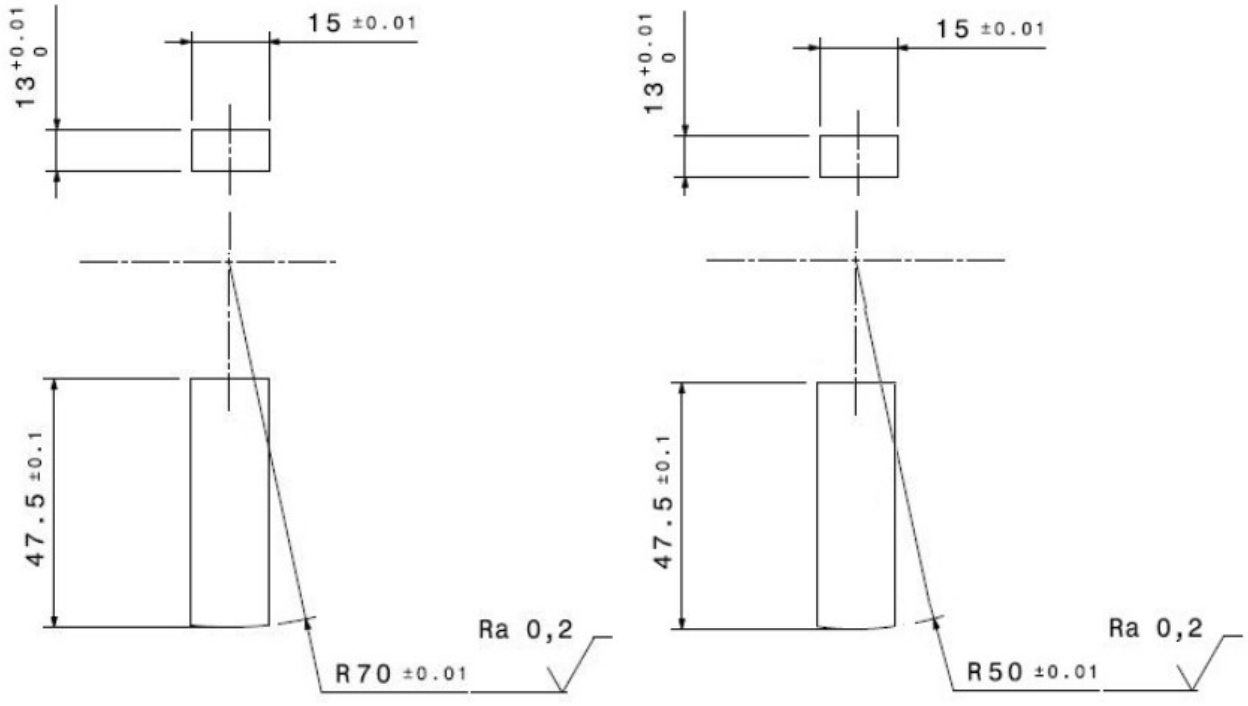

Figure 3-5: Fretting pads of the first group of tests (dimension in mm).

Group II Tests

The second group of experiments concerned an investigation on the size effect for fretting fatigue. Two size parameters were investigated for this study: The volume stressed under the contact and the size of the damaged area within the slip zones. To do so, the Group II Tests was divided into two sub-groups:

- The Group II-a Tests whose objective was to isolate the effect of the width of specimen, and so of the volume stressed under the contact zone.
- The Group II-b Tests whose objective was to study the impact of the damage area within the slip zone under the contact.

The results of the Group I Tests yielded experimental data with a specimen width, $W_{13} = 13mm$. The surface damaged area within the slip zones for these 13 mm thickness specimens can be computed as $A_{13}^{D} = 2 * 13(a_{13} - c_{13})$, being a_{13} the half-width of the contact, which is constant for all experiments conducted with the same pad radius (because the peak pressure was kept constant), and c_{13}, the half-width of the stick zone, which is a function of the tangential load applied.

The Group II-a Tests was designed so that two tests should have the same stress gradient (i.e. the same multiaxial index I_{13} and I_8 for the specimen widths of 13mm and 8mm respectively) under the contact zone and the same fretting damaged area (being A_{13}^{D} and A_{8}^{D} the specimen widths of 13mm and 8mm, respectively), but with a different volume of material being stressed. In other words, two experiments with the same pad radius, but with different widths of 13mm and 8mm, should be developed. Therefore, a loading configuration needs to be calculated to provide these tests with the following characteristics (Figure 3-6 (a)):

i. $A_{13}^{D} = A_{8}^{D}$ ➔ $13(a_{13} - c_{13}) = 8(a_8 - c_8)$
ii. $I_{13} = I_8$ at x=-a.

The Group II-b Tests was carried out to study the influence of the surface fretting damaged area on fretting fatigue life/strength. It has been developed also considering a smaller specimen width of 8mm for the comparative analysis. However, for this sub-group of tests, the only parameter which remains constant for the two corresponding tests is the multiaxial index under the surface for x=-a, being the fretted damage areas different, i.e., $I_{13} = I_8$ and $A_{13}^{D} \neq A_{8}^{D}$ (Figure 3-6 (b)).

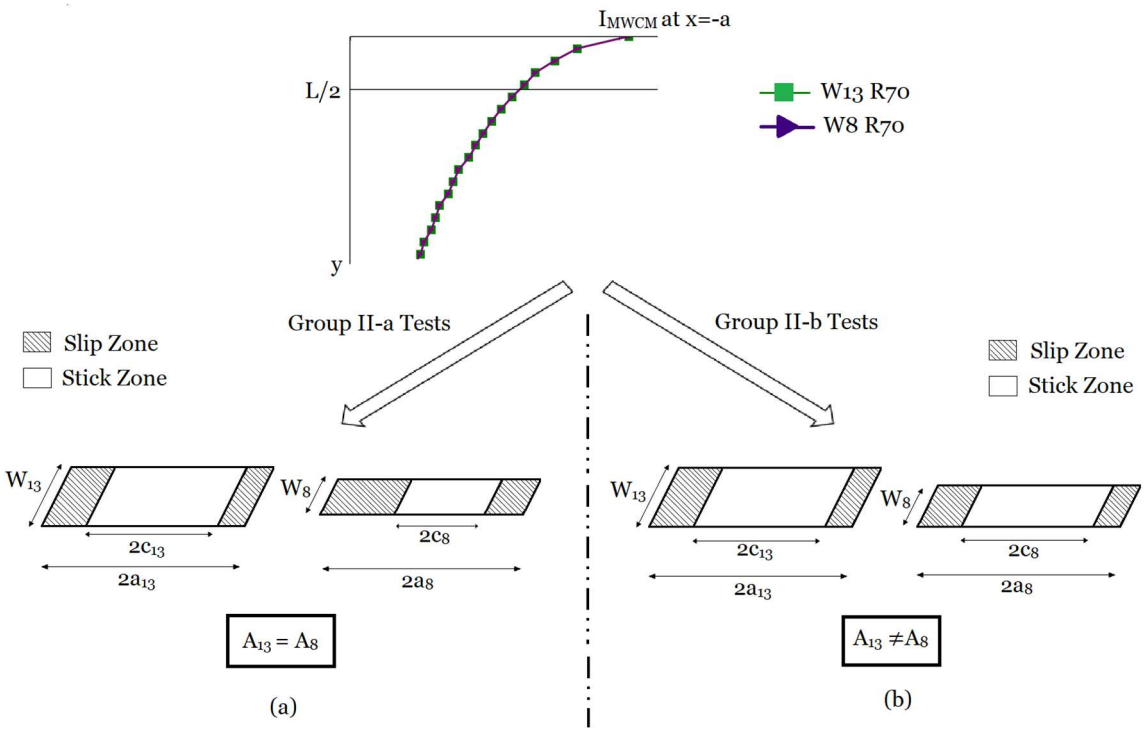

Figure 3-6: Schematic representation of the objectives of the Group II Tests: (a) Group II-a Tests with same fretting damaged area for the two specimen's widths, (b) Group II-b Tests for different fretting damaged areas.

Therefore, all experiments of the Group II Tests were carried out with a pad and specimen width of 8mm, and the pad radius considered is 70mm. The corresponding shape and dimension of both pad and specimen are presented in Figure 3-7 and Figure 3-8.

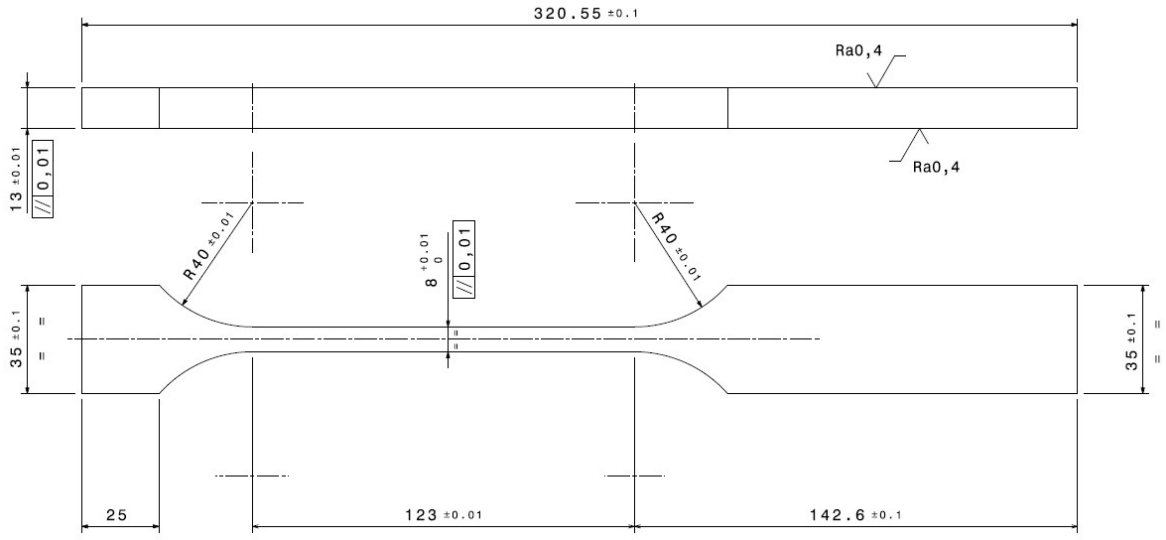

Figure 3-7: Fretting-fatigue main specimen of the second group of tests (dimension in mm)

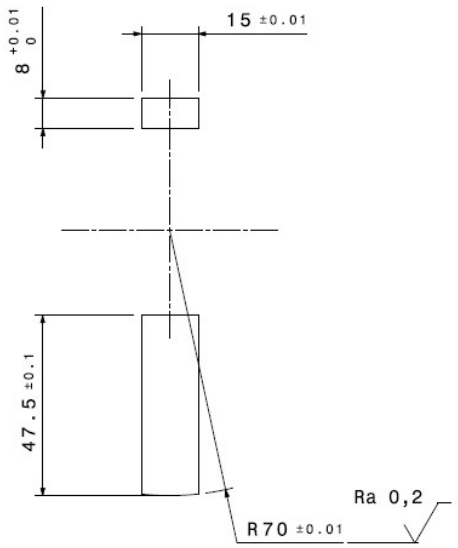

Figure 3-8: Fretting pad of the second group of tests (dimension in mm).

All fretting-fatigue specimens and pads were machined from a real fan disk randomly taken from production line by Safran Aircraft Engines in France. The specimens were then packed and sent to our laboratory in the University of Brasilia. Dimensions and surface roughness were controlled for the ground surfaces and for the cylindrical fretting pads with a confocal microscope. A three dimensional metrology machine equipped with probe sensor was used to measure the pad radii. Figure 3-9 depicts a photograph of main specimens and pads.

Figure 3-9: Photograph of fretting fatigue specimens and pads.

Description of the two vertical-actuators fretting-fatigue rig of the UnB

To conduct the tests, a two independent vertical-actuators fretting-fatigue rig available at the University of Brasília was used. A scheme with an overall view of such rig is shown in Figure 3-10. All its components were numbered and identified in the legend of such a Figure. Figure 3-11 depicts another schematic drawing now containing a detailed cut-view of the apparatus in the region of the contact between pad and specimen. The main 'dog-bone' specimen (8) is held between fixed and moveable jaws (6 and 7). The moveable jaw (7) is mounted to a load cell (4) and to a hydraulic actuator (3) capable of applying loads up to 250kN. This is used to apply the oscillatory fatigue load to the specimen. The cylindrical pad (11) and the roller bearing (10) are clamped against the specimen (8) by an Enerpac static hydraulic actuator (9) and a screw, respectively. This static actuator is connected by a hydraulic line to an external pump (13). The useful area of this pump is known, $A = 640mm^2$, and by knowing the desired pressure (in N), the pressure to apply (in bar) can be defined as follow:

$$P(bar) = \frac{10P(N)}{640} \tag{3.1}$$

A manometer (12) ensures the application of the correct pressure and an accumulator (12) ensures a correct constant normal load during the experiment. The cylindrical pad (11) and the roller bearing (10) are positioned on a carriage of the fretting-fatigue apparatus, which is connected to the upper vertical actuator (1) by four cylindrical bars (14). This hydraulic actuator (1), which can apply loads up to 100kN, is mounted to a load cell (2). Therefore, they are used to apply and to control the prescribed oscillatory fretting loads. The main advantage of using a two actuators fretting-fatigue rig, instead of a simple actuator one, as considered elsewhere (Nowell, 1988, Bellecave, 2015), is that it allows not only a more refined control and measurement of the fretting load, but also to apply the fatigue and fretting loads under different frequencies and/or phases. Indeed, in the case of a single actuator fretting machine, the fretting load is not applied directly to the pad carriage, but depends on a relation between the bulk fatigue load and the stiffness of the apparatus. Therefore, it is not possible to change the fretting load independently of the bulk load and there is limit value the fretting load can reach that is associated to the apparatus stiffness. Figure 3-12 and Figure 3-13 show photographs with a general and a detailed view of the fretting fatigue machine, respectively.

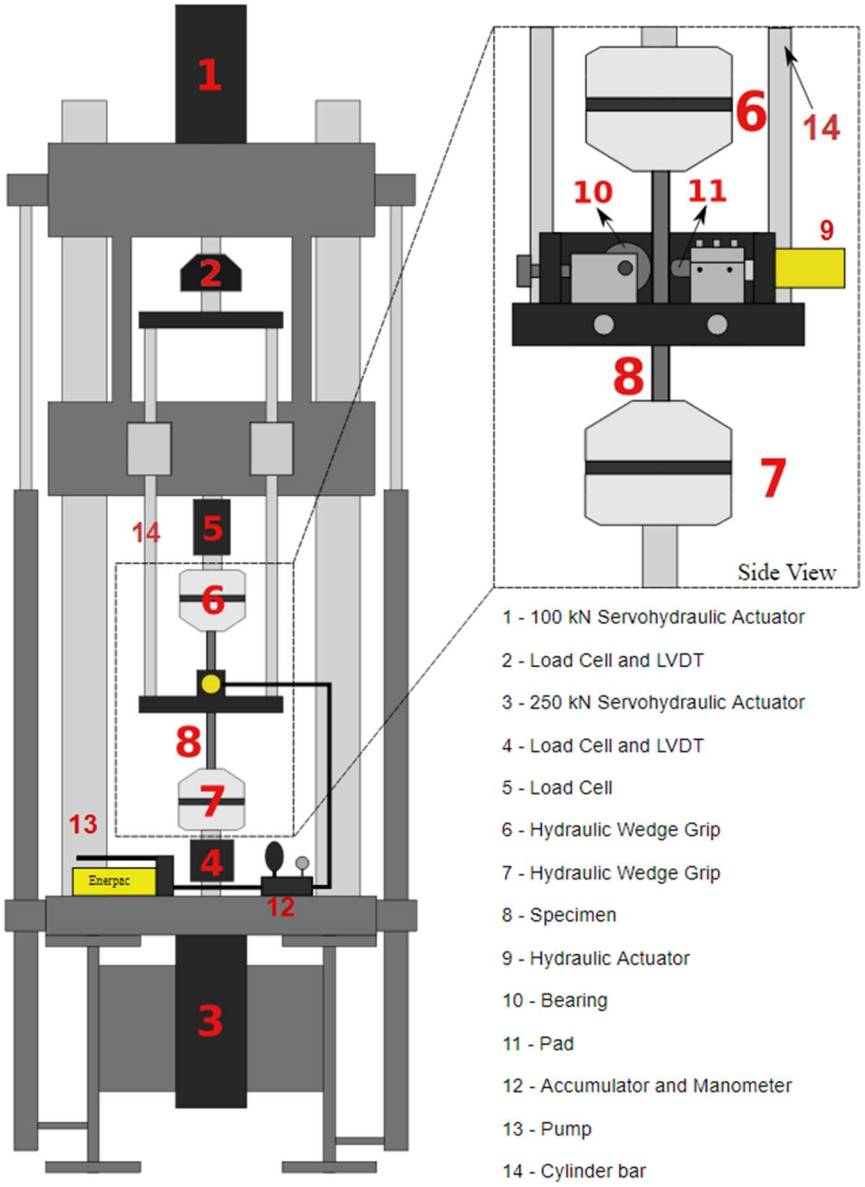

Figure 3-10: Detailed schematic view of the two actuators fretting-fatigue rig.

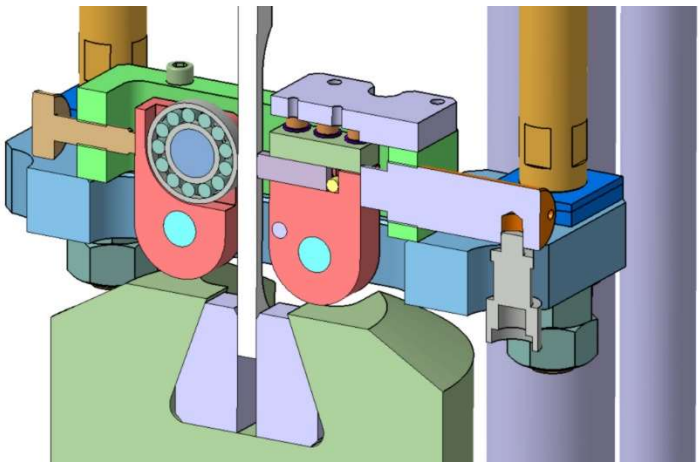

Figure 3-11: Schematic cut-view of the fretting-fatigue apparatus.

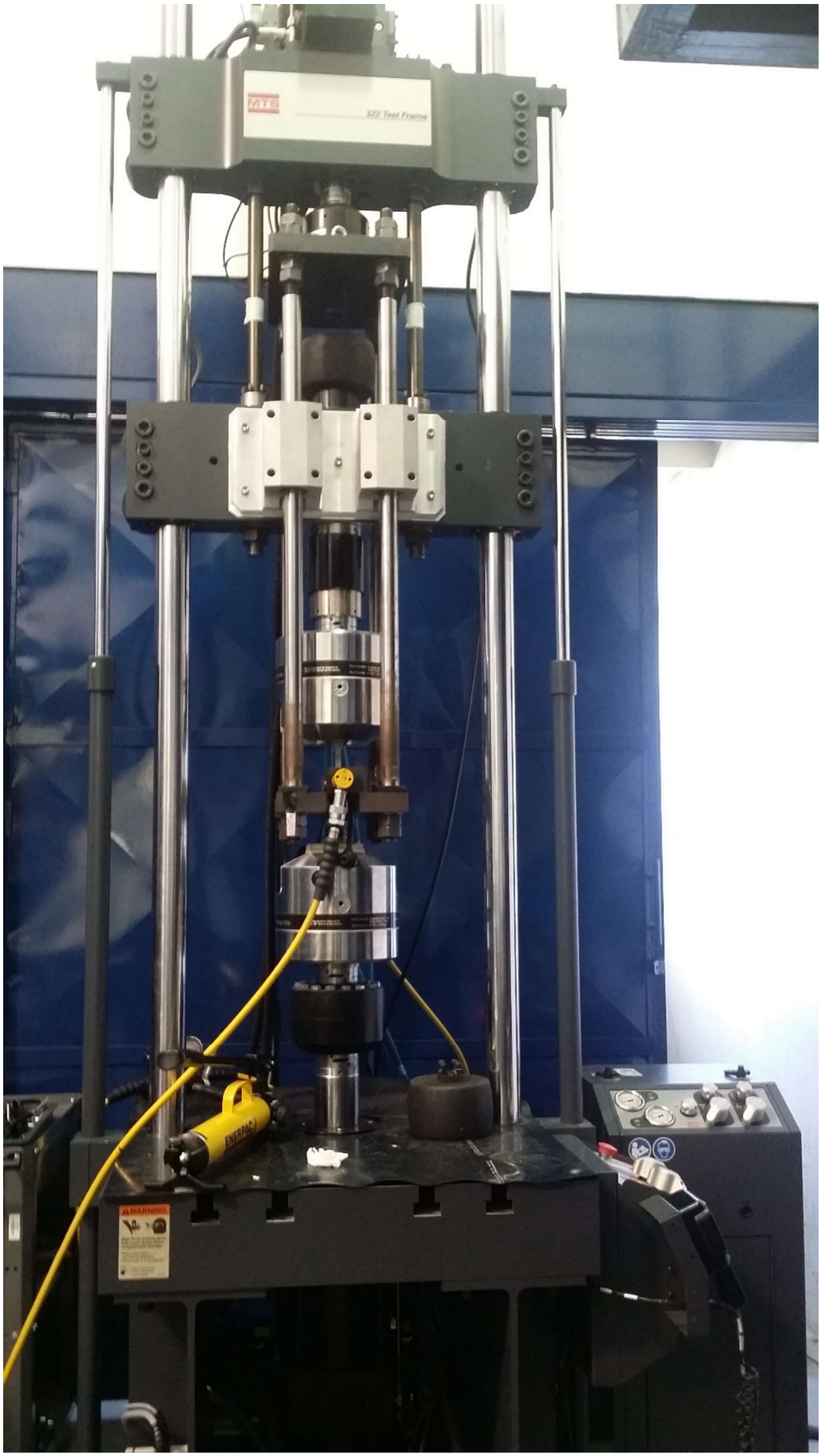

Figure 3-12: Photograph of the two vertical-actuators fretting fatigue rig of the UnB.

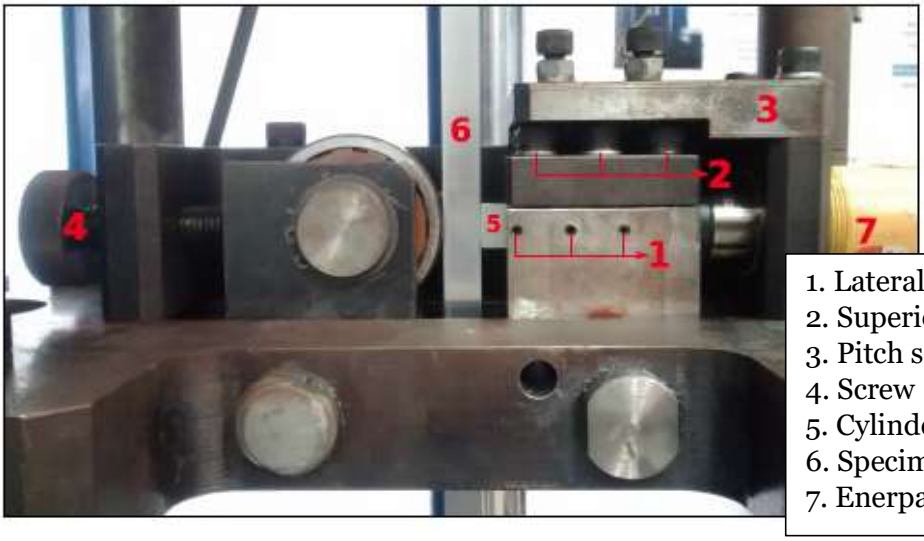

1. Lateral screws
2. Superior screws
3. Pitch screws
4. Screw
5. Cylinder pad
6. Specimen
7. Enerpac actuator RC-51

Figure 3-13: Photograph with a detailed view of the pad/specimen assembly in the two-actuator rig.

Methodology to conduct the fretting fatigue tests

As previously informed and for the sake of clarity, the experimental program in this thesis was divided in two groups of tests, each with the aim to investigate and to validate the influence of a different variable on the quantification of the fretting fatigue resistance/life of a Ti-6Al-4V cylinder on plane contact configuration. To carry out these tests the same fretting fatigue rig and experimental procedure are required regardless of the Test Group. The details the experimental procedure are now reported in this section.

Before starting the tests and to guarantee the specimens were machined as requested, the dimensions of the pads and specimens are checked using a calliper and the Confocal Laser Microscope, which also allows the assessment of the surface roughness. Each dimension was measured in three different positions and an average value was used to be compared with the nominal dimension. Before starting the test pads and specimens are chemically degreased.

One of the most important steps in the test procedure concerns the alignment of the pad. Indeed, a misalignment of the pad may induce edge stress concentrations, which give rise to anomalous corner-initiated failures. Thus, to obtain a correct alignment of the pad (Figure 3-14 (a)), a careful correction of its y-alignment (Figure 3-14 (b)) and of its angular position (Figure 3-14 (c))) should be performed with the help of six small pitch screws on the side of the pad carriers (Figure 3-13). The y-alignment of the pad should be controlled by visual inspection, and the angular position is verified with a Pressure Measuring Film (Fuji Prescale Film – Medium Pressure – Mono Sheet Type) until the desired alignment is obtained (Figure 3-15).

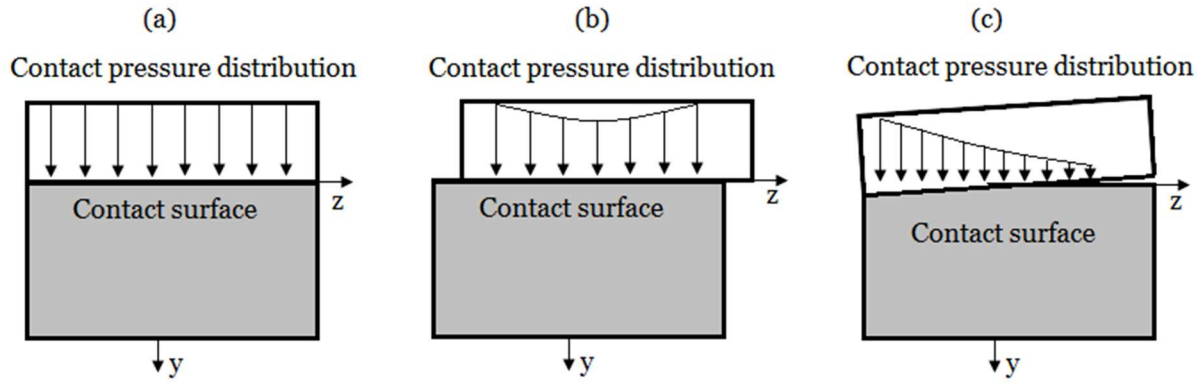

Figure 3-14: Possible alignment conditions of cylindrical pads and corresponding pressure distribution: (a) aligned; (b) and (c) misaligned.

Figure 3-15: Prints pressure of (a) misaligned pad; (b) aligned pad.

When a correct alignment of the pad is obtained (see Figure 3-15(b)), the experiment may begin. All the experiments in both Test Groups were conducted under a stress ratio R_σ = *0* for the bulk fatigue load. This mean normal force to the specimen is applied before the pad is clamped against the specimen with the prescribed normal load, which correspond to a peak pressure p_o=*500MPa* for all the tests. The sinusoidal fretting and bulk fatigue loads can then be applied in phase and under the same frequency. Figure 3-16 shows a schematic diagram of the load history that is used all tests for both Test Groups. One should notice however that, at the beginning of the test, the contact interface does not contain any superficial damage and hence the coefficient of friction is at its minimum value. Therefore, to avoid total slip due to the application of the full fretting load at once, the fretting actuator is initially operated under displacement control, as the precision of the actuator´s LVDT is of the order of 1μm. The amplitude of displacement of the pad is then increased in small steps (1 μm) at every 1000 cycles until the load desired for the fretting test is reached. This procedure is necessary to allow the mean coefficient of friction within the contact zone to slowly climb up and stabilize due to the growth of the slip zones. To assure the pad does not experience full slide when the displacement is increased at each step, attention must be paid to the displacement-force diagram provided by the sensors of the upper (100kN) fretting actuator. The typical "fretting loop" for a partial slip regime is depicted in Figure 3-17a. If a full slide would have taken place, this loop should contain horizontal straights lines (Figure 3-17b), i.e., a reasonable

displacement of the pad would have occurred under a constant tangential load. Finally, when the slip zones reached their final size for the fretting load designed for the test, the amplitude of displacement of the pad is slowly reduced to 0 mm and the test is switched to load control. Once again, the fatigue and fretting loads are gradually increased until the prescribed amplitude of loads for the experiment are reached (increments of 25N for the tangential load and of 250N for the fatigue load). For all tests performed, the loading ratio will be $R_B = 0$ for the bulk force and $R_Q = -1$ for the tangential force. The frequency will vary depending of the experiment's group. Indeed, if it was possible to obtain a correct response of the MTS with a frequency of 10Hz for the 13mm's experiments, it was observed that this frequency should not exceed 5Hz for the 8mm's specimens used in Group 2 experiments. During all the process, and regularly during the whole test, both loads and "fretting loop" are monitored on the scopes (Figure 3-18, Figure 3-19 and Figure 3-20) as well as the normal load in the manometer to ensure the precision of the test.

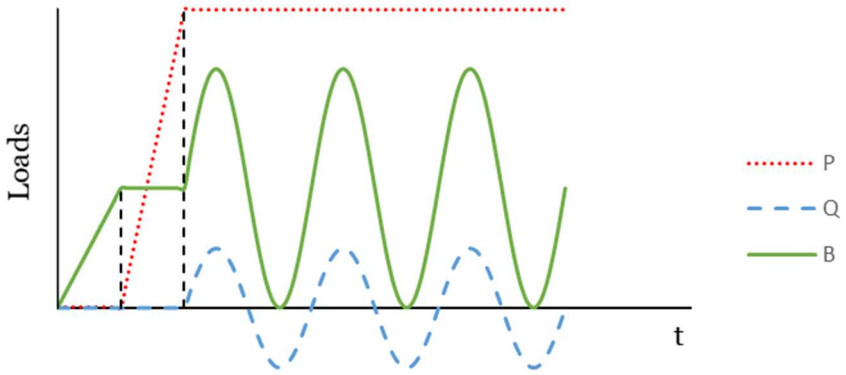

Figure 3-16: Illustration of the typical loading of the tests.

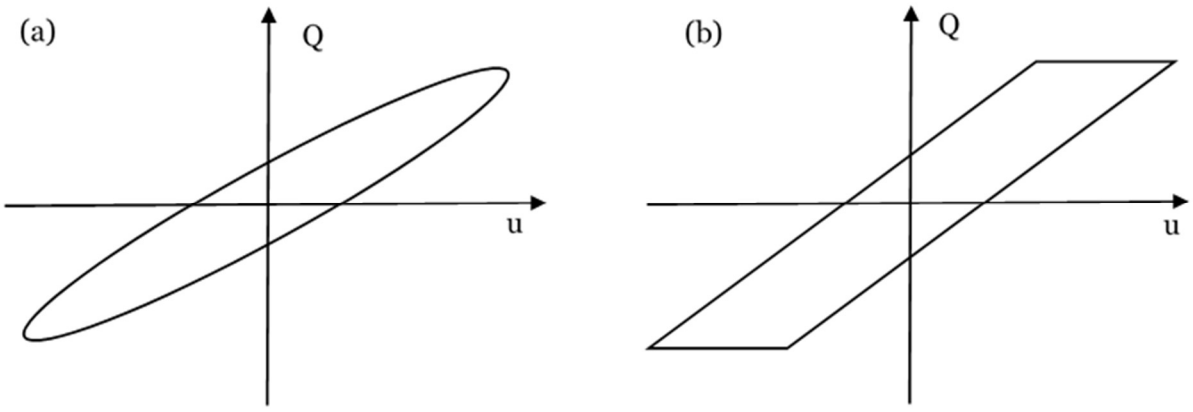

Figure 3-17: Fretting fatigue loops (a) Partial slip, (b) Full slip

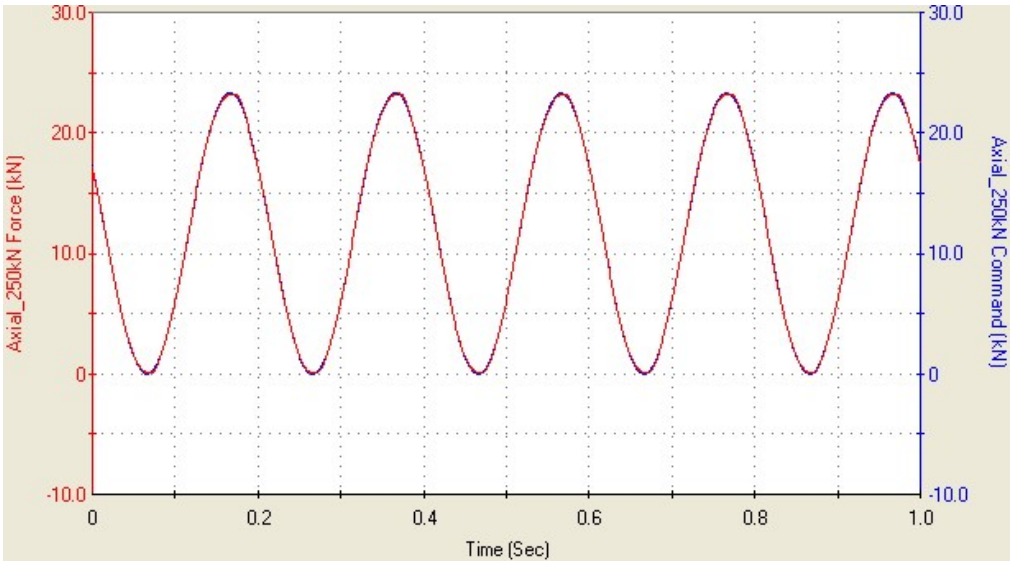

Figure 3-18: Station manager scope monitoring the fatigue load.

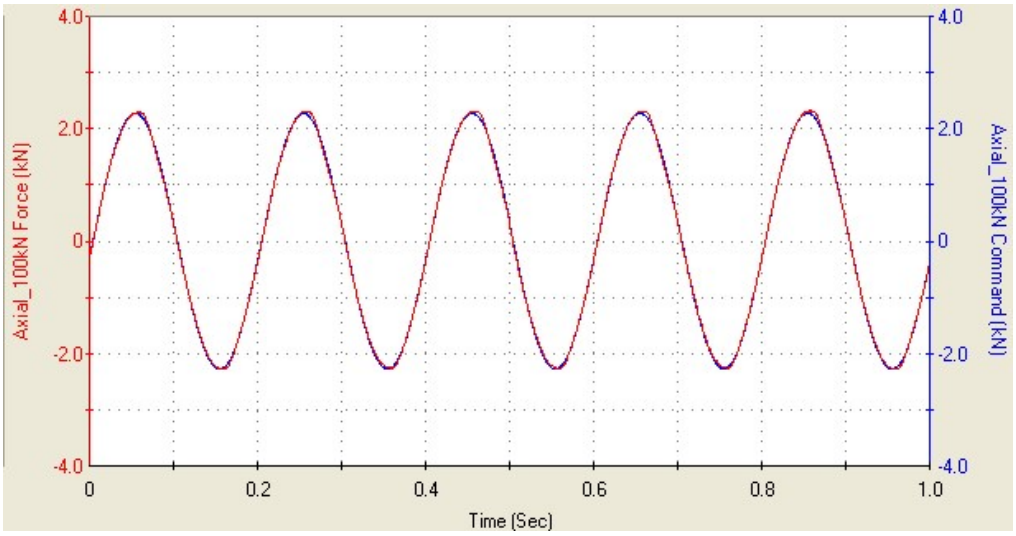

Figure 3-19: Station manager scope monitoring the fretting load.

Figure 3-20: Station manager scope monitoring the "fretting loop".

Two group of tests will be carried out during this work. In the first group, experiments are designed to test the ability of the crack analogue model, developed by Montebello (2015) as part of the COGNAC project, to deal with the gradient effect encountered in fretting fatigue. With the second group of tests, the aim was to investigate the size effect in fretting fatigue. All experiments of this study were carried out by using a two vertical actuator fretting fatigue rig available at the University of Brasilia.

Chapter 4. Experimental verification of the crack analogue model

4.1. Introduction

One of the major difficulties in dealing with the fretting fatigue problem come from the fact that it generates a multiaxial stress field under the contact region. Besides that, it usually presents a severe stress gradient close to the surface. There are different methodologies in the literature, which claim to be able to incorporate such characteristics of the fretting problem to the modelling. They have been usually divided into two main groups, the stress based models (Araújo et al., 2007, Araújo et al., 2014, Fouvry et al., 2014, Ferré et al., 2013, Araújo et al., 2008) and the stress intensity factor ones (Araújo et al., 2007, Fouvry et al., 2008, Dini et al., 2006, Araújo et al., 1999, Bellecave et al., 2014). A good level of accuracy has been obtained by both methods to estimate fretting fatigue life or strength. For instance, the Modified Wölher Curve Method (MWCM), in conjunction with the Theory of Critical Distance (TCD) (Susmel and Taylor, 2003) as proposed by Araújo et al. (2007), reached an accuracy of ±20% when predicting the fretting fatigue limit. On the other hand, with a short crack approach, first Araújo and Nowell (1999) and later Dini et al. (2006) were capable to estimate the fretting fatigue threshold for two different alloys, an Al 4% Cu and a Ti-6Al-4V. However, stress based models request refined meshes in order to take well into account the effect of the gradient in the vicinity of the contact. Meanwhile, the stress intensity approaches require time consuming computations to get the crack path resulting from the macroscopic loading. Therefore, these methodologies are difficult to be implemented in an industrial environment.

A crack analogue model has been developed by Giannakopoulos et al. (1998, 2000). This analogy relies on the similitude principle and the fact that the stress field at the end of a contact displays a strong similarity with a crack tip field. However, the approach of Giannakopoulos et al. (1998, 2000) is limited to problems where the friction zone is negligible and hence to contact with sharp edges. Based on this type of analogy, a new nonlocal method has been proposed Montebello et al. (2016) in an attempt to respond to the specific industrial needs by not assuming the friction zone inside the contact to be negligible. The main feature of this method is that it is geometrically independent, in the sense that the reference fields around the contact edges can be described as function of a set “stress intensity factors”. Moreover, it proved to be less time-consuming. Although it also requires a FEM model to be applied, the mesh does not need to be so much refined. Indeed, Montebello (2015) showed that for a mesh considering element sizes of 70μm within the contact zone, the resulting errors in the stress intensity terms were smaller than 5% when compared with the ones computed with

a 5µm element size mesh. Notice, however, that this somehow rough mesh would produce errors higher than 40% to compute the contact stresses compared with the fine one.

The aim of this chapter is not only to define experimental configuration (loading history and contact geometry) capable to challenge and validate this new method, but also to further investigate the role of the maximum normal stress on the limit between safe life and failure. Some authors (Fleury et al., 2017) have suggested that, under fretting fatigue conditions, the alternating shear stress is the main variable governing the crack initiation phenomenon, then the incorporation of the maximum normal stress in this case would be unnecessary and would turn the estimates extremely over conservative. These tests and analysis will seek to shadow some light on this issue.

Firstly, the experimental configuration and results of Group I of Tests in this study will be presented. The data were obtained at the University of Brasilia, using the two actuators Mechanical Test System with a fretting apparatus to test a cylinder against plane contact configuration, both made of a Ti-6Al-4V alloy, as detailed in section 0.

Then, the nonlocal intensity factors are computed via a Finite Element Analysis for the configurations tested. An attempt to correlate them with the number of cycles to failure was performed. At last, but not least, a comparative analysis to estimate the fretting fatigue limit was carried out by applying the Modified Wölher Curve Method (MWCM), in conjunction with the Theory of Critical Distance in terms of the nonlocal stress intensity factors. The role of the maximum normal stress to determinate the boundary between safe and failure zones is discussed when the MWCM is computed in terms of the nonlocal stress intensity parameters.

4.2. Group I Tests: Determination of tests configuration

Objective of the tests

As mentioned previously, the objective of the Group I of Tests is to provide a more general, robust and challenging validation of the crack analogue model proposed by Montebello (2015). Another objective of utmost importance for such tests is to explore the role of the bulk load for the determination of the boundary between safe life and failure. Indeed, the validation of this model was essentially conducted considering a limited set of data but under pure fretting loading conditions (i.e. without fatigue). Just few data for 35NiCrMo16 low-alloyed steel under fretting fatigue were considered in the analysis by Montebello et al. (2016). As this model was developed aiming to be used in the industrial context, and in particular for the aeronautical sector, its validation requires a much broader set of data under more realistic loading conditions and using materials of interest to produce the assemblies studied. As it has been

pointed out in section 3.2 (Chapter 3), Ti-6Al-4V have a set of mechanical properties of great interest for the aeronautical industry, and it is commonly used for the manufacturing of fan blades and disks of aeroengines. Thus, the Group I of Tests was carried using Ti-6Al-4V as specimens and pads material.

An important characteristic that we want to further exploit with these tests is the ability of the crack analogue model to properly take the gradient effect into account. To achieve this goal, this group of test was designed with the purpose of generating not only different stress gradients but also different magnitudes of stresses at the hot spot (the severest loaded material point). To that end, two set of pads with radii R=50mm and R=70mm were considered and the loads were determined so that the multiaxial fatigue index, computed with the Modified Wöhler Curve Method (MWCM) (section 2.3 of the Chapter 2), were identical at the critical distance, L/2 (Figure 4-1). According to the Theory of the Critical Distance (section 2.4 of the Chapter 2), tests which experiment the same level of relevant stress at the critical distance are supposed to have similar lifetimes. By applying this theory, the experiments of the Group I of Tests were designed within the objective of reaching specific target lives. Indeed, when the experiments are represented on an I^s-I^a map, a correlation between tests having similar lifetimes has to appear if the gradient effect is well taken into account. So, if one obtain experiments with different radii but similar lifetimes, the ability of the model to incorporate the gradient effect can be verified.

Thus, to determine the loading history for the fretting fatigue tests of the Group I Tests, the target lives have to be selected. In a recent past some fretting fatigue tests were carried out by Bellecave (2015) with the same Ti-6Al-4V alloy. He also studied a cylinder/plane contact with pad radii of 20mm and 70mm and used a single-rig actuator to conduct this experimental work (a complete description of this apparatus may be found in Bellecave (2015)). Among the results he obtained, it was noted that data were available for lives around 200 000 cycles, 500 000 cycles and for run out experiments (here considered as 1 000 000 of cycles) for both pad radii. To take advantage of these available experimental data, new tests with the pad radii of 50mm and 70mm will then be designed targeting to achieve 200 000 cycles, 500 000 cycles and run out. As the apparatus used during the experimental campaign of Bellecave (2015) was different from the two-vertical actuators one used for this work, some experiments with pad radius of 70mm will be reproduced to ensure the repeatability of the results.

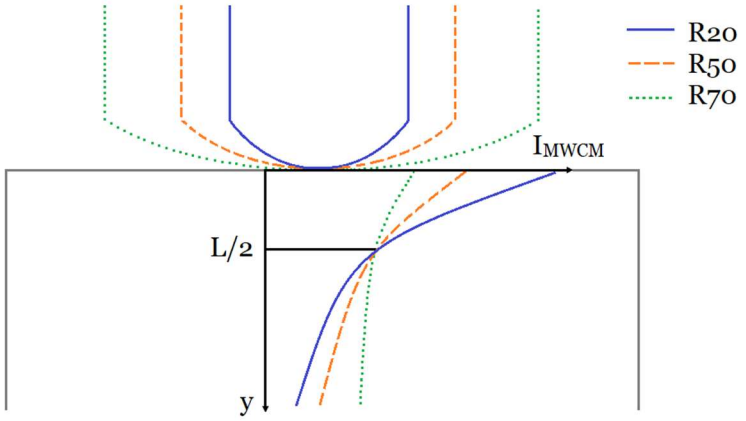

Figure 4-1: Schematic representation of the variation of the multiaxial fatigue parameter with distance from the contact surface at the trailing edge of the contact for three different pad radii.

Experiments conducted

To obtain the loads which will, theoretically, lead to 200 000 cycles, 500 000 cycles ant to run out experiments for the pad radii of 50mm and 70mm, the first step was to compute the Multiaxial Fatigue Index, I_{MWCM}, at the critical distance, $L/2$, for the tests carried out by Bellecave (2015) with pad radius of 20mm and which reached these target lives. This multiaxial index has been calculated with the Multiaxial Wöhler Curve Method (MWCM):

$$I_{MWCM} = \tau_a + \kappa \frac{\sigma_{n,max}}{\tau_a} \tag{4.1}$$

The equivalent shear stress, τ_a, and the maximum normal stress, $\sigma_{n,max}$, were computed with the Rectangular Hull Method (Section 2.3 of the Chapter 2) as proposed by Araújo et al. (2011). To simplify the computational process, κ will be considered as a constant material parameter, even if it is computed with respect to the fatigue limit determined at 10^6 cycles and presented in the section 3.2 of the Chapter 3: $\sigma_{-1} = 382\,MPa$ and $\sigma_{0,1} = 376\,MPa$. It should be noted that the equation (2.47) gives the expression of κ and λ in function of σ_{-1} and σ_0. Thus, an alternative writing of this equation is used:

$$\kappa = \frac{\sigma_a(\sigma_{-1} - \sigma_a)}{2\sigma_m} \tag{4.2}$$

It is obtained κ=*87MPa* for the Ti-6Al-4V alloy at room temperature.

In some quite recent work on fretting fatigue (Araújo et al., 2017) the critical distance for an Al 7050-T7451 alloy was assumed to vary with number of cycles to failure. A further

investigation by Sá et al. (2017) on the role of the critical distance for this same alloy showed that this variation was small for sharply notched specimens producing stress gradients similar to ones found under fretting conditions. Therefore, for the sake of simplification (usually required to model a complex three dimensional assembly in an industrial context) such a critical distance will be here considered as a material parameter, whose value was previously determined by Bellecave (2015): $L_{PM}=15\mu m$.

The methodology to determine the loading conditions for the new tests started by computing the distribution of the Multiaxial Fatigue Index at the critical distance and at the trailing edge of the contact (x/a=-1) for all tests of Bellecave considering the pad radius of 20mm and our three target lives. Then a search algorithm has been developed to determine the corresponding loads which would produce for R= 50mm and R=70mm the same value of the Multiaxial Fatigue Index, at the critical distance ($L/2=15\mu m$), that was computed for R=20mm, as depicted in Figure 4-2 for a run-out experiment. The firsts loadings determined for the pad radii of 50mm and 70mm by applying this methodology were not leading to the desired lives, nor to run out tests. This can be explain because in fatigue tests, lives cannot be exactly prescribed and some scatter is intrinsic of the phenomenon. Thus, a staircase procedure was applied around each loadings previously determined until reaching the target lives. Only these final loadings will be considered in this study.

The previous results obtained by Bellecave (2015) and used for the present work are presented in Table 4-1, and the new experimental results generated for $R=50mm$ and $R=70mm$ during this work are reported in Table 4-2. The tests of Bellecave were numerated from FF01 to FF16 and the ones of the present work from FFG01 to FFG19. All specimens and pads' widths are equal to 13mm and there are three pad radii involved: 20mm, 50mm and 70mm. The relevant test parameters are the stress ratio $\sigma_{b,max}/p_o$ and the load ratio Q_{max}/fP. The multiaxial index (I_{MWCM}) computed at the critical distance ($L_{PM}=15mm$) is given in MPa. The corresponding lifetimes of each experiment are reported as "Number of cycles". Run out conditions were established at 1 000 000 cycles, i.e, tests that did not break at this number of cycles were interrupted. All these results are represented in a S-N diagram (Figure 4-3) with the Multiaxial Fatigue Index computed at the Critical Distance in ordinate and the lifetime in abscissa.

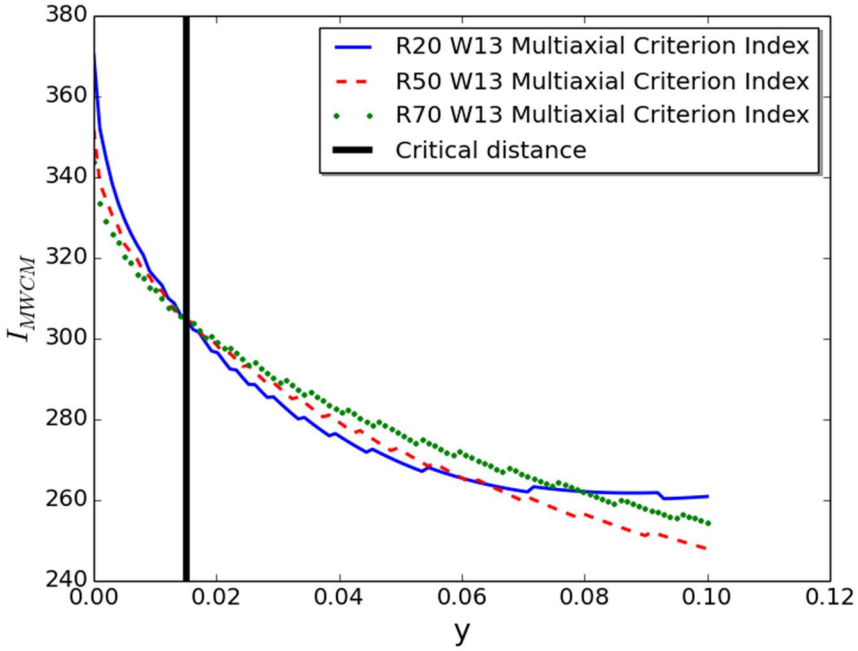

Figure 4-2: Variation of the multiaxial fatigue index with distance from the contact surface at the trailing edge of the contact for three different pad radii in Ti-6Al-4V.

Test	Width (mm)	Radius (mm)	$\sigma_{b,max}/p_o$	Q_{max}/fP	I_{MWCM} at $L/2=15\mu m$ (MPa)	Number of cycles
FF01	13	20	0,68	0,47	321	225 780
FF02	13	20	0,64	0,47	313	477 861
FF03	13	20	0,64	0,47	313	488 632
FF05	13	20	0,6	0,46	305	Run out
FF06	13	20	0,62	0,47	309	Run out
FF07	13	70	0,6	0,46	332	168 266
FF08	13	70	0,56	0,47	327	248 790
FF10	13	70	0,4	0,42	290	579 954
FF11	13	70	0,38	0,51	299	583 981
FF14	13	70	0,36	0,50	293	971 557
FF15	13	70	0,38	0,35	276	Run out
FF16	13	70	0,36	0,47	288	Run out

Table 4-1: Experimental parameters and results used in Bellecave's experiments (2015).

Test	Width (mm)	Radius (mm)	$\sigma_{B,max}/p_o$	Q/fP	I_{MWCM} at L/2=15μm (MPa)	Number of cycles
FFG01	13	50	0,6	0,47	327	164 690
FFG03	13	50	0,6	0,51	333	168 472
FFG02	13	50	0,6	0,55	337	189 147
FFG04	13	50	0,6	0,54	337	203 759
FFG08	13	50	0,4	0,44	285	541 220
FFG07	13	50	0,4	0,44	285	548 169
FFG09	13	50	0,27	0,49	266	Run out
FFG10	13	50	0,32	0,49	275	Run out
FFG16	13	50	0,32	0,49	275	Run out
FFG14	13	50	0,36	0,49	284	Run out
FFG11	13	70	0,6	0,46	332	166 150
FFG17	13	70	0,46	0,44	316	473 954
FFG18	13	70	0,46	0,44	316	412 440
FFG12	13	70	0,4	0,42	290	495 225
FFG19	13	70	0,36	0,43	282	Run out

Table 4-2: Results of Group 1 fretting-fatigue tests.

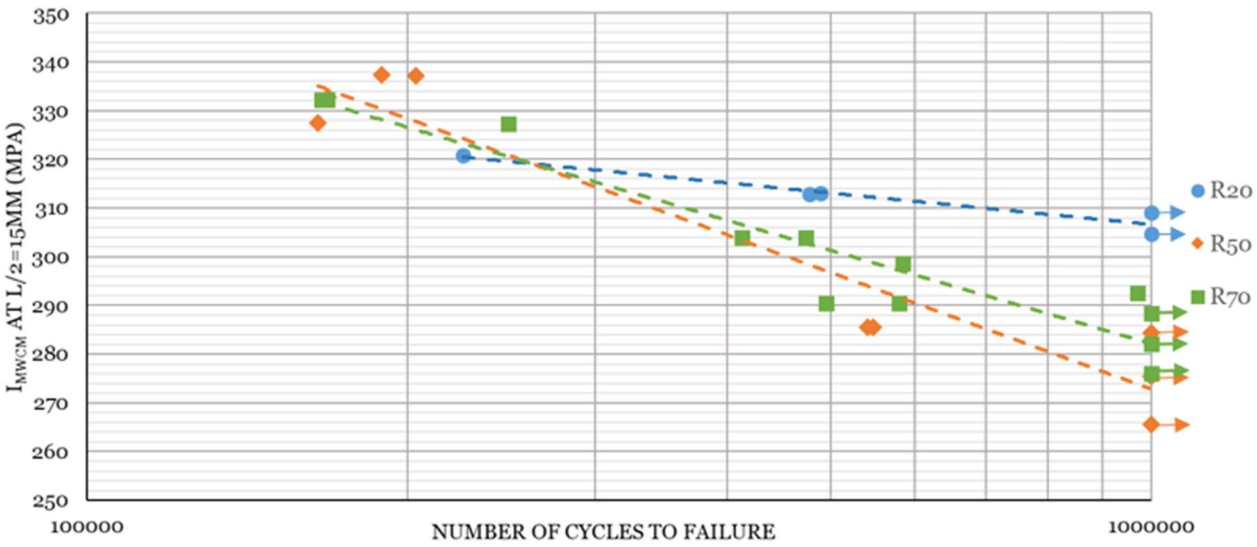

Figure 4-3: Multiaxial Fatigue Index in terms of the Modified Wöhler Curve Method at the Critical Distance against the number of cycles to failure from the experimental results.

Post failure investigation

In order to gain additional insight of the gradient effect into the fretting fatigue phenomenon, examinations of the fracture surface and fretted area of one broken specimen under the contact of the cylinder pad of R=70mm and one under the contact of the cylinder of R=50mm were conducted under a confocal microscope. Figure 4-4, Figure 4-5 and Figure 4-6 show different view of the main specimen used in test FFG11, which is an experiment carried out with a cylinder pad of radius R=70mm and which has a theoretical half-width, a, of 1,07mm and Figure 4-7, Figure 4-8 and Figure 4-9 of the specimen used in test FFG09, which is an experiment carried out with a cylinder pad of radius R=50mm and which has a theoretical half-width of 0,76mm. A number of important feature can be revealed from analysis of these pictures.

Figure 4-4 shows a view of the fretted area where fretting damage took place when the cylinder pad pressed against the flat specimen has a radius of 70mm. It can be noted that the crack initiated within the slip zone as it is theoretically predicted, even if it is difficult to evaluate the distance between the main crack and the edge of the contact as the scar did not have definite regular boundaries. However, it is important to notice the severity of the damages occurring in the fretted area, and there lack under the stick zone. Figure 4-5 depicts a photograph showing the initiation angle of the cracked area. The crack initiates in mode II (Stage I), with an angle of around 18° during approximately 1,5mm. Then, the propagation will continue in mode I (Stage II), perpendicular to the surface. Observation of the fracture surface, Figure 4-6, shows multiple crack initiation which interconnect after around 5,9mm to form a single crack propagation front.

A photograph of the fretted surface of the main fretting fatigue specimen used in test FFG09 shows also severe damages in the fretted area. Once more it is difficult to record the distance between the cracks and the boundary of the fretted area because the scar did not have definite regular boundaries. The crack initiation angle measured on Figure 4-8 is really smooth, of the order of 6° for around 4,2mm before the clear appearing of crack I growth. The analysis of the fracture surface is really similar to the one of the FFG11 test, only the size of the multiple crack initiation zone is different, the unique crack initiation front appears here after around 2,7mm to 4mm.

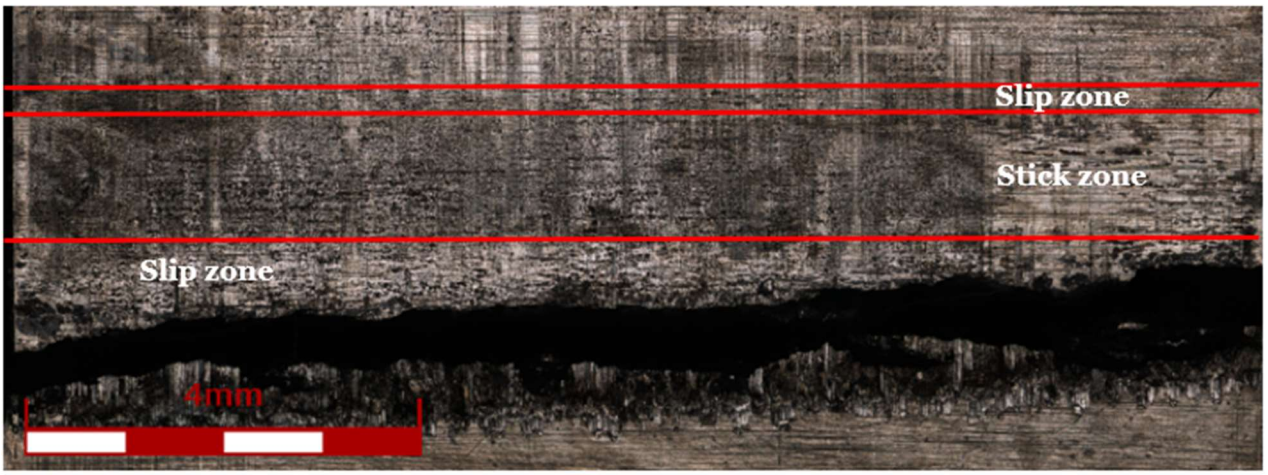

Figure 4-4: Fretted area of the specimen under the contact of the cylinder pad with radius R=70mm.

Figure 4-5: Angle of the crack initiation and profile of the crack propagation for the specimen under the contact of the cylinder pad with radius R=70mm.

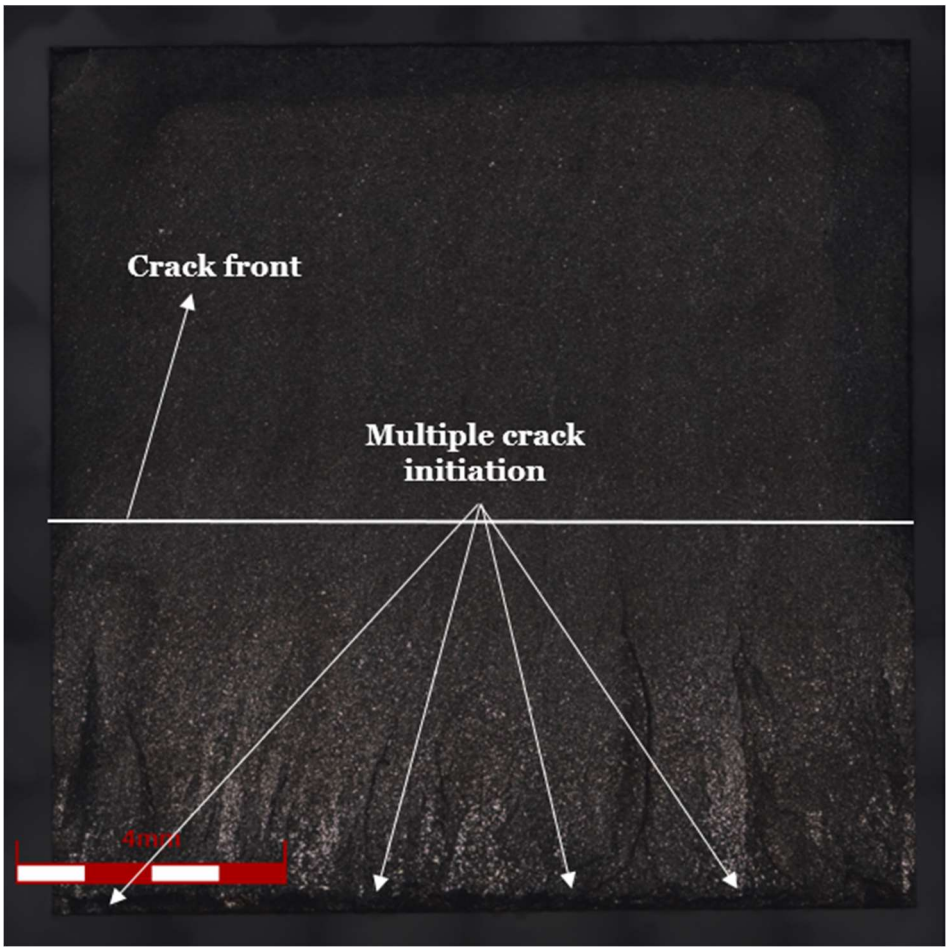

Figure 4-6: Confocal photograph of the fracture surface for the specimen under the contact of the cylinder pad with radius R=70mm.

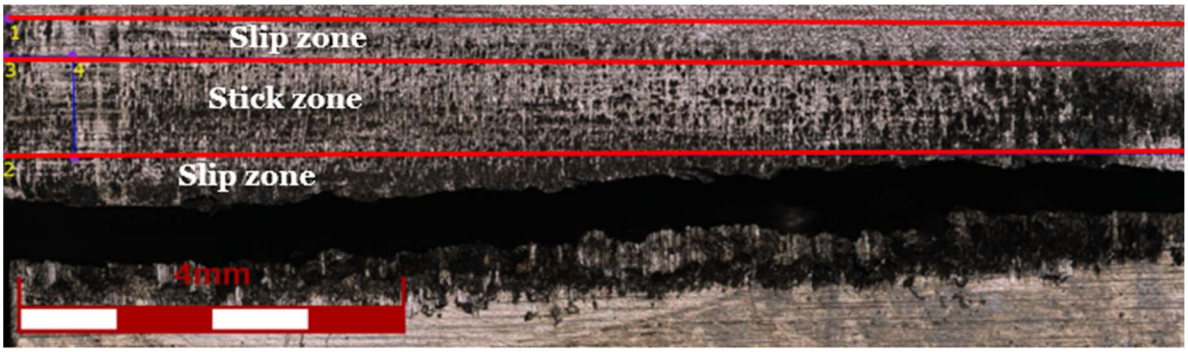

Figure 4-7: Fretted area of the specimen under the contact of the cylinder pad with radius R=50mm.

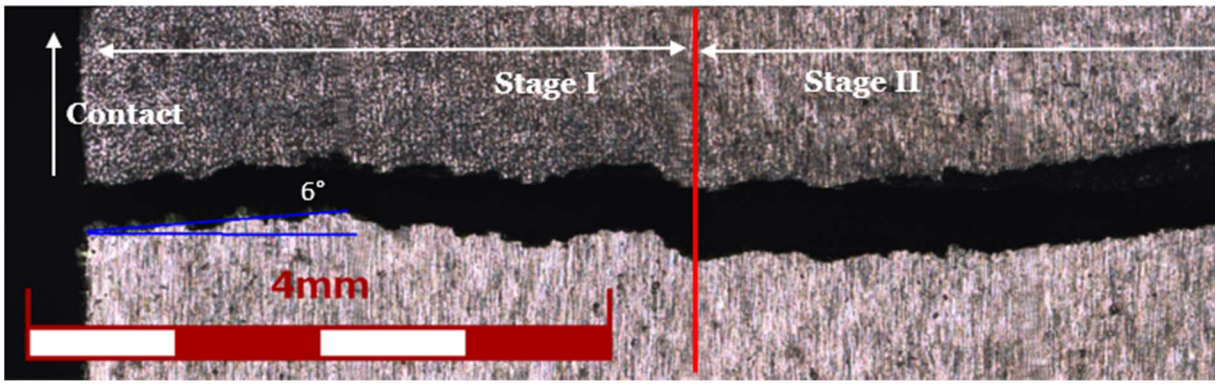

Figure 4-8: Angle of the crack initiation and profile of the crack propagation for the specimen under the contact of the cylinder pad with radius R=50mm.

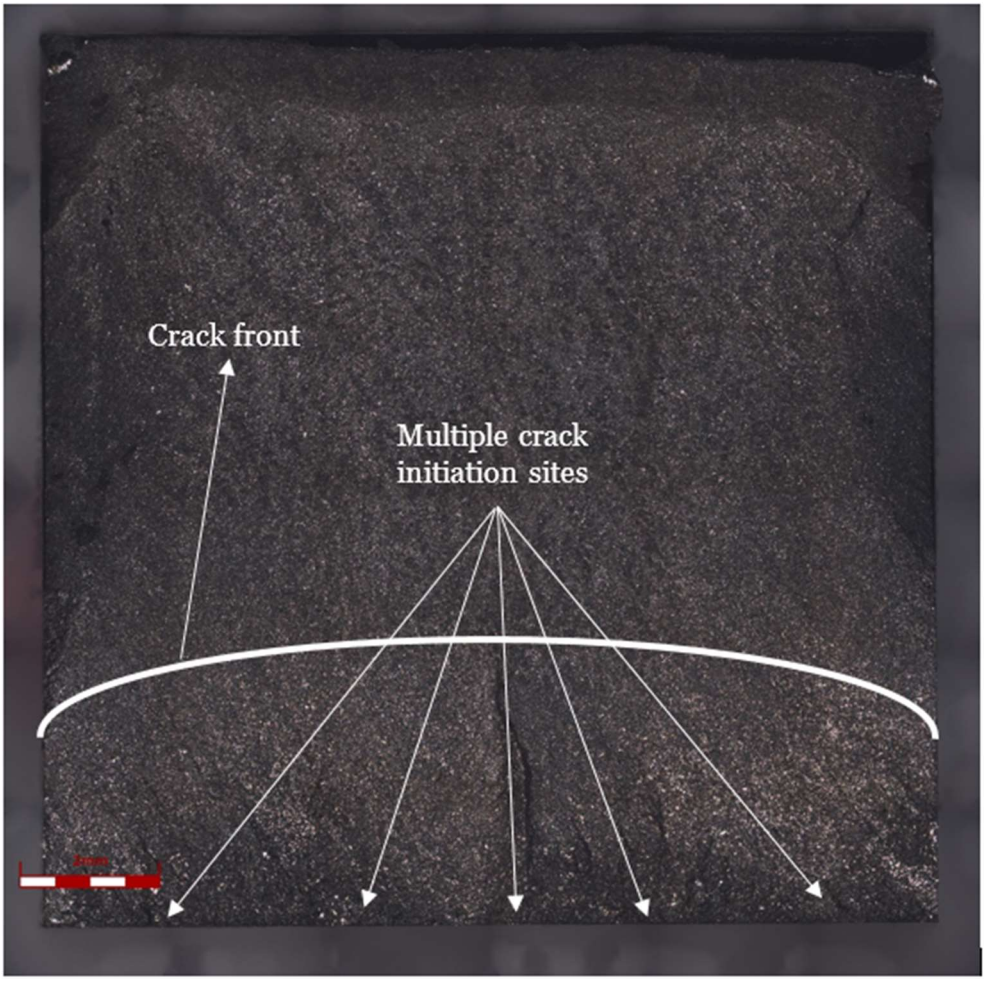

Figure 4-9: Confocal photograph of the fracture surface for the specimen under the contact of the cylinder pad with radius R=50mm.

Some remarks on the experimental results and microscope observations

The following remarks may be provided from the analysis of the experimental results:

i. There is a reasonable degree of scatter for the experiments performed under similar loading conditions, with an average standard deviation of around 15 000 cycles.
ii. Similar results were obtained for the tests carried out in the single-actuator fretting-fatigue rig and in the current the bi-actuator one (e.g., see Experiment FF07 and compare with experiment FFG11 and also compare FF10 with experiment FFG12).
iii. For the experiments performed during this thesis, tests which had similar values of the multiaxial index at the critical distance led to similar number of cycles to failure (compare Experiments FFG01-FFG04 with experiment FFG11, FFG07-FFG08 with experiment FFG12). The same observation can be made for run-out tests (see Experiments FFG14 and FFG19). However, the multiaxial index obtained at the critical distance for the run-out tests of Bellecave (2015), with a pad radius of 20mm, is higher than the ones obtained for the tests with pad radii of 50mm and 70mm tested here. This difference does not appear to be related to the change of fretting-fatigue rig but might be due to the use of a fixed critical distance to evaluate tests experiencing completely different lives (Araújo et al., 2017).
iv. For the experiments performed during this thesis, similar values of the multiaxial index at the critical distance lead to similar number of cycle to failure (Experiments FFG01-FFG04 with experiments FFG07/FFG08 with experiment FFG12). The same observation can be made for run-out tests (Experiment FFG14 with experiment FFG19). However, the value of the multiaxial index obtained at the critical distance for the run-out tests of Bellecave (2015) with a pad radius of 20mm is higher than the ones obtained for the tests with pad radii of 50mm and 70mm.
v. Concerning the post failure analysis, no full sliding should have taken place during the experiments as the first step of the test is controlled in displacement to increase the coefficient of friction. The absence of definite regular boundaries for the fretting scar may be explained by the displacement of the debris created under the contact during the experiment.
vi. For a considerable number of tests crack initiation took place in material planes essentially perpendicular to the surface (or in planes just slightly inclined to the surface). This cracking behaviour for fretting fatigue tests with Ti-6Al-4V was also reported by other authors (e.g., Araújo (2000)).

4.3. Analysis of the gradient effect

The objective of this analysis is to verify the ability of the crack analogue model proposed by Montebello (2015) to take the gradient effect into account. This validation was already

performed for the Ti-6Al-4V alloy in plain fretting conditions (Montebello et al., 2016) and it is proposed here to expand this methodology for fretting-fatigue conditions.

The experimental data presented above are expressed in terms of total fatigue lives while the present model was developed to study the crack initiation boundary. Recently, Hojjati-Talemi et al. (2014), have proposed an approach to estimate fretting-fatigue crack initiation and propagation lifetimes separately. Based on experimental results carried out for cylinder/plane contacts, they have found that the average crack initiation process represents up to 80% of the total estimated life. So it will be assumed that the experimental results obtained for broken specimens may be used to study this crack analogue model. Further, as the multiaxial fatigue model considered in this analysis was developed to tackle problems in the high cycle fatigue regime, i.e., under elastic conditions, the material constants required by the model are calibrated from fatigue tests where lives are registered after failure of the specimens. Therefore, the estimates provided here by the crack analogue model will be assessed by considering lives for the broken specimens.

Calculation of the non-local parameters

The methodology to determine the nonlocal parameters corresponding to the experimental data can be described as follows:

1. Firstly, it is necessary to implement a finite element model representative of the experimental loading and geometrical conditions. Material properties for the Ti-6Al-4V alloy are the ones reported in section 3.2, i.e: $E = 120GPa$ and $\upsilon = 0,29$. The normal and tangential forces were prescribed in N/mm and the fatigue load/stress in MPa. The mean bulk load was initially applied along the right surface, and then the cyclic fatigue was applied on the same surface while the normal force and the tangential fretting load were prescribed at the reference point RP1, located above the pad (Figure 4-11). The values of these loads were provided in Table 4-1 and Table 4-2 for each case of Group I tests. To reproduce the experimental conditions, displacements and rotation were forbidden on the left surface of the model, while a symmetric condition was implemented on the lower surface (Figure 4-11). Then, to obtain the velocity field required to compute the non-local parameter due to the normal load, a small variation of the pressure is generated just before its stabilisation (Figure 4-10). As mentioned in section2.5 of Chapter 2, CPE4R elements are used and the mesh size depends on the contact width, $2a$, computed with equation (2.18) and the numbers of nodes considered in each parts. For this analysis, 1000 elements were implemented and this led to a mesh size (S_M) of 12,1µm for the pad radius of 20mm, S_M=30,25µm for R=50mm and S_M=42,35µm for R=70mm. Figure 4-12 and Figure 4-13 show an

example of mesh that is implemented for the analysis. To describe the contact, the Lagrange multipliers technique was used and the Coulomb's friction law with a penalty ratio of 0,5 was employed to handle the relative slip.

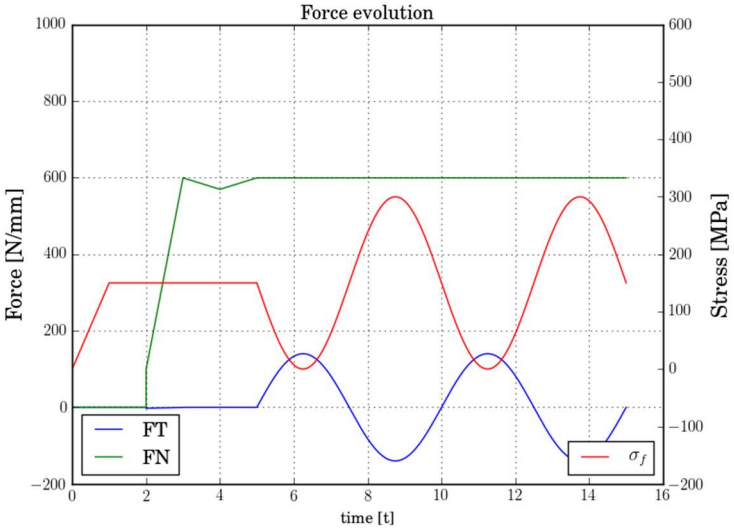

Figure 4-10: Typical loading history implemented in the FE model to compute the non-local parameters for the crack analogue model.

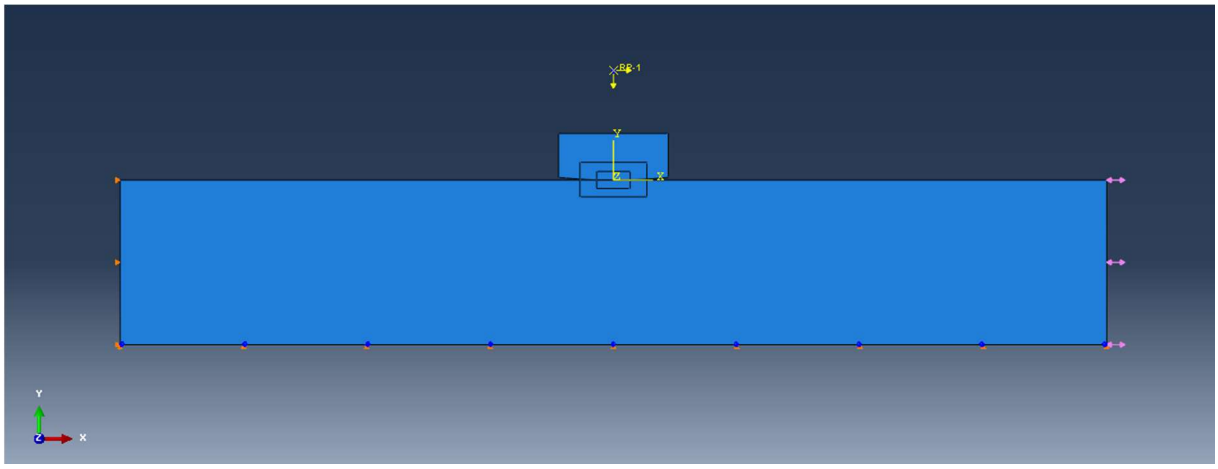

Figure 4-11: Loads and Boundaries conditions of the Finite Element model.

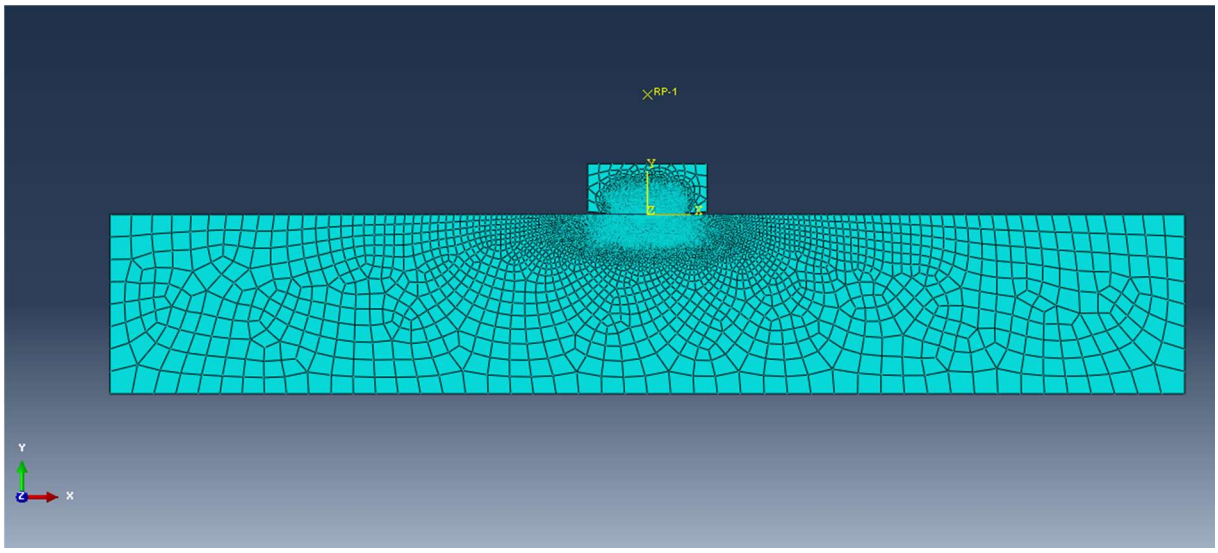

Figure 4-12: Global mesh of the finite element model.

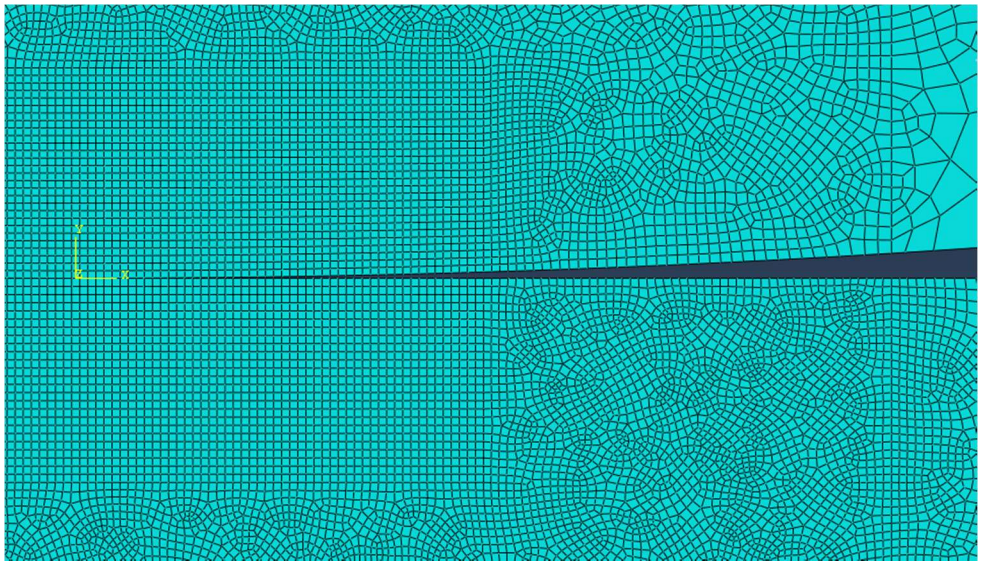

Figure 4-13: Details of the refined area.

2. The Finite Element (FE) analysis is performed. This takes around 10 minutes to be completed in a computer equipped with an Intel Xeon X3530 processor, 24GB RAM and a clock frequency equal to 2,8GHZ.
3. The validity of the model needs to be checked. To do so, and considering that this fretting contact configuration has an analytical solution for the stress field under the contact, as described in details in Chapter 2, a comparative analysis was conducted. In this setting, Figure 4-14 and Figure 4-15 show the numerical and analytical solutions for the normal and shear tractions on the contact surface, while Figure 4-16 depicts the variation of the first, stress components, σ_{xx}/p_o along the contact interface (in terms of normalised, *x/a, position)*, at instants of maximum value of the shear load

for a test with pad radius of 70mm, which present the rougher mesh. Similar results were obtained for R=20mm and R=50mm.

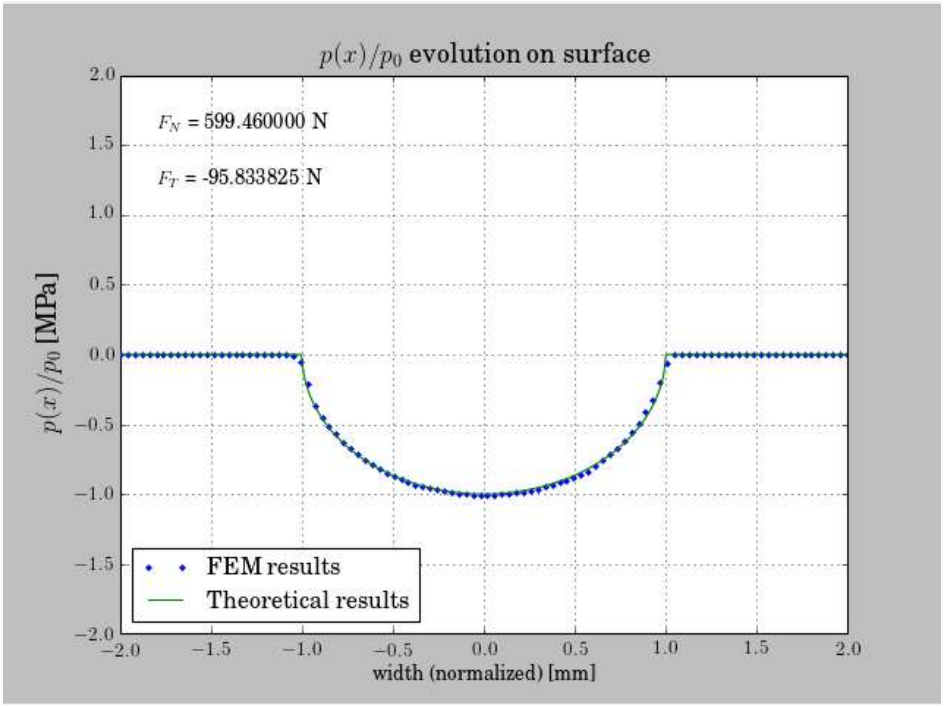

Figure 4-14: Comparison between the analytical formulation and the finite element model for the normal tractions at the surface for a pad radius of 70mm.

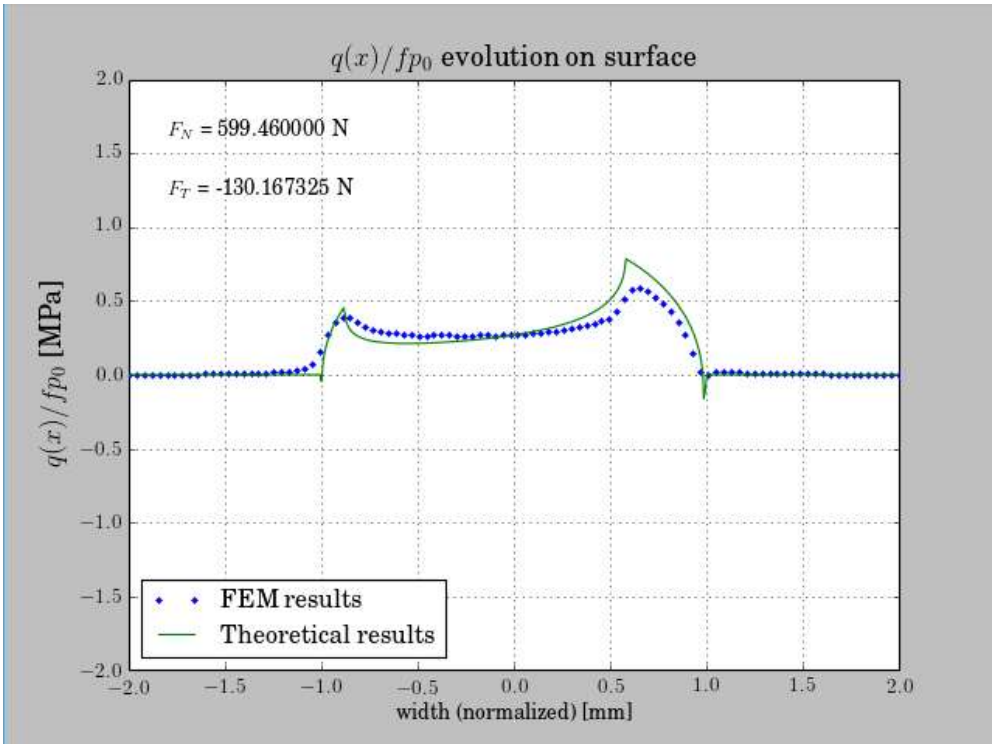

Figure 4-15: Comparison between the analytical formulation and the finite element model for the shear tractions at the surface for a pad radius of 70mm.

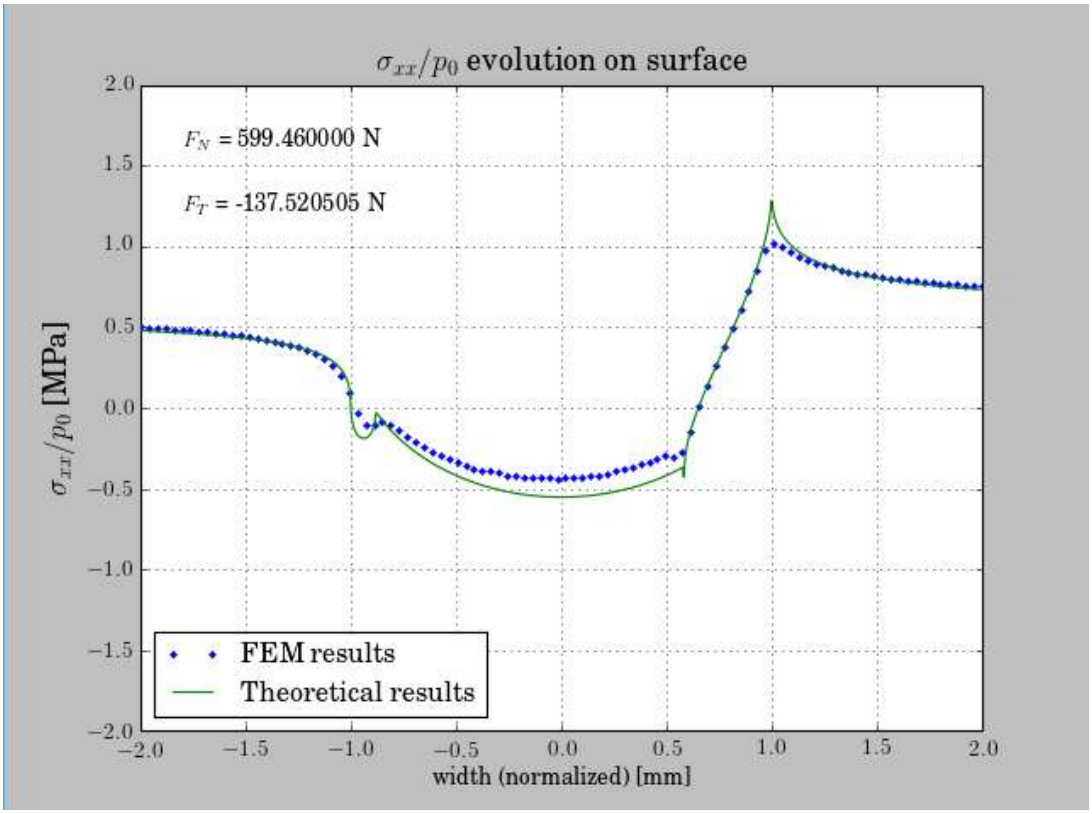

Figure 4-16: Comparison between the analytical formulation and the finite element model results for the first component of the stress, σ_{xx}, along the contact interface.

4. Determine the region where the data will be extracted. This region was described by Montebello (2015) as a circular region centred at the contact edge with a radius r such that r/R < 0,1, being R the radius of the pad. In Figure 4-10 it can be noted that the tangential and the bulk loads were implemented with a phase difference of 180°, consequently, the crack initiation is expected at the right hand side of the contact. Therefore, the circular region will be centred at the right contact edge. To respect the condition r/R<0,1 independently of the radius of the pad, it has been chosen a radius r equals to 110% of the semi-width of the contact, a:

$$\frac{r}{R} = \frac{1{,}1a}{R} = \frac{1{,}1 * 4(1-\nu^2)p_0 R}{ER} = \frac{1{,}1 * 4(1-\nu^2)p_0}{E} = 0{,}017 < 0{,}1 \qquad (4.3)$$

5. Extract the coordinates and the displacement fields for all time steps in the region defined in step 4.
6. Deduce the approximate velocity fields from the data extracted in step 5. It corresponds to the derivation of the difference between the current position of a node at time instant t and its original.

7. Select the time steps for the determination of the symmetric and anti-symmetric reference fields, $\boldsymbol{d^s}$ and $\boldsymbol{d^a}$. For the symmetric field the time step corresponds to the artificial variation of the pressure and for the anti-symmetric field to the step following the first peak reached by the tangential force.
8. Compute the displacement fields with the values extracted in step 6 at the time steps determined previously (equations (2.59) and (2.60)).
9. Project the reference fields on the velocity field to obtain the expression of the symmetric and anti-symmetric nonlocal parameters (equations (2.63) and (2.64)).

Application to the experimental results

For each experiment of the Group I tests and each data produced by Bellecave (2015) that was considered for our analysis (data depicted in the S-N curve in Figure 4-3). The equivalent velocity field was extracted using a finite element analysis as just detailed above. The nonlocal intensity factors were computed by post-processing the results. Only the symmetric and the anti-symmetric intensity factors will be represented in the I^s-I^a map (Figure 4-17, Figure 4-18 and Figure 4-19). The results were classified in terms of pad radius and number of cycles to failure.

One of the objectives of this study was to evaluate whether the new nonlocal parameters (I^s, I^a) could be somehow correlated with the life of a system submitted to a fretting fatigue loading. According to this hypothesis, one would expect that if tests present different stress gradient (different pad radii), but end at a similar life, a correlation law may appear between I^s and I^a. Indeed, as can be seen in Figure 4-17, for the experiments which broke around 200 000 cycles, and in Figure 4-18 for the tests which broke around 500 000 cycles, the tests corresponding to the different radii fell all very close to a same line in the nonlocal parameters map of I^s x I^a. This result suggests that tests having different stress gradients but with the same fatigue severity (computed by a critical plane multiaxial model) at a critical distance from the hot spot at the surface would have a similar life and present a linear correlation of I^s x I^a. Therefore, it seems reasonable to consider that the nonlocal parameters could be used to predict the life of components submitted to fretting fatigue.

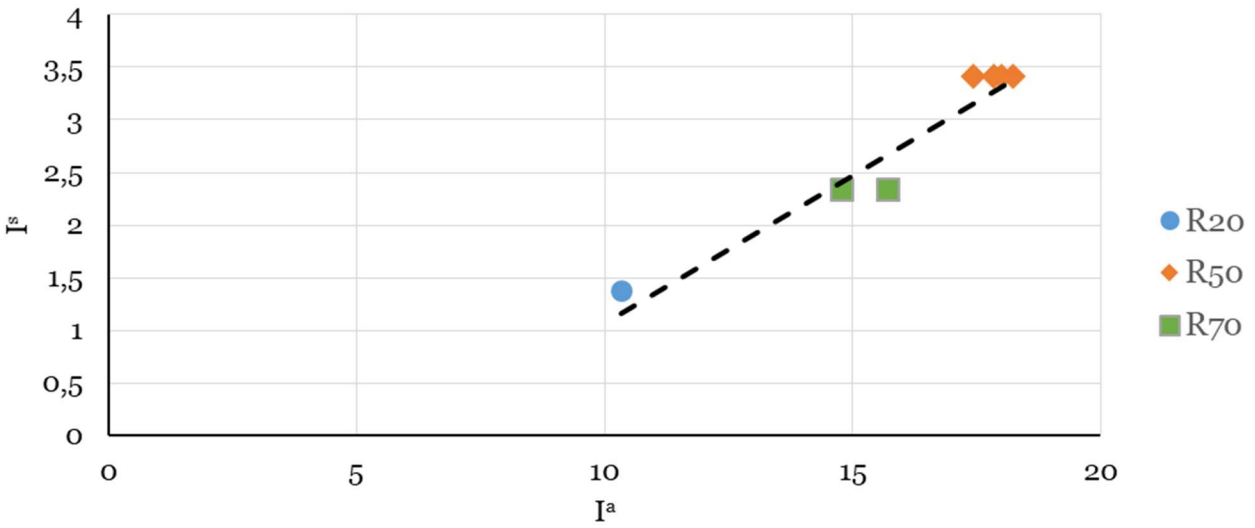

Figure 4-17: Nonlocal map for experiments configuration considering three different pad radii. All experiments represented on this map have broken around 200 000 cycles.

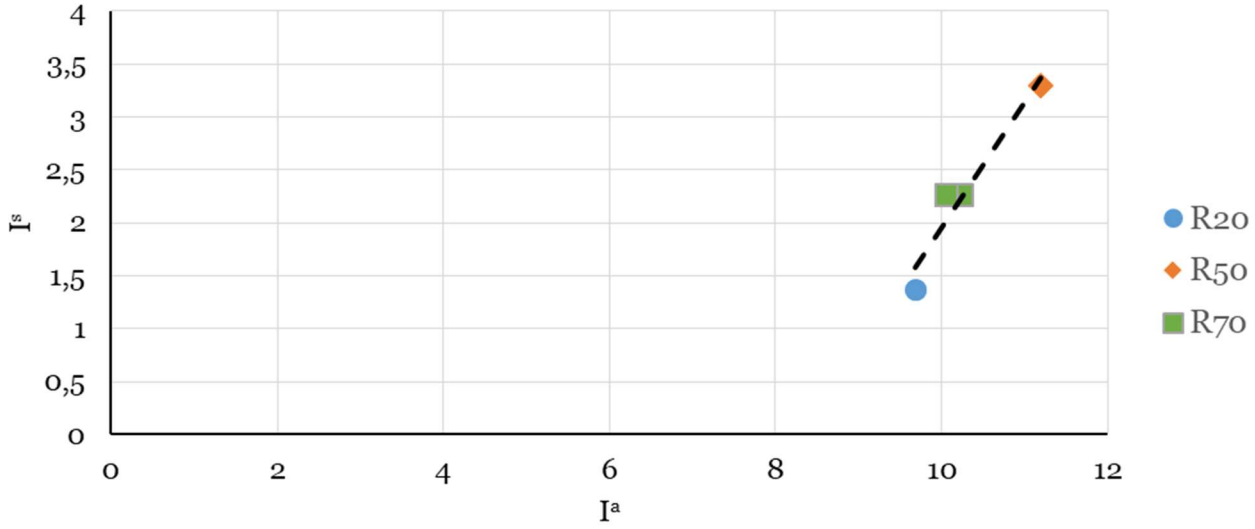

Figure 4-18: Nonlocal map for experiments configuration considering three different pad radii. All experiments represented on this map have broken around 500 000 cycles.

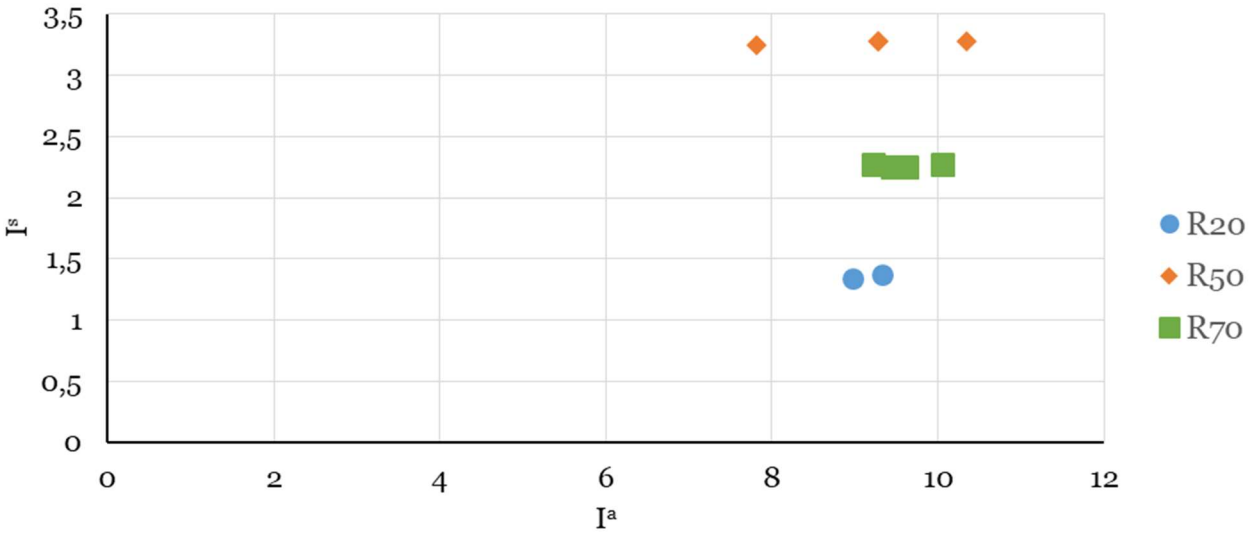

Figure 4-19: Nonlocal map for experiments configuration considering three different pad radii. All experiments represented on this map have ran-out.

4.4. Influence of the maximum normal stress on the crack initiation process

It is usually admitted by some authors that, under fretting conditions, the crack initiation process is mainly dominated by the normal and tangential contact forces (Nishioka and Hirakawa, 1969). Based on this hypothesis, Montebello (2015) only proposed that the crack initiation threshold was mode II dominated, i.e., he discarded the contribution of the normal stress to express the crack initiation boundary:

$$I^a_{max} = 2\frac{\Delta K_{th}}{K}\frac{\tau_{-1}}{\sigma_{-1}} \tag{4.4}$$

However, Venkatesh et al. (2001) have conducted four series of tests to study the effect of the bulk load on fretting fatigue. The results presented highlighted the role of the initiation and propagation of small cracks on the lives of the specimens. These results suggested that an increase of the bulk load could lead to a strong decrease of the lives of small cracks. This observation motivated us to investigate the role of the maximum normal stress for the determination of the crack initiation boundary. The resulting crack initiation boundary, as previously determined in section 2.5, is then formulated as:

$$I^a_{max,1} = 2\frac{\Delta K_{th}}{K}\frac{\tau_{-1} - \sqrt{2}\kappa + \sqrt{\left(\tau_{-1} - \sqrt{2}\kappa\right)^2 - 2\frac{K}{\Delta K_{th}}\sigma_{-1}\kappa(1-\sqrt{2})I_s}}{\sigma_{-1}} \tag{4.5}$$

Figure 4-20 and Figure 4-21 establish the frontier (vertical solid line) between safe life (for 10^6 cycles) and failure according to the MWCM written in terms of the nonlocal parameters. The dashed lines represent a ±10% bandwidth in the accuracy of the estimates, while the dotted trace lines correspond to ±25% bandwidth. Two approaches are compared here. First, the complete formulation of the multiaxial criterion (but written in terms of the nonlocal parameters) is considered, i.e., the equivalent shear stress and the maximum normal stress are assumed both to influence the crack initiation process (equation (4.5)) (Figure 4-20). With this formulation, all the points, expressed in terms of nonlocal intensity factors, fell within the nonlocal initiation boundary considering the ±25% bandwidth. Indeed, most results fell inside the ±10% bandwidth and the errors involved concerned conservative estimates, i.e, crack initiation was estimated while the assembly achieved run-out.

However, when only the equivalent shear stress amplitude is taken into account to characterize the crack initiation process under fretting fatigue conditions (equation (4.4)) (Figure 4-21), all data for the 3 different fretting configurations (R=20mm, R=50mm and R=70mm) are estimated to fail before 10^6 cycles.

Thus, it seems reasonable to assume that, for fretting fatigue, although the crack initiation process is usually dominated by shear stress amplitudes, the influence of the maximum normal stress is not negligible. Therefore, in a laboratory environment, equation (4.5) will give more accurate results to estimate the crack initiation frontier, but in an industrial context, the use of the simplified equation (4.4) which discards the effect of the normal stress to define such frontier for crack initiation, will be preferred, not only because it is easier to implement, but also because it yields more conservative results.

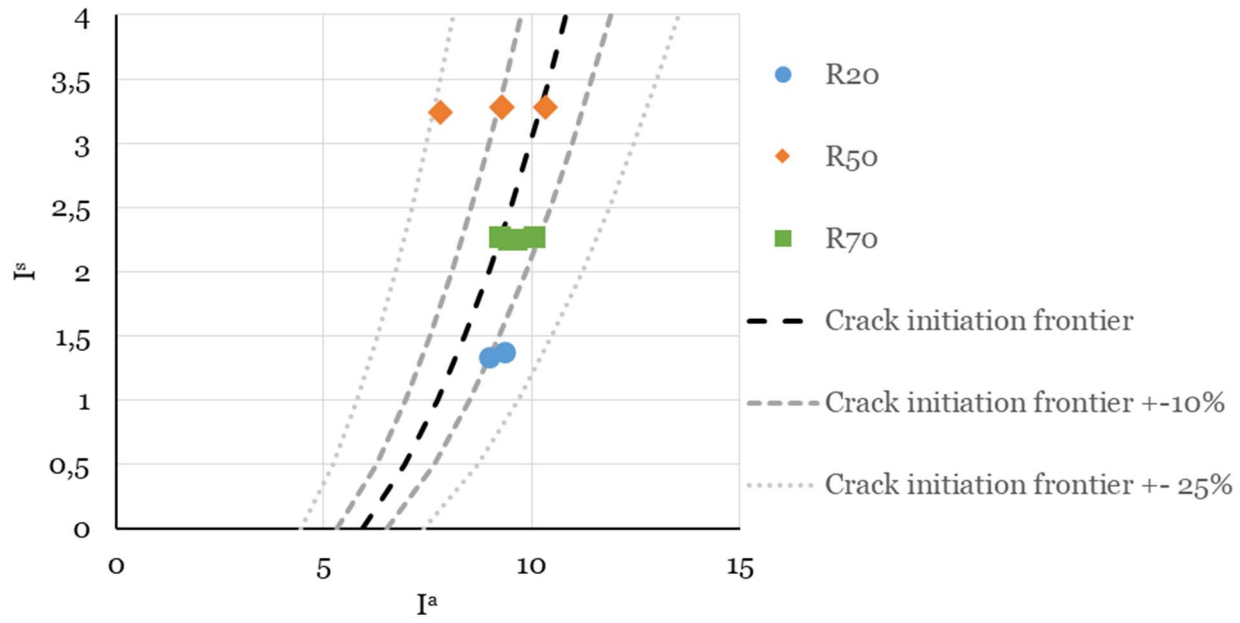

Figure 4-20: Boundary between safe and failure zones written terms of I^a and I^s and in accordance with equation (4.5) and the experimental results obtained for an infinite life (at 1 000 000 cycles).

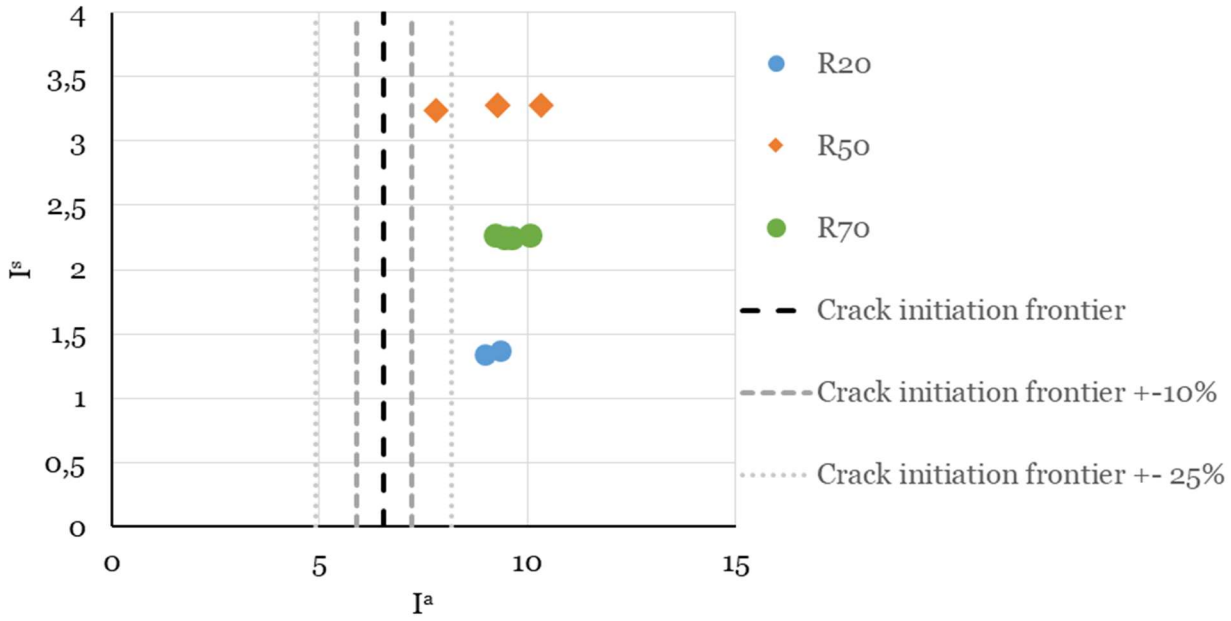

Figure 4-21: Boundary between safe and failure zones written terms of I^a and I^s and in accordance with equation (4.4) and the experimental results obtained for an infinite life (at 1 000 000 cycles).

4.5. Discussion of the analysis

A methodology was applied to try to predict the crack initiation boundary for the system submitted to fretting fatigue. This consisted of a multiaxial fatigue model (the Modified Wölher Curve Method), written in terms of two stress intensities/non-local parameters, applied in

conjunction with the Theory of the Critical Distances. These results showed that the application of this methodology was capable to estimate the crack initiation boundary with precision of ±10% in most cases considered in the experimental programme (Figure 4-20). This level of accuracy is similar to the one obtained by Araújo et al. (2007), who used a similar multiaxial criterion and theory of critical distance approach, but in stress basis, to model crack initiation under fretting fatigue conditions. In the case of the correlation between the nonlocal parameters I^a and I^s for a specific fatigue life, the results obtained for this Ti-6Al-4V (Figure 4-17,Figure 4-18 and Figure 4-19) seem to suggest that tests under a different stress gradient but that have a same fatigue index at the critical distance will have a linear correlation for finite lives (200.000 and 500.000 cycles). However, for tests under run out conditions, a larger dispersion was clearly present which do not allow us to firmly conclude that this linear correlation between I^s and I^a can be extended for run out tests. The conduction of further tests considering different materials and contact geometries would be necessary to draw a more firm conclusions anyway.

The comparative part of the study, concerning the effect of the maximum normal stress on determining the boundary between safe and failure zones, shows that, for this specific case (fretting crack initiation), the maximum normal stress has an effect on the computation of the fatigue damage, but is not a dominant variable. Indeed, it appears that the equivalent shear stress represents 75% of the definition of the crack initiation boundary. This result confirms the observation of Venkatesh et al. (2001).

One possible explanation for the dominant role of the normal stress in the crack initiation process is that, in ductile materials, the crack initiation process is usually associated with the formation of persistent slip bands, hence the amplitude of the shear stress in the early stages of crack initiation should play a much more important role in this process than the maximum normal stress.

In this work an “approximate velocity field” is determined with respect to a moving reference frame attached to the contact front and so, at a first glance, it should not be derived to obtain the stress tensor due to static loads, as the normal contact force. However, this methodology has been developed to handle more complex loadings and general contacts geometries, which cannot be solved using analytical approaches.

Future work will focus on two aspects. First, an attempt to use simplified kinematics will be considered to speed up the finite element analysis. The use X-FEM, as it is already been conducted for the study of fretting cracks, generates a good expectation (Giner et al.; 2011). On the other hand, the application of this nonlocal methodology to more complex geometries, such as an industrial assembly, e.g. the connection between blades and disc in aeroengines, and the establishment of experiments with 3 dimensional contacts may bring interesting results and

allow the reduction in the number of tests needed to validate the design of an industrial assembly against fretting fatigue, for which the analytical expressions cannot be applied.

Chapter 5. Study of the size effect on fretting fatigue

5.1. Introduction

Experimental campaigns carried out with single or two vertical actuators fretting fatigue rig, combined with different fatigue criteria (Araújo et al., 2007, Fouvry et al., 2014, Dini et al., 2006, Bellecave et al., 2014), or with wear analysis (Fouvry et al., 2013, Shen et al., 2015, Li et al., 2015, O'Halloran et al., 2017), have proved to be able to describe reasonably well the crack initiation and propagation phenomena. Although these models have become quite robust, being able to include not only the effects of the multiaxial stress state and of the non-proportional character of the stress history in fretting fatigue, but also the well-known stress gradient effects, their use have been usually confined to model/study laboratory contact configurations. It still remains difficult to transpose the experimental results obtained with these small laboratory contacts to large industrial interfaces.

The size effect, i.e. the change of response when the spatial dimensions are scaled up or down while the geometry and all other characteristics are preserved, is a problem of every physical theory. The size effect problem in fretting fatigue have started to receive attention these lasts years. As far as the author is aware, the works of the literature referencing this problem may be categorised into two categories. The first one usually considers effects of the size of the contact (or the size of the pad radius) on the fretting fatigue life or resistance (Bramhall, 1973, Nowell, 1988). One should notice that, somehow, this could be considered as a misuse of the term "size effect", as the reduction in life observed for tests under larger contact sizes is clearly related to the milder stress gradient that these tests had compared with the ones that had small contacts. Therefore, such effect was related to the stress gradient and not to a variation on the amount of material being stressed under the contact. The second category refers to tribological approaches (Fouvry et al., 2013). Up to now, there seems to be no tests and/or analysis dedicated tackle the real issue of the size effect on fretting fatigue from a mechanistic point of view.

The aim of this chapter is to show and discuss the results of an experimental campaign conducted to gain insight on the understanding of the size effect on fretting fatigue. To describe the size influence, two size parameters were considered: (i) the volume of material being stressed under the contact and (ii) the damaged area within the slip zone under the contact.

For each of these parameters, the design of the test configuration (load history and geometry) will be detailed, as well as the experimental results, in terms of lifetimes, obtained by following the methodology presented in Chapter 3. Then, a multiaxial fatigue model, the Modified Wöhler Curve Method, now written in its original formulation, i.e., in stress basis

(not considering the non-local stress intensities) was applied to these results in conjunction with the theory of the critical distance to quantify a possible impact of the two size parameters studied on the fretting fatigue lifetimes. Finally, the Weibull's theory was applied to the experimental results to evaluate the statistical relevance the results.

5.2. Group II-a Tests: Study of the influence of the width of the specimens on fretting fatigue

Objective of Group II-a Tests

The first parameter which has interested the author of this work is the width of the specimen. Indeed, when the size effect is studied, the first question that naturally arises is: what is the effect of a diminution, or an increase in the volume of material being stressed under the contact (keeping all the other parameters in the test unchanged) on the fretting fatigue life/resistance? Group II-a tests were proposed to tackle such an issue. To modify the stressed volume, the solution proposed was to change the width of the pads and specimens while at the same time maintaining their depth as well as their contact's area.

As experimental results of Group I of Tests are available, they will be used here as the results of a first "size" of stressed volume. For these experiments, the width of the contact zone was W_{13}=13mm, the pad radius considered was R=70mm and the peak pressure p_o = 500MPa. Therefore the corresponding volume of material being stressed under the contact zone is:

$$V_{13} = 2a_{13}T_{13}W_{13} = 361{,}17mm^2 \qquad (5.1)$$

with T_{13} being the thickness of the specimen.

To vary the size of the volume of material stressed under the contact in Group II-a of tests a specimen's whose width was 8mm was chosen but pad radius (R = 70mm) and a peak pressure (500MPa) were kept constant. This leads to a volume stressed V_8 = 222,26mm², which corresponded to a reduction in volume of 38,5% when compared to V_{13}. The methodology to determine the loadings such that the volumes stressed changed but the others tests parameters (e.g. the size of the damaged area within the slip zones and the stress gradient) were kept constant is developed on the following of this section, as well as the presentation of the results.

Determination of the loading history

In order to reach the objective of the Group II-a Tests, two parameters were kept equal between the experiments performed with a width of 13mm and the ones with a width of 8mm: the area of the slip zones where the fretting damage occurred, i.e. $W_{13}(2a_{13} - 2c_{13}) = W_8(2a_8 - 2c_8)$ (Figure 5-1) and the stress gradient under the contact for x/a = -1. One should notice that if the stress gradient is the same for both specimens (8 and 13 mm width) the multiaxial fatigue index computed by the MWCM criterion (computed in stress basis) will also be the same, i.e I_{13}=I_8.

As the peak pressure is equal for both contact width, $p_o = 500MPa$, as well as the pad radius, R=70mm, it stems from the equation (2.18) that the contact semi-width, a, remains the same, i.e. $a_{13} = a_8$. Consequently, the size of the stick zone for the 8 mm width specimen may be deduced from a simple equation:

$$c_8 = a - \frac{W_{13}}{W_8}(a - c_{13}) \tag{5.2}$$

and so the value of the corresponding tangential force, Q_8, may be found by applying the equation (2.23):

$$Q_8 = fP_8\left[1 - \left(1 - \frac{W_{13}}{W_8}\left(1 - \frac{c_{13}}{a}\right)\right)^2\right] \tag{5.3}$$

being P_8 the normal force for the specimen's width of 8mm. It can be noted here that the ratio Q_8/fP_8 will not be the same as the ratio Q_{13}/fP_{13}, hence it has been deduced that the stress gradient will not be exactly the same for the specimen's width of 8mm as for the specimen's width of 13mm. However, it was possible to obtain similar stress gradient by modifying also the bulk load/stress, without changing the theoretical damaged area. To determine the bulk load which best fit the stress gradient obtained for the contact's width of 13mm, a numerical procedure was implemented. This procedure can be described in the following steps:

i) The multiaxial parameter, I_{13}, is computed from the surface until $y = 0{,}1mm$ and at $x/a = -1$, for the 13mm specimen. This index was computed by applying the Modified Wöhler Curve Method in a stress basis and by calculating the equivalent shear stress amplitude with the Maximum Rectangular Hull Method. The detailed procedure can be found in the section 2.3.

ii) The corresponding values of the multiaxial parameter for $W = 8mm$, I_8, are then computed. The process starts by assigning a low value to the bulk load for the configuration with $W = 8mm$.

iii) The two multiaxial parameters are compared. If I_8 does not correspond to I_{13} within a tolerance of ±10%, at the critical distance, the value of the bulk load is increased by steps of 1MPa. Otherwise, the value obtained for the bulk load is saved.

Figure 5-2, Figure 5-3 and Figure 5-4 present the graphics of the variation of the multiaxial index, I_{MWCM}, under the surface from the trailing edge of the contact. As can be seen in such graphs, it is possible to find a load combination where the variation of the multiaxial index for both specimens is nearly identical at least up to the critical distance. The loads necessary to obtain these variations, the new experimental data obtained with the Group II-a Tests, as well as the experimental results used from the Group I Tests are all reported in Table 5-1. Tests were numerated from FFS05 to FFS09 for the specimen's width of 8mm and from FFG11-FFG17 to FFG19 for the specimen's width of 13mm. All pads have a radius of 70mm. The relevant tests parameters are the stress ratio $\sigma_{b,max}/p_{o,}$ the load ratio Q_{max}/fP and the theoretical damaged area, A_{th}^{D}, given in mm². The corresponding lifetimes of each experiment are reported as "Number of cycles". Run out conditions were established at 1 000 000 cycles, i.e, tests that did not break at this number of cycles were interrupted.

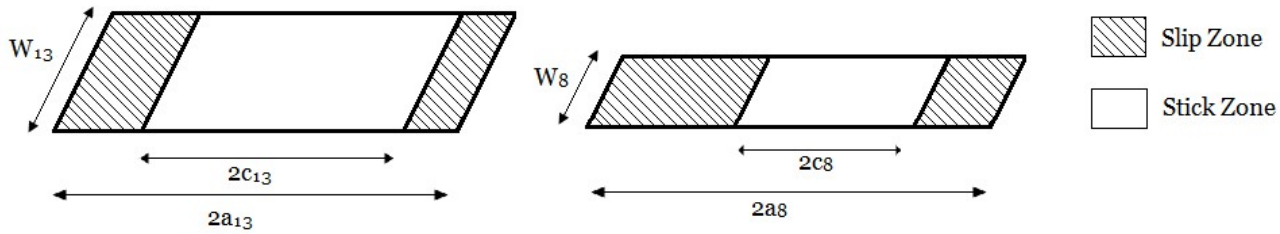

Figure 5-1: Scheme of the damaged area for both specimen widths.

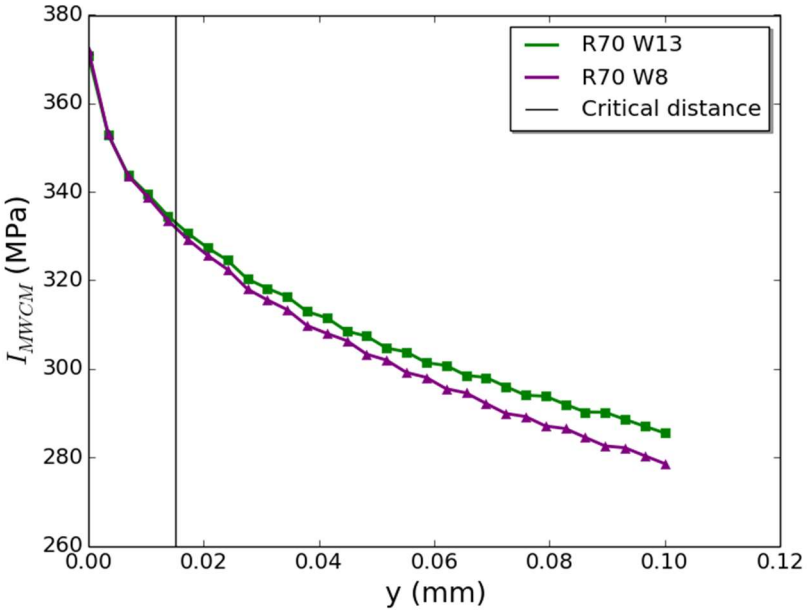

Figure 5-2: Evolution of the stress under the contact at x/a = -1 for both specimen widths (For W_{13}: $\sigma_{B,max}/p_0$ = 0,6; Q/fP =0,46. For W_8: $\sigma_{B,max}/p_0$ = 0,45; Q/fP =0,68).

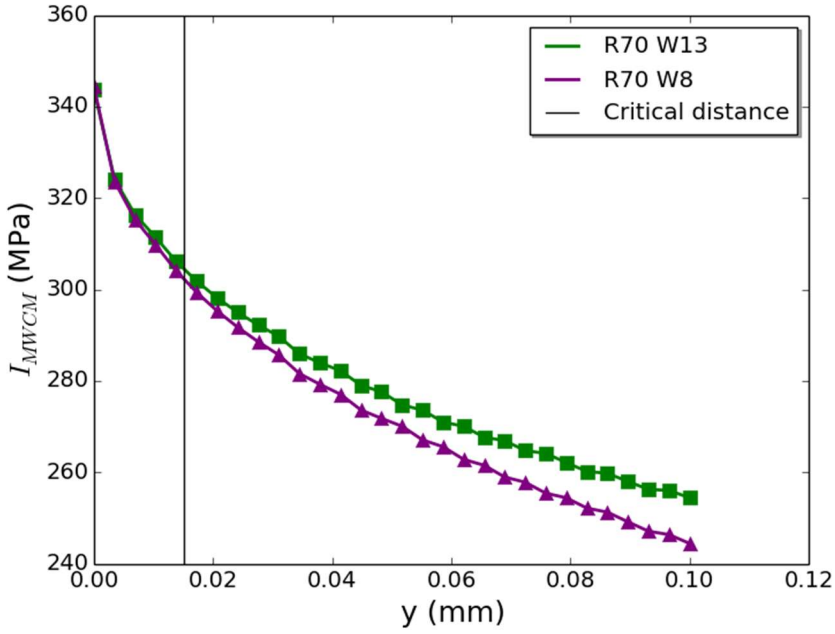

Figure 5-3: Evolution of the stress under the contact at x/a = -1 for both specimens widths (For W_{13}: $\sigma_{B,max}/p_0$ = 0,46; Q/fP =0,44. For W_8: $\sigma_{B,max}/p_0$ = 0,30; Q/fP =0,65).

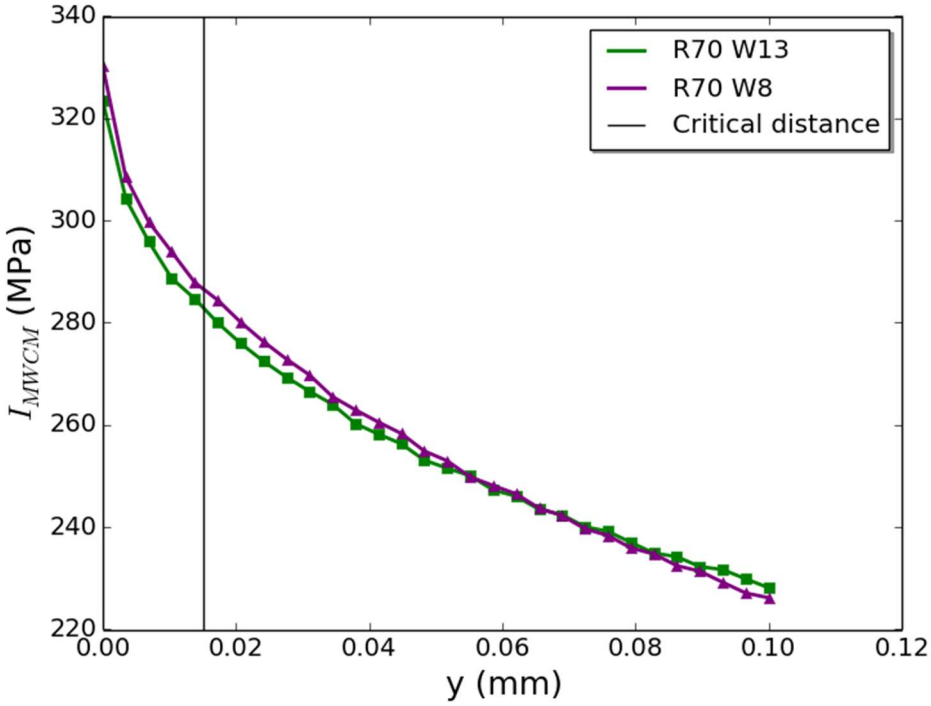

Figure 5-4: Evolution of the stress under the contact at x/a = -1 for both specimens widths (For W_{13}: $\sigma_{B,max}/p_0$ = 0,36; Q/fP =0,43. For W_8: $\sigma_{B,max}/p_0$ = 0,24; Q/fP =0,63).

Test	Width (mm)	Radius (mm)	$\sigma_{B,max}/p_0$	Q/fP	I_{MWCM} at L/2=15µm (MPa)	A_{th}^{D}(mm²)	Number of cycles
FFS05	8	70	0,45	0,68	331	7,43	153 047
FFS07	8	70	0,45	0,68	331	7,43	240 321
FFS06	8	70	0,45	0,68	331	7,43	261 871
FFG11	13	70	0,6	0,46	332	7,37	166 150
FF07	13	70	0,6	0,46	332	7,37	168 266
FFS09	8	70	0,3	0,65	301,5	7,01	671 534
FFG17	13	70	0,46	0,44	304	6,99	473 954
FFG18	13	70	0,46	0,44	304	6,99	412 440
FFS08	8	70	0,24	0,63	287	6,70	1 000 000
FFG19	13	70	0,36	0,43	282	6,81	1 000 000

Table 5-1: Experimental results of the first section of the Group II-a Tests.

The evolution of the multiaxial index, in the sense of the Multiaxial Wöhler Curve Method, in conjunction with the theory of the critical distance has been plotted in the Figure 5-5 for both widths.

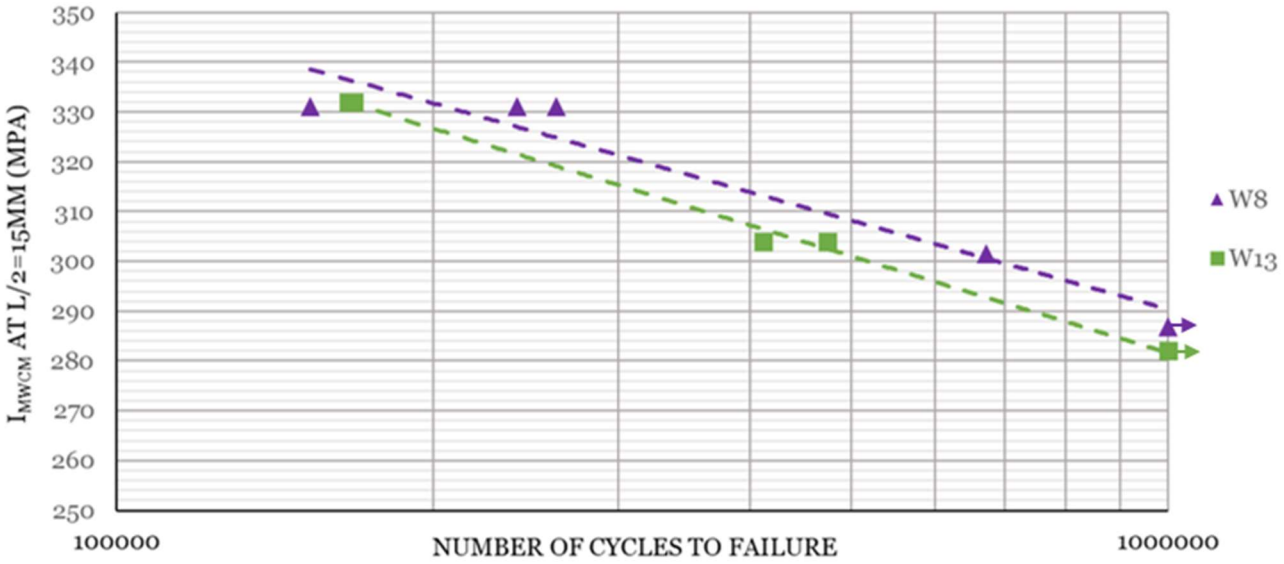

Figure 5-5: Evolution of the multiaxial index computed at the critical distance as a function of the number of cycle to failure for both specimens widths.

Fretted area examination

The analysis of the Group II-a Tests was based on the hypothesis that not only there was nearly equal variation of the multiaxial fatigue index with distance from the surface for both specimens/pad widths studied, but that the damaged area within the slip zone was the same between tests although there were different volumes of materials being stressed under the contact zones. This hypothesis was theoretically verified, with a difference of around 1% between these areas (Table 5-1) for each loading condition. However, an experimental verification was necessary.

To obtain the fretting scar of the different experiments, tests were repeated and interrupted after 50 000 cycles to avoid all risk of failure. Then, a chemical attack was realised to remove debris generated by the fretting on the surface. A solution composed of 8g of ammonium persulphate, $(NH_4)_2S_2O_8$, 1mL of hydrofluoric acid, HF and 99mL of water, H_2O was used. Finally, specimens were observed with a confocal microscope and the slips and stick zones were isolated and measured. Figure 5-6 presents an example of the fretting scars obtained for the specimen's whose widths was 8mm (Figure 5-6 (a)) and for the ones with 13mm (Figure 5-6 (b)).

Several observations can be obtained by analysing these photographs. First, even if most of the debris was removed from the surface, the limits of the slip zones are not always clear nor regular, particularly for the specimens of 8mm width. Thus, a tolerance of ±10% will be considered for the measured widths of the stick ($2a_m$) and of the slip zones ($2c_m$), as well as for the measured fretting damaged areas (A_m^D). These values are reported in Table 5-2, together with the theoretical values ($2a_{th}$, $2c_{th}$ and A_{th}^D) for each test conducted. The values resulting from the tolerance applied appear into parenthesis. Also from Figure 5-6 one can identify the slip zones, where a clear superficial damage occurred, and the stick zone, which remains intact. Finally, the effect of the bulk load can be noticed. Indeed, the upper slip zone appears to be larger than the lower one in both cases.

(a)

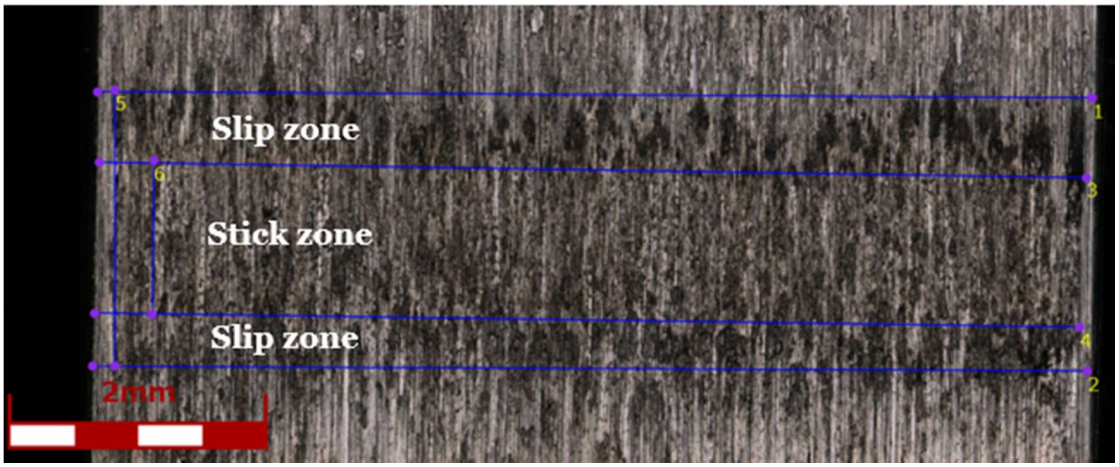

(b)

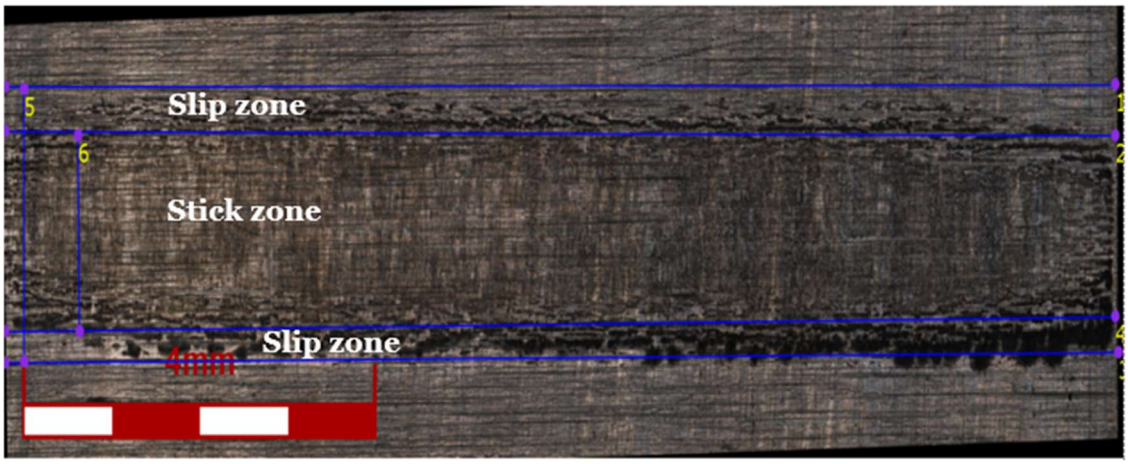

Figure 5-6: Fretting scar of tests which led to failure around 200 000 cycles: (a) with a specimen's width of 8mm, (b) with a specimen's width of 13mm

Tests	Specimen's width (mm)	$2a_{th}$ (mm)	$2c_{th}$ (mm)	A_{th}^{D} (mm²)	$2a_m$ (mm)	$2c_m$ (mm)	A_m^D (mm²)
FFS05/ FFS06/ FFS07	8	2,14	1,21	7,43	2,15 (1,94-2,37)	1,20 (1,08-1,32)	7,60 (6,84-8,36)
FFG11/ FF07	13	2,14	1,57	7,36	2,14 (1,93-2,35)	1,55 (1,40-1,71)	7,67 (6,90-8,43)
FFS09	8	2,14	1,26	7,01	2,10 (1,89-2,31)	1,25 (1,13-1,38)	6,80 (6,12-7,48)
FFG17/ FFG18	13	2,14	1,60	6,99	2,11 (1,90-2,32)	1,53 (1,38-1,68)	7,54 (6,79-8,30)
FFS08	8	2,14	1,30	6,70	2,10 (1,89-2,31)	1,29 (1,16-1,42)	6,48 (5,83-7,13)
FFG19	13	2,14	1,61	6,81	2,13 (1,92-2,34)	1,55 (1,40-1,71)	7,54 (6,79-8,30)

Table 5-2: Theoretical and measured values of the global contact and stick zones for the Group II-a Tests loading conditions.

Some remarks on the experimental results and microscope observations

The stress gradients (expressed in terms of the fatigue index computed with the Multiaxial Wöhler Curve Method) resulting from the loads applied for the tests FFS05 to FFS09 (8mm width specimens) have, up to the critical distance, a very similar variation with distance from the surface to the tests carried out with the 13mm width specimens (Figure 5-2, Figure 5-3 and Figure 5-4). The difference in terms of the multiaxial index is nearly null at the surface and less than 1% at the critical distance for two corresponding tests. It can be noted that the multiaxial index is slightly smaller for the 8mm broken specimens than for the 13mm ones, and that it is slightly higher for the run-out test with 8mm specimens than for the specimens with 13mm. Moreover, the difference between the theoretical fretting damaged areas within the contact for the 13mm and for the 8mm specimens is less than 2%. Therefore, the only parameter which, theoretically, varied significantly between the tests which used the 8mm specimens (FFS05 to FFS09) and the ones with the 13mm ones (FFG11-FFG17 to FFG19 and FF07) was the volume of material stressed under the contact zone.

Three tests were carried out with a width of 8mm, Q/fP=0,68 and $\sigma_{B,max}/p_o$=0,45 (FFS05 -FFS07). Although there is a dispersion between the results (around ±50 000cycles), these 3 tests broke around 200 000 cycles. Only one test was carried out for Q/fP=0,65 and

$\sigma_{B,max}/p_o$=0,3 and for Q/fP=0,63 and $\sigma_{B,max}/p_o$=0,24, hence no conclusion can be firmly expressed, but the evolution of the tendency curve of the results is coherent and so the experimental results should be considered reliable.

The microscope observations of the surface (Figure 5-6) and the results presented in Table 5-2 show a slight difference between the theoretical contact sizes and the measured ones. For both specimen's width, the peak pressures, p_o, leading to these contact sizes would be up to 2,5% lower than the theoretical ones. Similarly, a disparity between the theoretical slip zones size and the measured ones appeared. This difference appears to be more significant for the specimens whose width was 13mm. In these cases the measured values of the slip zones were up to 4,5% lower than the corresponding theoretical values. For the 8mm specimens this reduction was lower than 1%. These differences between the theoretical and measured values of the contact and slip zones sizes also lead to differences between the theoretical and the measured fretting damaged areas. Indeed, a decrease up to 15% of the damaged area is observed for the tests with the 8mm specimens, while an increase up to 10% of this damaged area appeared for the tests with the 13mm specimens.

Lifetimes obtained for the tests with the 8mm and the 13mm specimens were similar (Figure 5-5). Under similar loading conditions, the test with specimens whose width was 8mm were around 10% longer than the ones with the 13mm specimens. This difference is of the order of the dispersion of the fretting fatigue tests results. Moreover, the same level of stress lead to run-out tests in both configurations. The highest difference in terms of number of cycles to failure, appears between Tests FFS09 and FFG17-18. Indeed, in this case, the test with the 8mm specimen lasted around 50% longer than the ones with 13mm. This experiment corresponded to the test which presented the strongest disparity in terms of damaged area with a reduction of 20% of this areas for the test carried out with the 8 mm specimen.

5.3. Group II-b Tests: Influence of the damaged area on fretting fatigue

Objective of the Group II-b Tests

The first section of this group of tests has shown that the width of the specimen does not have a significant influence on the crack initiation process. Hence, the Group II-b Tests will focus now on investigating the influence of the size of the fretting damaged area. Indeed, the post failure investigation carried out in section 4.2 of Chapter 4 has shown that cracks initiate preferentially within the slip zone, at, or close to, the trailing edge of the contact. Hence, it may be postulated that, statistically, if the slip zone is smaller, less superficial damage would be present and consequently one could expect less crack initiation points.

To verify this hypothesis, a methodology similar to the one followed for the first section of tests will be applied: Experiments will be carried out with a specimen whose width was of 8mm, a pad radius of 70mm and then comparisons will be conducted with the experimental results of the first group of tests (Table 4-2) which considered 13 mm specimens. One should notice that again, the load configuration will be designed so that the variation of the multiaxial fatigue index with distance from the surface will be the same for the tests with 8 and 13 mm specimens. However, the corresponding damaged areas, A_{th}^{D}, will no longer be equal between them.

Determination of loading history

As the size of the damaged area is no longer the same between tests with specimens of 13mm and of 8mm width, it does not exist anymore a constraint on the value of the tangential force *Q*. Thus, it has been decided to keep the same value of the bulk force for the two configurations, i.e. $\sigma_B^8 = \sigma_B^{13}$, σ_B^8 and σ_B^{13} being the bulk stresses associated with the loads applied to the 8 and 13 mm specimens, respectively. This means that the ratio $\sigma_{B,max}/p_o$ will be the same for both.

To determine the value of the tangential load, which yields a similar stress gradient evolution for *W=8mm* and for *W=13mm*, a similar numerical procedure as for the first sub-section of tests was applied:

i) The multiaxial parameter, I_{13}, is computed for the 13mm specimens at the trailing edge of the contact, *x/a=-1*, from the surface up to *y=0,1mm*. As previously performed, the multiaxial index is computed by applying the Modified Wöhler Curve Method. The equivalent shear stress amplitude in this model is calculated by the Rectangular Hull Method.

ii) The corresponding values of the multiaxial parameter for *W=8mm*, I_8, are computed. Initially, a low value is assigned to the tangential load for the *8mm* specimen.

iii) The two multiaxial parameters are then compared. If, at the critical distance, I_8 does not correspond to I_{13} within a tolerance of ±20% the value of the tangential force is increase by step of 10N. Otherwise, convergence is achieved and the value of the tangential force is saved.

iv) Once an approximate value of the tangential load is obtained, the procedure is further refined by restarting the search with the temporary value for the tangential force found in the previous step. Then, a new reduced tolerance is set to 10% and the load increments reduced to 1N. The search goes on until convergence is achieved.

The resulting graphics of the procedure showing the variation of the Multiaxial Index, $I_{MWCM,}$ under the surface, are depicted in Figure 5-7, Figure 5-8 and Figure 5-9. It should be noticed that, for all experiments in this group, the values obtained for the tangential load led to a same ratio *Q/fP* for both specimens width, and so to the same size of the stick zone, *2c* (Figure 5-10), although the theoretical fretting damaged areas, A_{th}^{D}, were different. The results in terms of number of cycles to failure are reported in Table 5-3 for both specimens width (8 and 13mm). The pad radius was 70mm. Relevant information on the loadings history is also reported in such a Table, as the stress ratio $\sigma_{B,max}/p_o$ and the load ratio *Q/fP*, as well as the corresponding values of the multiaxial index, I_{MWCM}, at the critical distance. The theoretical damaged areas, A_{th}^{D}, are specified in mm². Figure 5-11 shows the evolution of the multiaxial index calculated at the critical distance as a function of the number of cycles to failure for both specimen widths.

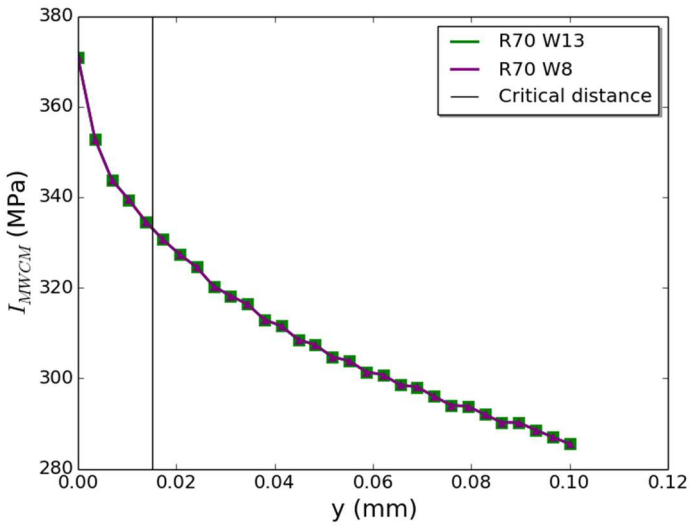

Figure 5-7: Evolution of the multiaxial fatigue index under the contact at x/a = -1 for both specimen widths ($\sigma_{B,max}/p_o$ = 0,6; Q/fP =0,46).

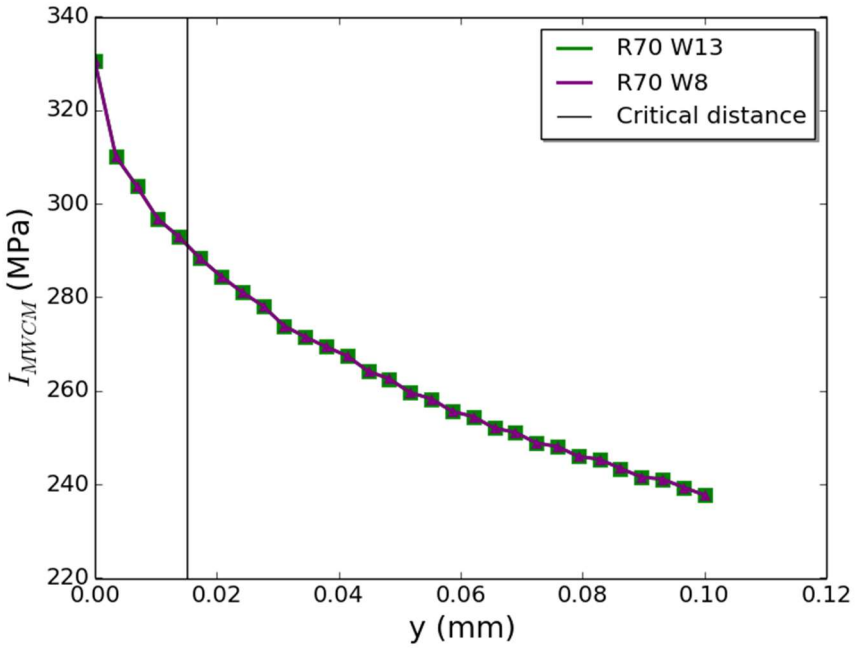

Figure 5-8: Evolution of the multiaxial index under the contact at x/a = -1 for both specimen widths ($\sigma_{B,max}/p_0$ = 0,4; Q/fP =0,42).

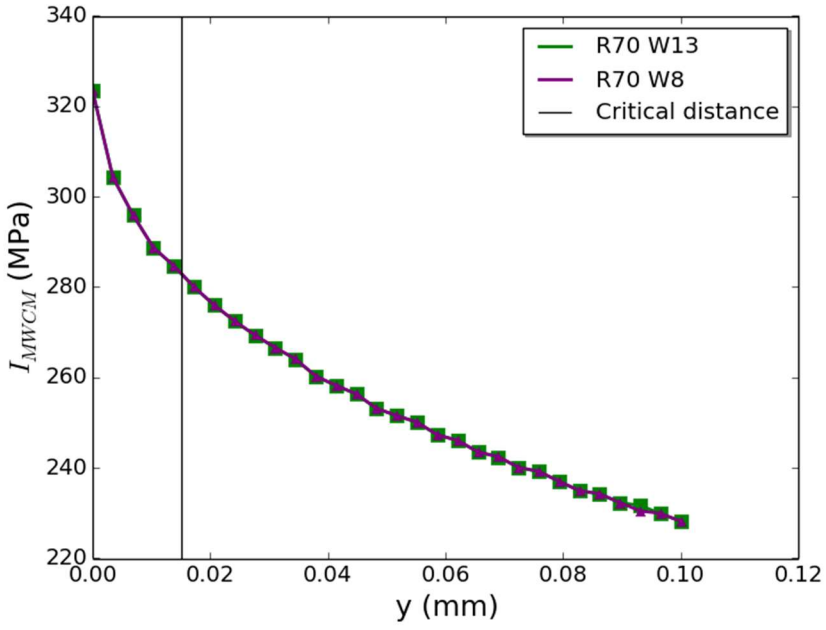

Figure 5-9: Evolution of the multiaxial fatigue index under the contact at x/a = -1 for both specimen widths ($\sigma_{B,max}/p_0$ = 0,36; Q/fP =0,43).

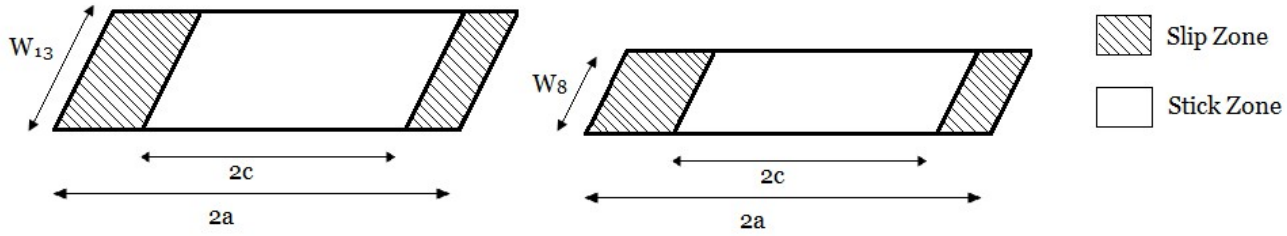

Figure 5-10: Scheme of the different contact areas for 13mm and 8mm specimens, width with the same stick zone size, but different fretting damaged areas.

Test	Width (mm)	Radius (mm)	$\sigma_{B,max}/p_o$	Q/fP	I_{MWCM} at $L/2=15\mu m$ (MPa)	A_{th}^{D}(mm²)	Number of cycles
FFS10	8	70	0,6	0,46	332	4,53	207 185
FFG11	13	70	0,6	0,46	332	7,37	166 150
FF07	13	70	0,6	0,46	332	7,37	168 266
FFS11	8	70	0,4	0,42	290	4,08	528 519
FFG12	13	70	0,4	0,42	290	6,62	495 225
FF10	13	70	0,4	0,42	290	6,62	579 954
FFS12	8	70	0,36	0,43	282	4,19	1 000 000
FFG19	13	70	0,36	0,43	282	6,81	1 000 000

Table 5-3: Experimental results of the Group II-b Tests.

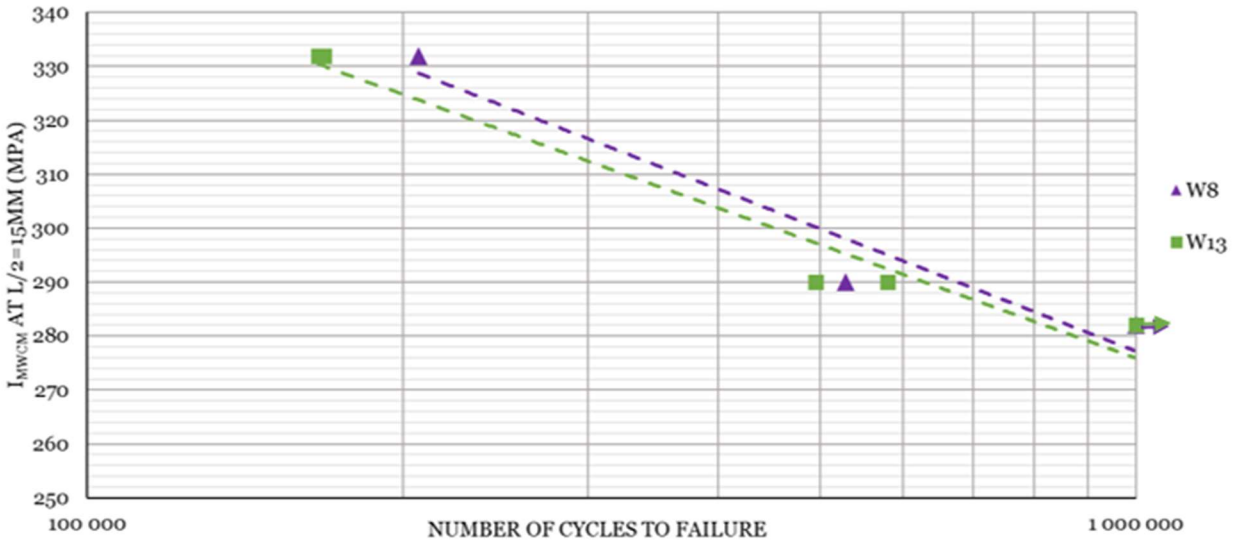

Figure 5-11: Evolution of the Multiaxial Index as a function of the number of cycles to failure for both specimen widths.

Fretted area examination

The analysis of the Group II-b Tests was based on the hypothesis of a significant reduction of the damaged area within the slip zones for the tests carried out with the 8mm specimens in comparison with the 13mm ones. This decrease in the specimen´s width provoked a reduction of around 39% in the superficial damaged area compared with the 13 mm specimens. Table 5-4 reports not only the theoretical and measured values of the contact ($2a_{th}$ and $2a_{m}$) and of the stick zone sizes ($2c_{th}$ and $2c_{m}$) but also the corresponding fretting damaged areas. Figure 5-12 presents an example of the fretted scar observed for a run-out experiment for the different specimen's width. The same chemical attack as presented in section 5.2 of the present Chapter was used to remove most of the oxides debris. However, if the slip zones appear to be quite well delimited for the 13mm specimens (Figure 5-12 (b)), their limits were not so clear nor regular for the 8mm ones (Figure 5-12 (a)) and had to be estimated.

In the photographs presented in Figure 5-12, the eccentricity due to the bulk load applied does not appear clearly. However, the lower slip zone in each photo seem to be slightly larger for both specimens. In these zones, severe damages appear while the stick zones remain intact.

(a)

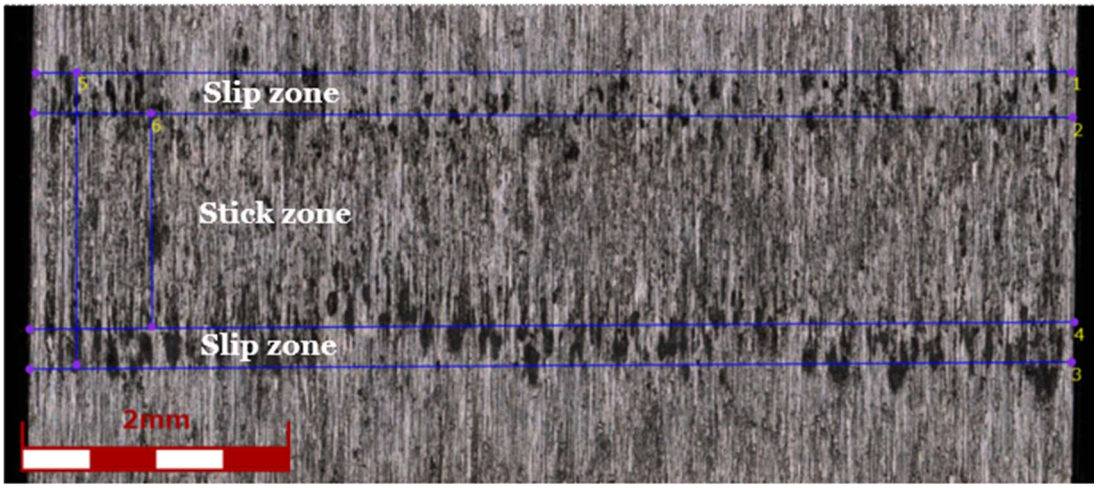

(b)

Figure 5-12: Fretting scar of run-out test: (a) specimen's width of 8mm, (b) specimen's width of 13mm

Tests	Specimen's width (mm)	$2a_{th}$ (mm)	$2c_{th}$ (mm)	A_{th}^{D} (mm²)	$2a_m$ (mm)	$2c_m$ (mm)	A_m^D (mm²)
FFS05/FFS06/ FFS07	8	2,14	1,57	4,53	2,14	1,54	5,54
FFG11/FF07	13	2,14	1,57	7,37	2,14	1,55	7,78
FFS09	8	2,14	1,63	4,08	2,11	1,60	4,09
FFG17/FFG18	13	2,14	1,63	6,62	2,10	1,59	6,47
FFS08	8	2,14	1,61	4,19	2,19	1,59	4,77
FFG19	13	2,14	1,61	6,81	2,18	1,59	7,58

Table 5-4: Theoretical and measured values of the contact and stick zone sizes, as well as for the fretting damaged areas for the Group II-b Tests loading conditions.

Some remarks on the experimental results and microscope observations

All the experiments carried out with the specimens and pads whose width was of 8mm have the same Q/fP and $\sigma_{B,max}/p_o$ ratios of their corresponding experiments carried out with the 13 mm specimen and pads. This yielded a same variation of the multiaxial index under the surface (and at x/a=-1) between tests FFS10 and FFG11-FF07 (Figure 5-7), FFS11 and FFG12-FF10 (Figure 5-8) and FFS12 and FFG19 (Figure 5-9). On the other hand, the theoretical fretting damaged areas was decreased by 39% for the 8 mm specimens when compared with the 13 mm ones.

The results of this Group II-b of tests revealed that lives were quite similar for fretting fatigue tests having the same pad radius but with different specimen and pad widths. These tests were designed to have the same variation of the multiaxial index although the fretting damaged areas within the slip zones were different. Therefore the size of these damage areas does not appear to influence fretting live for this alloy.

After the microscope examinations, it appears that the actual contact widths, *2a,* are greater than the theoretical ones, while the stick zones, *2c*, are smaller. This results in an increase of the damaged size areas, $A_m^D > A_{th}^D$, for both widths of specimen. This phenomenon, already observed in the section 5.2 of the present Chapter, will not be a problem for the present analysis. Indeed, although the actual damaged areas are smaller than the theoretical ones for the 13 and 8mm specimens, the ratio between the actual damaged areas of the 13 and 8mm specimens was approximately the same as the ratio for the theoretical damaged areas.

5.4. Post-failure investigation

Observations of the fretted and the fracture surface were conducted under a confocal microscope. Figure 5-13, Figure 5-14 and Figure 5-15 show different views of the specimen used in test FFS08, an experiment which broke just after 1 000 000 of cycles and was assumed to be a run-out test for the analysis.

Figure 5-13 shows an example of the damage caused on the specimen surface by the fretting mechanism. The lower slip zone, where crack occurred, appear clearer and larger than the upper slip zone. Cracks leading to failure seems to appear within the slip zone of the lower part of the specimen. The angle between the crack initiation plane and the direction perpendicular to the surface, which is illustrated in the photo shown in Figure 5-14, is around 20° and reflects a mode II crack propagation (Stage I). This pattern was observed for the different experiments with a width of 8mm. The transition to a mode I crack growth (Stage II), perpendicular to the surface, occurred after the crack reached a size around 1,7mm. Finally, multiple cracks initiation can be seen in the fracture surface (Figure 5-15). They further propagate in a plane perpendicular to the main fatigue load, until one unique crack front appeared after around 5mm.

The observation of the fretted and fracture surfaces of the specimens of 8mm revealed a similar aspect to the 13mm ones. Similar damages were observed on the surface and the same mechanisms of multiple cracks initiation and propagation. However, the crack plane presented an higher inclination for the specimen of 8mm.

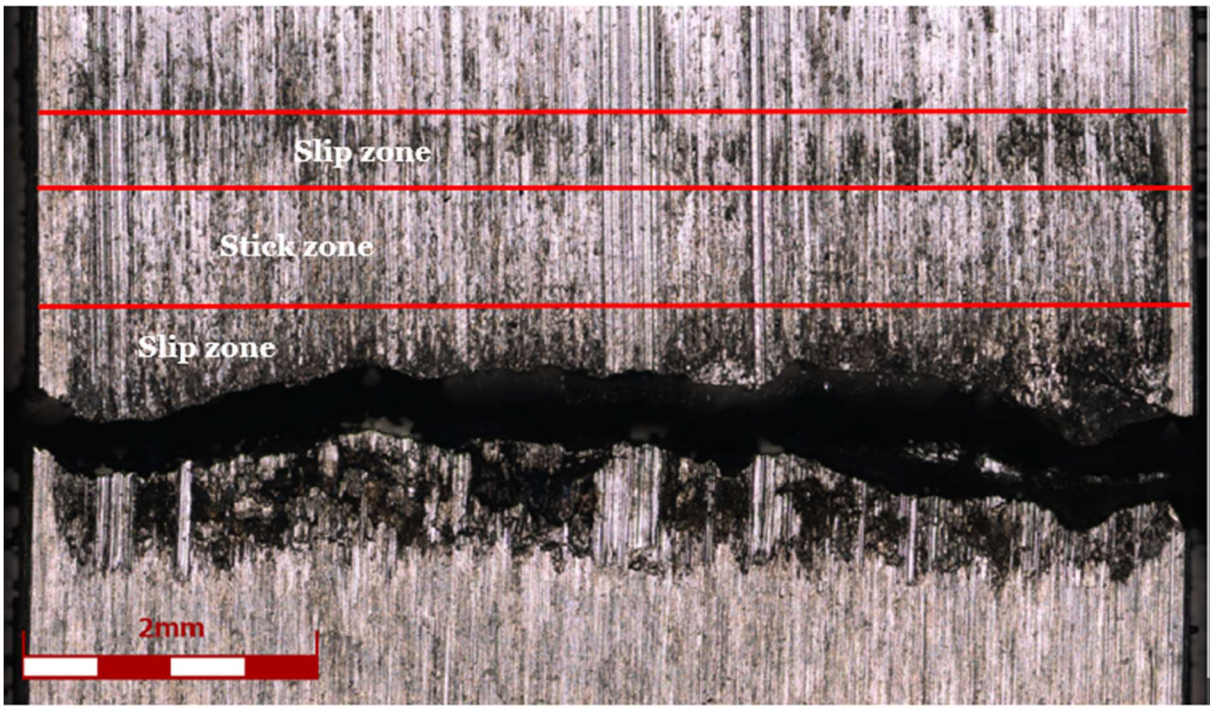

Figure 5-13: Fretted area of the 8mm specimen for pad radius R=70mm.

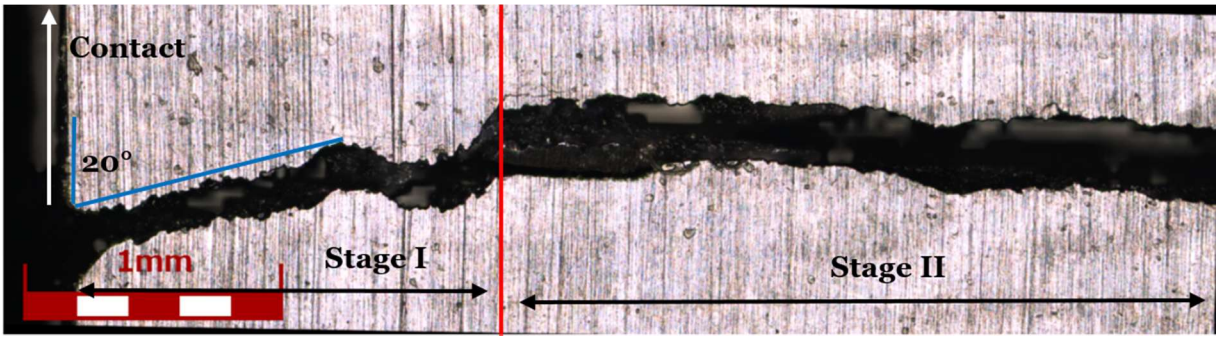

Figure 5-14: Angle of crack initiation and direction of further crack propagation for the 8mm specimen and test with pad radius R=50mm.

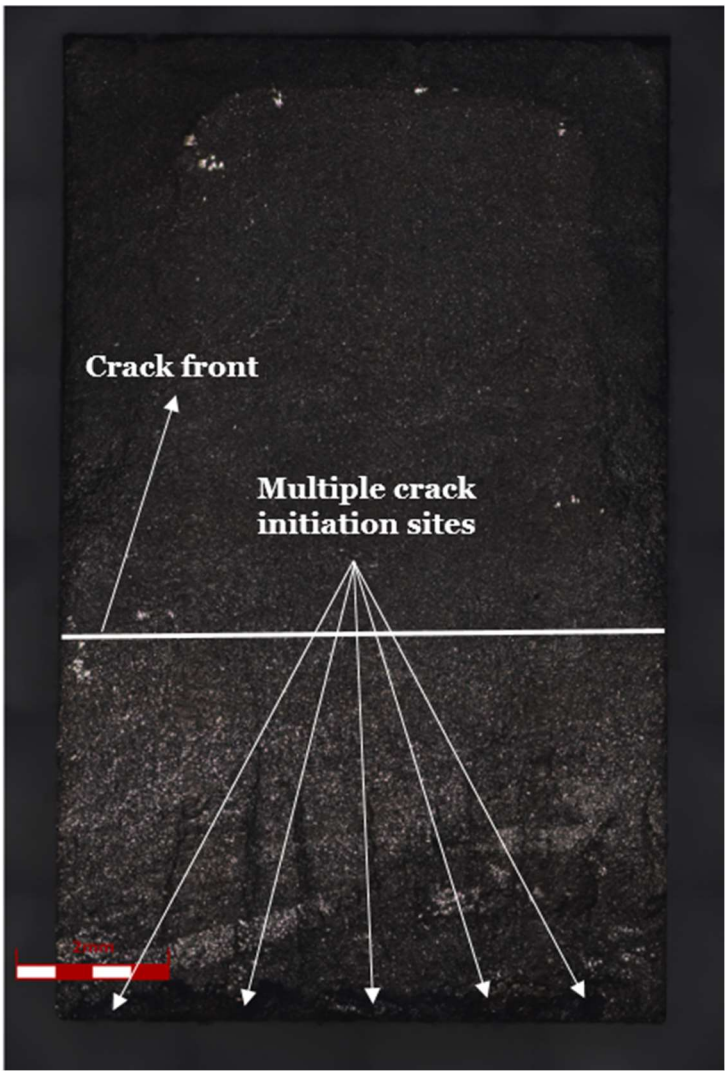

Figure 5-15: Confocal photograph of the fracture surface for the 8mm specimen and pad radius R=50mm.

5.5. Determination of the volume's influence using the Weibull's theory

Theory

The Weibull's theory is based on the theory of the weakest link proposed by Freudenthal (1968). It can be applied for materials with a low toughness because, for these materials the first crack which initiates will lead to the total failure, and so the probability of failure will depend on the probability for crack initiation. This imply a dependence between the volume being stressed and the failure of the material. Indeed, the bigger the stressed volume is, the higher the chance to initiate a crack is and so the faster the failure will happen.

The expression of the failure probability of a material given by Weibull (1951) is based on the observation that a really low applied stress will not lead to the failure and so the

probability is null, while a very high applied stress will always lead to the failure and so the probability equals to one. This may be expressed as follows (Weibull, 1951):

$$P_R(\sigma) = 1 - Exp\left[-\left(\frac{\sigma}{\sigma_W}\right)^m\right] \quad (5.4)$$

As the stress resulting from the fretting fatigue loading is multiaxial, the expression of the probability of Weibull will be expressed, for this study, in terms of the multiaxial index I_{MWCM}:

$$P_R(I_{MWCM}) = 1 - Exp\left[-\left(\frac{I_{MWCM}}{I_W}\right)^m\right] \quad (5.5)$$

Then, the failure's probability of the material depends on the exponent m, a material parameter which set the width of the distribution, and the nominal stress, I_W, which sets the value of the multiaxial index around which failure occurred for the material. To identify these parameters, the experimental results obtained with a specimen width of 13mm and a pad radius of 70mm were used; the corresponding volume stressed was V_W = 13mm^3; then the failure probability has been determined for each level of stress. The infinite life considered, i.e. the maximum number of cycles reached without failure, for this campaign was 1 000 000 of cycles. The Weibull's diagram was carried out (Figure 5-16), and the following parameters were extracted:

- m = 30,784
- I_W = 345 MPa

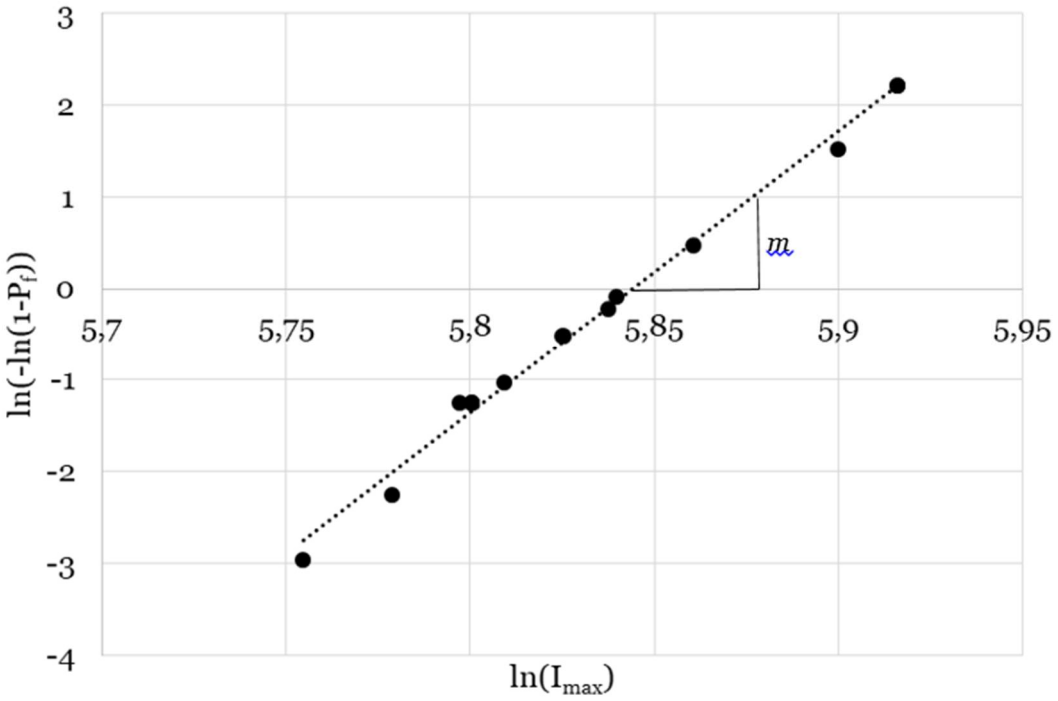

Figure 5-16: Theoretical representation of the Weibull's diagram used for the determination of the coefficient m and the nominal stress I_W.

This theory allows to highlight the failure probability of a material, but also to deal with the size effect. Indeed, according to the weakest link theory, a crack initiation in one element of the volume will lead to the failure of the whole volume. It follows that, as the parameters of the probability's law are determined for a given volume V_W, if a new experiment is conducted with a volume $V = N.V_W$ under an homogeneous stress σ, the probability of failure of the material, $P_R(\sigma)$, will be equal to the product of the probability of failure of each sub-volume V_W:

$$P_R(\sigma)^V = 1 - Exp\left[-\frac{V}{V_W}\left(\frac{\sigma}{\sigma_W}\right)^m\right] \qquad (5.6)$$

This formulation is valid for a homogeneous stress on the material. However, as it has been seen earlier, the stress under the contact will decrease rapidly. However, this stress may be considered homogeneous in an infinitesimal volume under the contact. Hence, the previous reasoning may be applied for an infinite number of sub-volumes, V_i, in the material:

$$P_R(I_{MWCM})^V = 1 - Exp\left[-\int_V \frac{dV}{V_W}\left(\frac{I_{MWCM}}{I_W}\right)^m\right] = 1 - Exp\left[-\frac{1}{V_w}\int_V \left(\frac{I_{MWCM}}{I_{max}}\right)^m dV \left(\frac{I_{max}}{I_W}\right)^m\right] \quad (5.7)$$

where I_{max} is the maximum value of the multiaxial index among all the material points analysed inside the effective volume. The integral is known as the effective volume V_{eff}:

$$V_{eff} = \int_V \left(\frac{I_{MWCM}}{I_{max}}\right)^m dV \quad (5.8)$$

It follows that:

$$P_R(I_{MWCM})^V = 1 - Exp\left[-\frac{V_{eff}}{V_W}\left(\frac{I_{max}}{I_W}\right)^m\right] \quad (5.9)$$

Application to the experimental results

The Weibull´s probability model has been applied here to statistically validate a possible effect of the size in our experimental results. The first step was to determine the effective volume in which the model would be applied. In the case of the fretting-fatigue, cracks initiate under the contact. Hence, only the zone between $x=-a$ and $x=+a$, will be considered. To capture the entire effect of the stress gradient, the effective volume will start, in the direction y, at the surface ($y=0$) and go until the opposite side of the specimen ($y=13$). Concerning the direction z, as the plain strain hypothesis is applied for both geometries, only the centre of the contact will be considered (Figure 5-17) and the results will be multiplied by the width of the specimen, W. It results:

$$V_{eff} = \int_V \left(\frac{I_{MWCM}}{I_{max}}\right)^m dV = W \int_{x=-a}^{x=a}\int_{y=0}^{y=13} \left(\frac{I_{MWCM}}{I_{max}}\right)^m dxdy \quad (5.10)$$

The effective volume was computed with respect to the equation (5.10). Then, the corresponding probabilities of failure were calculated (equation (5.9)) and the results are presented in the Figure 5-18.

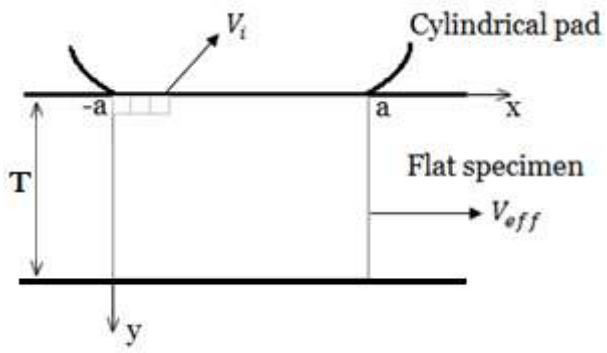

Figure 5-17: Volume studied for the Weibull's probability of failure analysis.

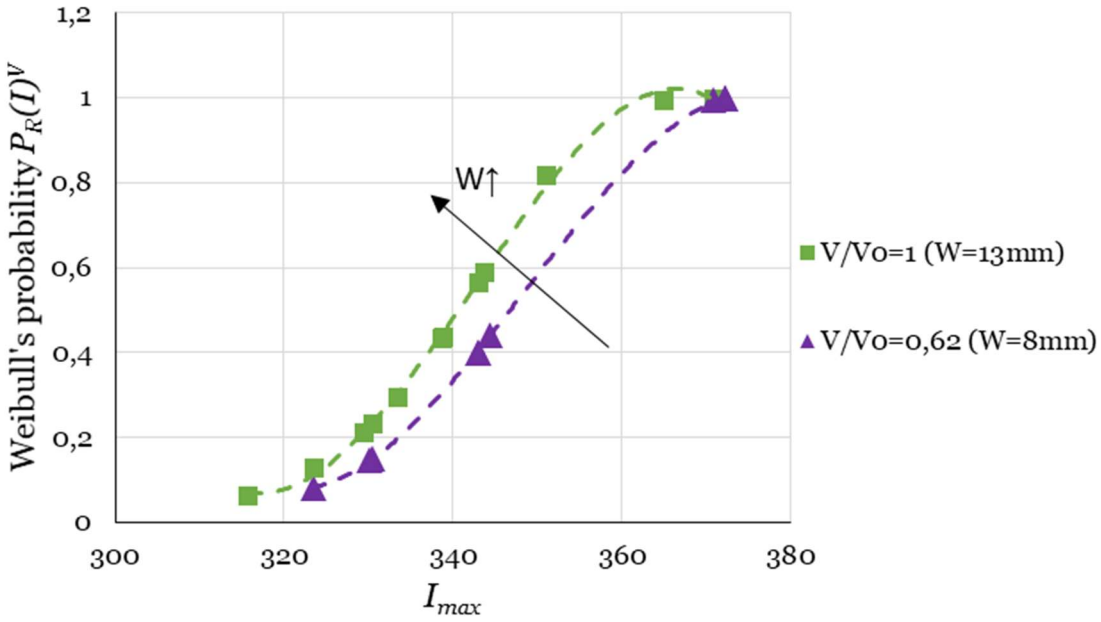

Figure 5-18: Probability of failure of the tests carried out with a width of 13 mm and a width of 8mm computed by the multiaxial index (I_{MWCM}) at the critical distance.

Preliminary remarks

In agreement with the Freudenthal theory (Freudenthal, 1968), the results presented above predict a higher probability of failure with a lower amplitude of stress, here represented by the maximum value of the multiaxial index, for the experiment carried out with a pad and specimen width of 13mm than for the 8mm ones. To determine the sustainability of the results, the classical S-N diagram was plotted with the maximum of the multiaxial index in ordinate and the number of cycles to failure in abscissa (Figure 5-19).

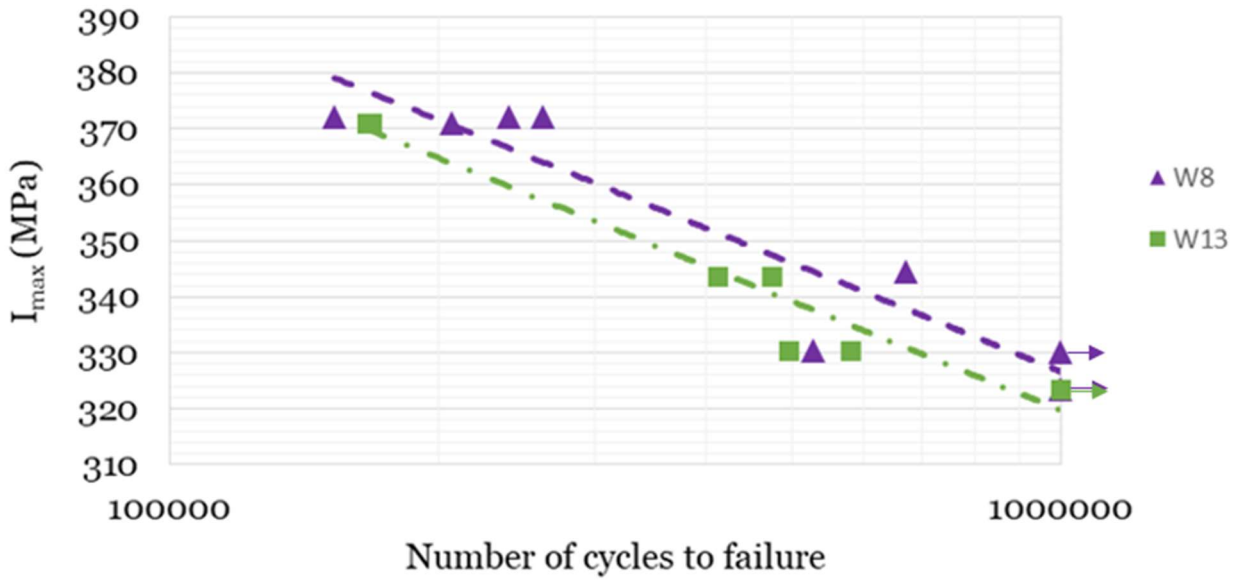

Figure 5-19: Comparison of the maximum of the multiaxial index, I_{max} which leads to the failure for the two contact's width.

According to the Weibull's theory, for a same level of stress, the probability of failure is higher for a specimen whose width was 13mm than for the 8mm specimens. This result is confirmed by the S-N diagram where it appears that the maximum amplitude of stress leading to run out tests, i.e. tests with a low probability of failure, is higher for the tests carried out with the 8mm specimens. However, it should be noticed that, in both cases, the difference between the curves for the 8mm and 13mm specimens, is of the order of 2%.

5.6. Discussion of the results

Two parameters were investigated to understand the role of the size effect on fretting fatigue: the stressed volume and the fretted damaged area. The results showed that, when the volume of material stressed under the contact is reduced by 39% (by decreasing the specimens width from 13 to 8mm) but the stress gradient, represented in terms of the Multiaxial Index (computed by the Modified Wöhler Curve Method), is maintained roughly the same for both configurations, as well as the damaged areas, the specimens with a width of 8mm lasted on average around 10% longer than the one with a width of 13mm. However, this first results have to be examined carefully because it appears that it was not possible to maintain the evolution of the multiaxial index exactly the same for the two corresponding tests with different widths, mainly for distances longer than the critical one. Moreover, the microscope examination of the fretted scars has shown that the resulting damaged area are different from the expected ones.

Thus, a firmly conclusion cannot be drawn, however, it seems that the reduction, or increase, of the volume stressed do not have a relevant influence on the fretting fatigue strength.

The second part of the study, concerning the reduction of the damaged area, have led more reliable results. Indeed, by changing the area within the slip zones, it became possible to maintain the stress gradient exactly equal between the two specimens with different widths because it was possible to keep all the other relevant experimental parameters, i.e. the stress ratio σ_B/fP and the load ratio Q/fp_o, constant. These experiments have led to quite similar lifetimes when the same multiaxial index was applied. This result led to the conclusion that nor the decrease of the stressed volume, nor the one of the damaged area within the slip zone influence the fretting fatigue strength for experimental studies carried out within partial slip conditions. This result was confirmed by the statistical study. Indeed, the application of the Weibull's theory have shown that the probability of failure only decreased by 2% when the volume of material stressed under the contact was decreased by 39%.

One possible explanation for the negligible role played by the tribological aspect in the fretting fatigue resistance under partial slip conditions may be associated with the numerous cracks initiated within the slip zones (Figure 5-15). Indeed, at the beginning of the experiment, a specimen presenting a larger width will, statistically, present more preferential sites for the initiation of cracks. However, the fretting mechanism will severely damage the surface within the slip zone (Figure 5-13) whatever the specimen width considered is. Thus, a large amount of defects will be created on the surface and numerous small cracks will initiate (Figure 5-15) even for the smaller specimen width, making the statistical aspect negligible. Finally, the main mechanism leading to the failure of a specimen is the propagation of these small cracks, which is controlled by the stresses applied.

In this study, the fretted zone obtained with the specimens width of 8mm and the ones of 13mm were examined. The microscope observations have shown a small increase of the contact area at the middle of the specimen and a decrease of it at the contact edges. This phenomenon, known as the edge effect, was more pronounced for the specimen's width of 13mm than for the specimen's width of 8mm. One should notice that the analytical study of the elastic contact problem assumes plane strain conditions. A three dimensional Finite Element Analysis conducted by Bellecave (2015) tried to quantify this edge effect. He showed that, for the fretting problem involving the 13 mm specimens the ratio between the out of plane normal stress and the in plane normal stresses computed at the centre of the specimen was $\frac{\sigma_{zz}}{\nu(\sigma_{xx}+\sigma_{yy})} = 0{,}8$, i.e. quite close from the plane strain condition ($\frac{\sigma_{zz}}{\nu(\sigma_{xx}+\sigma_{yy})} = 1$) assumed in the analytical formulation. This FEA study has not been repeated for the 8mm specimen but clearly this ratio would be greater.

Chapter 6. Conclusions

6.1. Overview

Since the first observations of the fretting corrosion by Eden et al. (1911), over a century ago, numerous studies have been carried out to better understand the fatigue phenomenon under fretting conditions. In particular, the gradient effect generated at the contact interface of the two bodies is now better understood and it exists a large amount of models to take it into account (Dini et al., 2006, Araújo et al., 2007, Ferré et al., 2013, Fouvry et al., 2014). However, the main parts of these studies were conducted under laboratory conditions and it still remains difficult and numerically expensive to apply the existing models to industrial configurations.

The general aim of this study was to investigate new ways to deal with the fretting fatigue within industrial objectives. In this setting, a new crack analogue model was challenged under more realistic fretting fatigue loading conditions for a titanium alloy, the Ti-6Al-4V, widely used in the aeronautical industries. Furthermore, the role of the size effect on fretting fatigue was perhaps systematically investigated for the first time. The new experiments we have conducted to investigate such effect were designed so that the size effect itself was addressed and not the stress gradient effect as studied by other authors elsewhere (Bramhall, Nowell, 1988, Araújo 2000). These studies reported a “size” effect phenomenon, which was in fact provoked by stress gradient effects/differences among tests. One should notice here that effects of size on fretting fatigue have a strong interest in the industrial context.

6.2. Main conclusions

Group I of Tests and Crack Analogue Model

The experimental program in this study was conducted using a two vertical and independent actuators servo-hydraulic fretting fatigue machine in the Department of Mechanical Engineering at the University of Brasília. As far as the author is aware, there are only three laboratories in the world where such type of test rig is available, being the other two located in Ecole Centrale de Lyon and in the University of Oxford. The fretting configuration considered in our experiments was composed of a single cylindrical fretting pad and a roller bearing loaded against a flat dogbone tensile test piece. The use of a two vertical actuators fatigue rig allows to apply the fatigue and fretting loads independently and so to have a better control of them, besides allowing the application of phase differences or the conduction of

asynchronous tests. Here, in this section, we will present the main conclusions of the Group I of Tests conducted with such experimental rig and contact configurations.

The Group I of Tests was obtained using two different pad radii 50mm and 70mm) and a “dog bone” tensile specimen, both with 13 mm width. Tests with a 20 mm pad radius were available from the work of Bellecave (2015) and were considered for the analysis. The loads for our tests were determined so that the value of the multiaxial index at the critical distance was equal for both sets although they were different at the surface. Therefore, they had different stress gradients and superficial stress levels at the hotspot, but the same severity of loading in the so called critical distance according to the MWCM model. These tests configurations resulted in similar lifetimes.

The crack analogue model, originally proposed by Montebello et al. (2016) was challenged with these new fretting fatigue tests (results of Group I of tests). Also notice that these tests used loading programs which considered the presence of a fatigue bulk load applied to the Ti-6Al-4V specimens. The nonlocal stress intensity factors, I^a and I^s, were computed for three different stress gradients, obtained with pad radii of 20mm, 50mm and 70mm, and with loads designed to achieve different but specific fretting fatigue lifetimes. As fretting crack initiation mechanisms usually represent the main part of the life (Hojjati-Talemi et al., 2014), the experimental lives here obtained in terms of number of cycles to total failure were used to validate the crack initiation model.

It was found that, when different stress gradients are considered but the resulting lifetimes are similar, it seems to exist a clear correlation between the experimental results in a nonlocal map (I^s-I^a). For the broken tests, at around 200 000 cycles and 500 000 cycles, this correlation was represented by a straight line. However, the results obtained for unbroken specimens at 1 000 000 cycles presented a higher dispersion and we cannot conclude that such a linear correlation can be extended to run-out tests.

In his work, Montebello (2016) has suggested that for run-out tests a crack initiation boundary may be found by applying a multiaxial fatigue criterion to the nonlocal stress intensity factors. In the original formulation of this crack initiation boundary (Montebello, 2016), the effect of the maximum normal stress was discarded and an over-conservative frontier was obtained when we represented it for our experimental results. Consequently, we decided to add the maximum normal stress to the formulation of the crack initiation boundary. With this modification, we were able to predict the crack initiation frontier with a precision of ±10%.

Group II of Tests and Size Effect

The Group II of tests was carried out using a 70mm pad radius and a pad/specimen's width of 8mm and 13mm. In this group, two parameters representative of the size effect were investigated, the volume of material, V, stressed under the contact and the fretted damaged area, A^D. During this study, experimental results obtained with two stressed volumes were compared, the first obtained for a specimen's width of 13mm, V_{13} = 361,17mm², and the second for a specimen's width of 8mm, V_8 = 222,26mm². The tests were carried out by maintaining the fretted damage area and the stress gradient roughly constant between two corresponding tests (Group II-a). The experimental results have shown an increase of around 10% of the life when the stressed volume has been reduced by 39%. However, it existed a small difference between the stress gradients developed between the 13 and 8mm specimens. It was observed that the actual fretted damage areas for the lowest stressed volume were smaller than the ones observed for the biggest stress volume. These differences, probably associated to computation issues and to edge effects do not allowed us to firmly conclude that the increase of the strength is only driven by the reduction of the stressed volume.

Then, in Group II-b, experiments were conducted by maintaining the peak pressure, p_o, the stress ratio σ_B/p_o and the load ratio Q/fP equal for the 8mm and 13 mm specimens. By doing so, the stress gradient was exactly the same for both configurations, but now, not only the resulting volume of material stressed under the contact changed, but also the damaged area within the slip zones were reduced by approximately 39%. We did not observe differences between the experimental results, in terms of fatigue lifetimes, obtained with the different specimens widths for these tests. This methodology allowed us to separate the effect of the stress gradient from the size effect and it showed that it does not seem to exist any size effect for fretting fatigue under the partial slip conditions considered here. Moreover, the decrease of the fretted damaged area between two corresponding tests allowed us to conclude that the subsurface stress field have a stronger influence on the final fatigue life than the superficial fretting damages.

6.3. Suggestions for future work

Studies to extend the fretting fatigue model from laboratory scale to industrial configurations are clearly important since in principle they are applied to provide a safe life design of critical components of real structures. Strikingly, the specialised literature contains few reports on this subject. The methodologies applied in this work to address this problem have shown good preliminary results, however they should be confronted to different materials and geometrical configurations to validate their application in practical situations.

Some authors (Fouvry et al., 2013, Shen et al., 2015, Li et al, 2015), suggest that fretting fatigue crack initiation is influenced by the amount of damage in the slip zones and have proposed models which included damage parameters to predict it. The author accepts that when the study is carried out under gross slip conditions or reciprocal sliding (O'Halloran et al, 2017), the large increase of superficial damage may motivate the use of such models, which have shown an reasonable level of success in predicting the fretting crack initiation life. Maybe a similar study as the one proposed in this work should be implemented considering these loading conditions, i.e. gross slip and reciprocal sliding conditions, to evaluate the real influence of the damaged area on the final fatigue life.

Finally, most of the studies and experimental work in fretting fatigue are conducted at room temperature while the temperatures in aeroengines can reach up to 1700°C. Nalla et al. (2003) have shown that the increase of the temperature have a negative effect on the fatigue strength of the Ti-6Al-4V. Thus, a heating system may be implemented to the fretting apparatus to carry out experiments at high temperature (Figure 6-1), as it has been proposed by Saengsai et al. (2014). Others systems involving a local increase of the temperature at the contact interface, using laser for example, can also be alternatives for a future work.

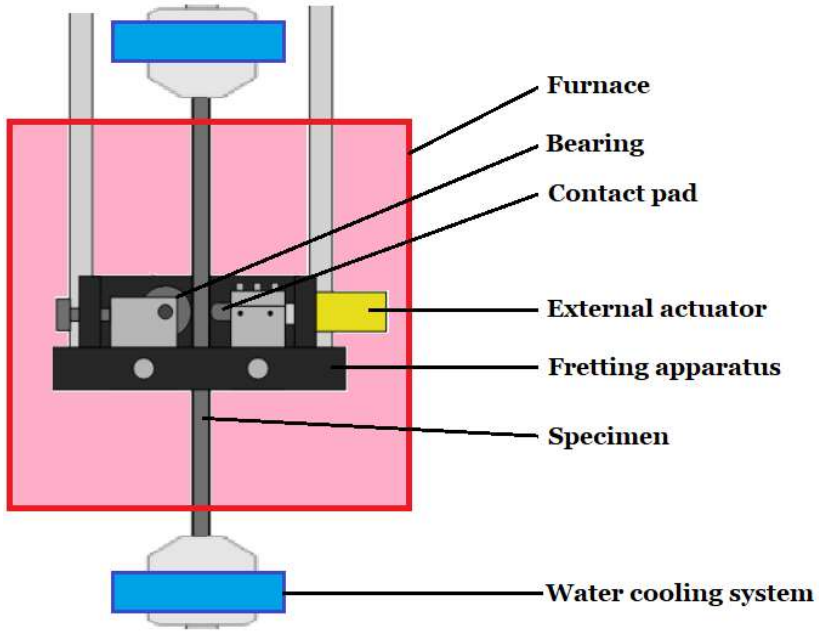

Figure 6-1: Schematic view of a proposed experimental set-up for fretting fatigue tests at high temperatures in air.

References.

Alexandrov, V.M., Pozharskii, D. A. (2001). "Three-dimensional contact problems". *Kluwer Academic Publishers*.

Anderson, T.L. (1995). "Fracture Mechanics: Fundamentals and Applications", 2nd Edition, *CRC Press*, Boca Raton, FL.

Araújo, J.A. (2000). "On the Initiation and Arrest of the Fretting Fatigue Cracks". PhD thesis of the University of Oxford.

Araújo, J.A., Nowell, D. (2002). "The effect of rapidly varying contact stress fields on fretting fatigue". *International Journal of Fatigue*, 24(7), pp. 763-775.

Araújo, J.A., Susmel, L., Taylor, D., Ferro J.C.T., Mamiya E.N. (2007). "On the use of the theory of critical distances and the Modified Wöhler curve method to estimate fretting fatigue strength of cylindrical contacts". *International Journal of Fatigue,* 29(1), pp. 95-107.

Araújo, J.A., Dantas, A. P., Castro, F. C., Mamiya, E. N., Ferreira, J. L. A. (2011). "On the characterization of the critical plane with a simple and fast alternative measure of the shear stress amplitude in multiaxial fatigue". *International Journal of fatigue*, 33(8), pp. 1092-1100.

Araújo, J.A., Castro, F. C. (2012). "A comparative analysis between multiaxial stress and ΔK-based short crack arrest models on fretting fatigue". *Engineering Fracture Mechanics*, 93, pp. 34–47.

Araújo, J.A., Carpinteri, A., Ronchei, C., Spagnoli, A., Vantadori, S. (2014). "An alternative definition of the shear stress amplitude based on the maximum rectangular hull method and application to the C-S (Carpinteri-Spagnoli) criterion". *Fatigue and Fracture Engineering of Materials and Structures*, 37(7), pp. 764-771.

Araújo, J.A., Castro, F. C., Pommier, S., Bellecave, J., Mériaux, J. (2016). "On the design and test of equivalent configurations for notch and fretting fatigue". *Fatigue and Fracture of Engineering Materials and Structures*, 39(10), pp. 1241-1250.

Araújo, J.A., Susmel, L., Pires, M. S. T., Castro, F. C. (2017). "A multiaxial stress-based critical distance methodology to estimate fretting fatigue life". *Tribology International*, 108, pp. 2-6.

Archard, J. F. (1953). "Contact and rubbing of flat surfaces". *Journal of Applied Physics*, 24, pp. 981-988.

Bantounas, I., Dye, D., Lindley, T.C. (2010). "The role of microtexture on the faceted fracture morphology in Ti-6Al-4V subjected to high-cycle fatigue". *Acta Materialia*, 58(11), pp. 3908-3918.

Bellecave, J. (2015). "Stress Gradients in Fretting Fatigue". PhD thesis of the Ecole Normale Supérieure de Cachan and the Universidade de Brasilia.

Bellows, S., Muju, S. Nicholas, T. (1999). "Validation of the step test method for generating Haigh diagram for Ti-6Al-4V". *International Journal of Fatigue*, 21(7), pp. 687-697.

Bramhall, R. (1973). "Studies in fretting fatigue". PhD thesis of the Oxford University.

Brown, M. W. and Miller, K. J. (1973). "A theory for fretting fatigue under multiaxial stress-strain conditions". *Proc ImechE*, 187(1), pp. 745-755.

Carpinteri, A., Ronchei, C., Spagnoli, A., Vantadori, S. (2014). "Lifetime estimation in the low/medium-cycle regime using the Carpinteri-Spagnoli multiaxial fatigue criterion". *Theoretical and Applied Fracture Mechanics*, 73, pp. 120-127.

Castro, F. C., Araújo, J.A., Zouain, N. (2009). "On the application of multiaxial high-cycle fatigue criteria using the theory of critical distances". *Engineering Fracture Mechanics*, 76(4), pp. 512-524.

Cattaneo, C. (1938). "Sul contatto di due corpi elastici: Distribution locale dei sforzi". *Rendiconti dell'Accademia nazionale dei Lincei* 27, pp.342-348.

Chambon, L., Journet, B. (2006). "Modelling of fretting fatigue in a fracture-mechanics framework". *Tribology International*, 39(10), pp. 1220-1226.

Ciavarella, M., Macina, G. (2003a). "A note on the crack analogue mode for fretting fatigue". *International Journal of Solid and Structures*, 40(4), pp.807-825.

Ciavarella, M., Macina, G. (2003b). "New results for the fretting-induced stress concentration on Hertzian and flat rounded contacts". *International Journal of Mechanical Science*, 45(3), pp. 449-467.

Ciavarella, M., Berto, F. (2017). "A simplified extension of the Crack Analogue model for fretting fatigue with varying normal load". *Theoretical and Applied Fracture Mechanics*, In press, Corrected proof.

Conner, B. P., Lindley, T. C., Nicholas, T., Suresh, S. (2004). "Application of a fracture mechanics based life prediction method for contact fatigue". *International Journal of Fatigue*, 26(5), pp. 511-520.

Crupi, V., Epasto, G., Guglielmino, E. (2017). "Influence of the microstructure [alpha + beta and beta on very high cycle fatigue behaviour of Ti-6Al-4V alloy". *International Journal of Fatigue*, 95, pp. 64-75.

Dang Van, K. (1973). " Sur la résistance à la fatigue des métaux". Sci. Tech. L'armement, (47), pp. 429–53.

Dang Van, K., Griveau, B., Message, O. (1989). "On a New Multiaxial Fatigue Limit Criterion: Theory and Application". *Biaxial and Multiaxial Fatigue*, EGF3 (Edited by M. W. Brown and K. J. Miller), Mechanical Engineering Publications, London, pp. 479-496.

Delahaye, T. (2004). ‘’Développement d’une méthode probabiliste de calcul en fatigue multiaxiale prenant en compte la répartition volumique des contraintes”. PhD thesis at the Université de Bordeaux I.

Dini, D., Nowell, D., Igor N. Dyson (2006). “The use of notch and short crack approaches to fretting fatigue threshold prediction: Theory and experimental validation”. *Tribology International*, 39(10), pp. 1158-1165.

Dundur, J. (1969). “Discussion of edge-bonded dissimilar orthogonal elastic wedges under normal and shear loading”, *Journal of Applied Mechanic*, 36, pp. 650-652.

Eden, E.M., Rose, W.N., Cunningham, F.L. (1911). “The endurance of metals”. *Proceedings of the Institute of Mechanical Engineering*, 4, pp. 839-974.

El Haddad, M. H., Smith, K. N., Topper, T. H. (1979). “Fatigue crack propagation of short cracks”. *Transactions of the ASME*, 101(1), pp. 42-46.

Endo, K., Goto, H. (1975). “Initiation and propagation of fretting fatigue cracks”. *Wear*, 38, pp. 311-324.

Fatemi, A. and Socie, D. F. (1988). ‘A Critical Plane Approach to Multiaxial Fatigue Damage Including Out of Phase Loading”. *Fatigue Fracture of Engineering Materials and Structures*, 11(3), pp. 939-947.

Fenner, A.J., Field, J.E. (1960). “A study of the onset of the fatigue damage due to fretting”. *Transactions of the North East Coast Institution of Engineers and Shipbuilders*, pp. 1959-1960.

Fenner, A.J. and Field, J.E. (1958). "Fatigue under fretting conditions." *Revue Metallurgique*, 55, pp. 475-478.

Ferré, R. (2013). “Etude expérimentale et modélisation de la durabilité d’un contact aube/disque de soufflante grenaillé revêtu soumis à des chargements de fretting/fatigue/usure”. PhD thesis of the Ecole Centrale de Lyon.

Findley, W. N. (1959). “A theory for the effect of mean stress on fatigue of metals under combined torsion and axial load or bending”. *Journal of Engineering for Industry*, B81, pp. 301-306.

Fleury, R. M. N., Hills, D. A., Ramesh, R., Barber, J. R. (2017). “Incomplete contacts in partial slip subject to varying normal and shear loading, and their representation by asymptotes”. *Journal of the Mechanics and Physics of Solids*, 99, pp. 178-191.

Fouvry, S., Kapsa, P., Vincent, L. (2000). “A multiaxial fatigue analysis of fretting contact taking into account the size effect”. *Fretting Fatigue: Current Technology and Practices*, ASTM STP 1367, D. W. Hoeppner, V. Chandrasekaran, and C. B. Elliott, Eds., American Society for Testing and Materials, West Conshohocken, PA.

Fouvry, S., Elleuch, K., Simeon, G. (2002). "Prediction of crack nucleation under partial slip fretting conditions". *The Journal of Strain Analysis for Engineering Design.*

Fouvry, S., Merhej, R. (2013). "Introduction of a power law formulation to quantify the contact size effects on friction and wear responses of dry oscillating sliding contacts: Application to a chromium steel interface", *Wear*, 301(1-2), pp. 34-46.

Freudenthal, A. M. (1968). "Statistical approach to brittle fatigue". *Fracture, an Advanced Treatise*, II, pp. 591-619.

Gladwell, G.M.L. (1980). "Contact Problems in the Classical Theory of Elasticity", *Sijthoff and Noordhoff*, Alphen aan den Rijn.

Giannakopoulos, A.E., Lindley, T.C., Suresh, S. (1998). "Aspects equivalence between contact mechanics and fracture mechanics: theoretical connections and a life-prediction methodology for fretting-fatigue". *Acta Materialia*, 46(9), pp.2955-2968

Giannakopoulos, A. E., Lindley, T. C., Suresh, S., Chenut, C. (2000). "Similarities of stress concentrations in contact at round punches and fatigue at notches: implications to fretting fatigue crack initiation". *Fatigue and Fracture of Engineering Materials and Structures*, 23(7), pp. 561-571.

Giner, E., Sabsabi, M., Fuenmayor, F. J. (2011). "Calculation of K_{II} in crack faces contacts using X-FEM. Application to fretting fatigue." *Engineering Fracture Mechanics*, 78, pp. 428-445.

Hertz, R. (1881). "Über die berührung fester elastischer körper". *Journal für die reine und angewandte Mathematik,* 92, pp.156-171

Hills, D. A., Nowell, D., O Connor, J. J. (1988). "On the mechanics of fretting fatigue". *Wear*, 125(1-2), pp. 129-146.

Hills, D.A., Nowell, D., Sackfield, A. (1993). "Mechanics of Elastic Contacts", *Butterworth Heinemann*, Oxford

Hills, D.A., Nowell, D. (1994). "Mechanics of fretting fatigue". *Kluwer academic publishers.*

Hines, J.A., Lutjering, G. (1999). "Propagation of microcracks at stress amplitudes below the conventional fatigue limit in Ti-6Al-4V". *Fatigue and Fracture and Engineering Materials and Structures*, 22(8), pp. 657-665.

Hojjati-Talemi, R., Wahab, M.A., De Pauw, J., De Baets, P. (2014). "Prediction of fretting fatigue crack initiation and propagation lifetime for cylindrical contact configuration". *Tribology International*, 76, pp. 73-91.

Horger, J. H. (1953). "Influence of Fretting Corrosion on the Fatigue Strength of Fitted Members", *Symposium on Fretting Corrosion*, STP 144, ASTM, Philadelphia.

Hutson, A. L., Nicholas, T., Goodman, R. (1999). "Fretting fatigue of TI-6Al-4V under a flat-on-flat contact". *International Journal of Fatigue*, 21(7), pp. 663-670

Hutson, A. L., Nicholas, T. (2000). "Fretting fatigue behaviour of TI-6Al-4V against Ti-6AL-4V under flat-on-flat contact with blending radii". *Fretting Fatigue: Current Technology and Practices*, ASTM STP (Edited by D. W. Hoeppner, V. Chandrasekaran and C. B. Elliot), Am. Soc. for Testing and Materials, West Conshohoken, PA, USA, pp. 308–321.

Irwin, G. R. (1957). "Analysis of stresses and strains near the end of a crack traversing plate". *Journal of Applied Mechanics*, 1.24, pp. 361-364.

Irwin, G. R. (1958). "Elasticity and Plasticity / Elastizität und Plastizität". *Handbuch der Physik / Encyclopaedia of Physics*, Ed. by S. Flügge, Vol. 3/6, Berlin, Heidelberg: Springer Berlin Heidelberg.

Ivanova, S.G., Cohen, F.S., Biederman, R.R., Sisson Jr. R.D. (1999). "Role of the microstructure in the mean stress dependence of fatigue strength in Ti-6Al-4V alloy". English.

Ivanova, S.G., Biederman, R.R., Sisson Jr., R.D. (2002). "Investigation of Fatigue Crack Initiation in Ti-6Al-4V during Tensile-Tensile Fatigue". *Journal of Materials Engineering and performance*, 11(2), pp. 226-231.

Johnson, K.L. (1985). "Contact Mechanics", *Cambridge University Press*, Cambridge

Kanninen, M.F., Popelar, C.H. (1985). "Advanced Fracture Mechanics". *Oxford engineering Science Series*, Oxford University Press, 1985.

Karhunen, K. (1946). "Uber lineare methoden in der wahrscheinlichkeitsrechnung," Ann. Acad. Sri. Fennicae, ser. Al. Math. Phys., vol. 37.

Kuno, M., Waterhouse, R.B., Nowell, D., Hills, D.A. (1989). "Initiation and growth of fretting fatigue cracks in the partial slip regime", *Fatigue and Fracture of Engineering of Materials and Structures*, 12(5), pp. 387-398.

Lanning, D.B., Nicholas, T., Haritos, G.K. (2005). "On the use of critical distance theories for the prediction of the high cycle fatigue limit stress in notched Ti-6Al-4V". *International Journal of Fatigue*, 27(1), pp. 45-57.

Lazzarin, P., Milani, V., Quaresimin, M. (1997). "Scatter bands summarizing the fatigue strength of aluminium alloy bolted joints". *International Journal of Fatigue*, 19(5), pp. 401-407.

Le Baviant, K., Pommier, S., Prioul, C. (2002). "Local texture and fatigue crack initiation in a Ti-6AL-4V titanium alloy". *Fatigue and Fracture of Engineering Materials and Structures*, 25(6), pp.527-545.

Lee. H., Mall, S. (2004). "Effect of dissimilar mating materials and contact force on fretting fatigue behaviour of Ti-6Al-4V". *Tribology International*, 37(1), pp. 35-44.

Li, B., Santos, J. L. T., de Freitas, M. (2000). "A unified numerical approach for multiaxial fatigue limit evaluation". International Journal of Mechanics of Structures and Machines, 28 (2000), pp. 85-103.

Li, X., Zuo, Z., Qin, W. (2015). "A fretting related damage parameter for fretting fatigue life prediction". *International Journal of Fatigue*, 73, pp. 110-118.

Liu, H.W., Corten, H.T., Sinclair, G. M. (1956). "Fretting fatigue strength of titanium alloy RC 130B. Department of Theoretical and Applied Mechanics, University of Illinois.

Lindley, T. (1997). "Fretting fatigue in engineering alloys*", International Journal of Fatigue*, 19(93), pp. 39-49.

Mamiya, E. N., Araújo, J.A. (2002). "Fatigue limit under multiaxial loadings: on the definition of the equivalent shear stress". *Mechanics Research Communications*, 29(2-3), pp. 141-151.

Mamiya, E. N., Castro, F. C., Araújo, J.A. (2009). "Prismatic hull: A new measure of shear stress amplitude in multiaxial high cycle fatigue". *International Journal of Fatigue*, 31(7), pp. 1144-1153.

Mamiya, E. N., Castro, F. C., Araújo, J.A. (2014). "Recent developments on multiaxial fatigue: the contribution of the University of Brasília". *Theoretical and Applied Fracture Mechanics*, 73, pp. 48-59.

McColl, I. R., Ding, J., Leen, S. B. (2004). "Finite element simulation and experimental validation of fretting wear". *Wear*, 256, pp. 114-1127.

McDiarmid, D. L. (1991). "A general criterion for high cycle multiaxial fatigue failure". *Fatigue and Fracture of Engineering Materials and Structures*, 14(4), pp. 429-453.

McDowell, J.R. (1953). "Fretting Corrosion Tendencies of Several Combinations of Materials", *Symposium on Fretting Corrosion*, STP 144, ASTM, Philadelphia, pp. 24-39.

Mériaux, J. (2010). "Etude expérimentale et modélisation de l'endommagement d'un contact aube/disque de soufflante soumis à des chargements de fretting fatigue". PhD Thesis of the Ecole Centrale de Lyon.

Mindlin, R. D. (1949). "Compliance of elastic bodies in contact", *Journal of Applied Mechanics*, 16, pp. 259-268.

Mindlin, R. D., Deresciewicz, H. (1953). "Elastic spheres in contact under varying oblique forces." *Journal of Applied Mechanics*, 20, pp. 327-344.

Montebello C. (2015). "Analysis of the stress gradient effect in Fretting Fatigue through a description based on nonlocal intensity factors". PhD thesis of the Ecole Normale Supérieure de Cachan.

Montebello, C., Pommier, S., Demmou, K., Leroux, J., Mériaux, J. (2016). ''Analysis of stress gradient effect in fretting fatigue trough nonlocal intensity factors". *International Journal of Fatigue,* 82, pp.188-98.

Moshier, M.A., Nicholas, T., Hillberry, B.M. (2001). "Load history effects on fatigue crack growth threshold for Ti-6Al-4V and Ti-17 titanium alloys". *International Journal of Fatigue*, 23, Supple. 0, pp. 253-258.

Muskhelishvili (1953). *Some basic problems of mathematical theory of elasticity*. Noordhoff, Groningen.

Naboulsi, S. and Mall, S. (2003). "Fretting fatigue crack initiation behaviour using process volume approach and finite element analysis", *Tribology International*, 36(2), pp. 121-131.

Nagai, K., Yuri, T., Umeza, O., Ogata, T., Ishikawa, K., Ito, Y. (1993). "High cycle fatigue properties of Ti-6Al-4V alloys at cryogenic temperatures". *Titanium*, ED. By Caplan IL Froes FH. Warrendale (PA), pp.1827-1834.

Nalla, R.K., Boyce, B.L., Campbell, J.P., Peters, J.O., Ritchie, R.O. (2002). "Influence of microstructure on high-cycle fatigue of Ti-6Al-4V: Bimodal vs. lamellar structures". *Metallurgical and Materials Transactions"*, 33(13), pp.899-918.

Nalla, R.K., Altenberger, I., Noster, U., Liu, G.Y., Scholtes, B., Ritchie, R.O. (2003). "On the influence of mechanical surface treatments – deep rolling and laser shot peening – on the fatigue behaviour of Ti-6Al-4V at ambient and elevated temperatures". *Material Science and Engineering*, 355(1-2), pp.216-230.

Neuber, H. (1936). "Theorie der technischen Formzahl". *Forschung auf des Gebiete des Ingenieurwesens*, 7 (6), pp. 271-274.

Neuber H. (1958). "Theory of Notch Stresses". *Kerbspannungslehre*.

Nishioka, K., Hirakawa, K. (1969). "Fundamental investigations of fretting fatigue (part4) – The effect of mean stress". *Bulletin of JSME*, 12(51), pp.408-414.

Nowell, D. (1988). "An analysis of fretting fatigue". *PhD thesis*.

Oberwinkler, B., Riedler, M., Eichlseder, W. (2010). "Importance of local microstructure for damage tolerant light weight design of Ti-6Al-4V forgings". *International Journal of Fatigue*, 32(5), pp.808-814.

O'Halloran, S. M., Shipway, P. H., Connaire, A. D., Leen, S. B., Marte, A. M. (2017). "A combined wear-fatigue design methodology for fretting in the pressure armour layer of flexible marine risers". *Tribology International*, 2017, 108, pp. 7-15.

Papadopoulos, I. V. (1994). "A new criterion of fatigue strength for out-of phase bending and torsion of hard metals". *International Journal of Fatigue*, 16, pp. 377–84.

Papadopoulos, I. V. (1995). "A high-cycle fatigue criterion applied in biaxial and triaxial out-of-phase stress conditions". *Fatigue and Fracture of Engineering Materials and Structures*, 18(1), pp. 79-91.

Papadopoulos, I. V. (1998). "Critical plane approaches in high-cycle fatigue: on the definition of the amplitude and mean value of the shear stress acting on the critical plane". *Fatigue and Fracture of Engineering Materials and Structures*, 21(3), pp. 269-285.

Papanikos, P., Meguid, S.A. (1994). "Theoretical and experimental studies of fretting-initiated fatigue failure of aeroengine compressors discs", *Fatigue and Fracture of Engineering of Materials and Structures*, 17(5), pp. 539–550.

Peters, M., Gysler, A., Lutjering, G. (1984). "Influence of texture on fatigue properties of Ti-6Al-4V". *Metallurgical Transactions*, 15(8), pp. 1597-1605.

Peterson, R. E. (1959). "Notch sensitivity". *Metal Fatigue*, pp. 293-306.

Petiot, C., Vincent, L., Van, K.D., Maouche, N., Foulquier, J., Journet, B. (1995). "An analysis of fretting-fatigue failure combined with numerical calculations to predict crack nucleation". *Wear*, 181, pp.101-111.

Pommier, S., Hamam, R. (2007). "Incremental model for fatigue crack growth based on a displacement partitioning hypothesis of mode I elastic-plastic displacement fields". *Fatigue and Fracture of Engineering Materials and Structures*, 30 (7) (2007), pp. 582–598.

Pommier, S., Lopez-Crespo, P., Decreuse, P. (2009). "A multiscale approach to condense the cyclic elastic-plastic behaviour of the crack tip region into an extended constitutive model". *Fatigue and Fracture of Engineering Materials and Structures,* 32 (11), pp. 899–915.

Proudhon, H., Buffière, J.-Y., Fouvry, S. (2007). "Three-dimensional study of a fretting crack using synchrotron x-ray micro-tomography". *Engineering Fracture Mechanic*, 74(5), pp. 782–793

Sá, M. V. C., Ferreira, J. L. A., Araújo, J.A (2017). "Notched multiaxial fatigue of Al7050-T7451: on the need for an equivalent process zone size". *Frattura ed Integrità Stutturale*, 41, pp. 90-97.

Saengsai, A., Otsuka, Y., Mutoh, Y. (2014). "Fretting fatigue behavior of SUS304 stainless steel under pressurized hot water". *Tribology International*, 79, pp. 52-58.

Shen, F., Hu, W., Voyiadjis, G. Z., Meng, Q. (2015). "Effects of fatigue damages and wear on fretting fatigue under partial slip condition". *Wear*, 338-339, pp. 394-405.

Smith, K. N., Watson, P., Topper, T. H. (1970). "A Stress-Strain Function for the Fatigue of Metals". *Journal of Materials*, 5(4), pp. 767-778.

Socie, D. F. (1987). "Multiaxial Fatigue Damage Models". *Transactions of the ASME. Journal of Engineering Materials and Technology*, 109(4), pp. 293-298.

Stoschka, M., Tan, W., Eichlseder, W., Stockinger, M. (2009). "Introduction to an approach based on the (α+β) microstructure of elements of alloy Ti-6Al-4V". *Procedia Engineering*, 1(1), pp.31-34.

Susmel, L. and Taylor, D. (2003). "Two methods for predicting the multiaxial fatigue limits of sharp notches". *Fatigue and Fracture of Engineering Materials and Structures*, 26(9), pp. 821-833.

Susmel, L., Tovo, R., Lazzarin, P. (2005). "The mean stress effect on the high-cycle fatigue strength from a multiaxial fatigue point of view". *International Journal of Fatigue*, 28(8), pp.928-943.

Susmel, L. and Taylor, D. (2007). "A novel formulation of the theory of critical distances to estimate lifetime of notched components in the medium-cycle fatigue regime". *Fatigue and Fracture of Engineering Materials and Structures*, 30(7), pp. 567-581.

Susmel, L. and Taylor, D. (2008). "The Modified Wöhler curve method applied along with the theory of critical distances to estimate finite life of notched components subjected to complex multiaxial loading paths". *Fatigue and Fracture of Engineering Materials and Structures*, 31(12), pp. 1047-1064.

Szolwinski, M. P. and Farris T. N. (1996). "Mechanics of Fretting Fatigue Crack Formation". *Wear*, 198(1-2), pp. 93-107.

Tanaka, K. (1983). "Engineering formulae for fatigue strength reduction due to crack-like notches". *International Journal of Fatigue*, 22, pp. R39-R45.

Taylor, D. (1999). "Geometrical effects in fatigue: a unifying theoretical model". *International Journal of Fatigue*, 21(5), pp. 413-420.

Timoshenko, S.P., Goodier, J.N. (1951). "Theory of Elasticity", *McGraw-Hill*, New-York.

Tomlinson, G.A. (1927). "The Rusting of Steel Surfaces in Contact", *Proceedings of the Royal Society*, 115(771), pp. 472-483.

Tomlinson, G.A., Thorpe, P.L., Gough, H.J. (1939). "An investigation of the Fretting Corrosion of Closely Fitting Surfaces", *Proceedings of the Institution of Mechanical Engineers*, 141(1), pp. 223-249.

Venkatesh, T. A., Conner, B. P., Lee, C. S., Giannakopoulos, A. E., Lindley, T. C., Suresh, S. (2001). "AN experimental investigation of fretting fatigue in Ti-6Al-4V: the role of contact conditions and microstructure". *Metallurgical and Materials transactions*, 32A, pp. 1131-1146.

Warlow-Davies, F.J. (1941). "Fretting Corrosion and Fatigue Strength", *Proceedings of the Institute of Mechanical Engineers*, 146(1), pp. 32.

Waterhouse, R. B. (1992). "Fretting Fatigue", *International Materials Reviews*, 37(1), pp. 77-98.

Westergaard, H. M. (1939). "Bearing Pressure and Cracks". *Journal of Applied Mechanics*". pp. 49-53.

Weibull, W. (1951). "Wide applicability". *Journal of applied mechanics*, 103(730), pp. 293-297

Whitney, J. M., Nuismer, R. J. (1974). "Stress fracture criteria for laminated composites containing stress concentrations". *Journal of Composite Materials*, 8, pp. 253-265.

Wolfram, L. J. (1983). "Friction of skin". *Journal of the Society of Cosmetic Chemists*, 34(8), pp. 465-476.

Wu, G.Q., Shi, C.L., Sha, W., Sha, A.X., Jiang, H.R. (2013). "Effect of microstructure on the fatigue properties of Ti-6Al-4V titanium alloys". *Materials and Design*, 46, pp.668-674.

Zuo, J.H., Wang, Z.G., Han, E.H. (2008a). "Effect of microstructure on ultra-high cycle fatigue behaviour of Ti-6Al-4V". *Material Science and Engineering*, 473(1-2), pp. 14-152.

Zuo, J.H., Wang, Z.G., Han, E.H. (2008b). "Fatigue behaviour of Ti-6Al-4V alloy in vacuum and at low temperature". *Advanced Materials Research*, Vol. 41-42, pp. 83-90.

université PARIS-SACLAY
ÉCOLE DOCTORALE
Sciences mécaniques et énergétiques, matériaux et géosciences (SMEMAG)

Titre : Etude des effets de gradient de contraintes et des effets de taille en fatigue du contact.

Mots clés : Fatigue de contact, Effet de taille, Effet de gradient

Résumé : La fatigue de contact fait référence au processus d'endommagement situé à l'extrémité du contact entre deux corps soumis à des chargements de fatigue. La prédiction de ce phénomène est d'une importance majeure dans la détermination de la durée de vie de certains systèmes tels que les disques de turbines. Au voisinage du front de contact, le champ de contraintes est maximal en surface et présente un fort gradient sous le contact. De plus, la différence d'échelle entre les essais effectués en laboratoire et les systèmes industriels a motivé l'étude de l'effet de taille sur les modèles de fatigue des systèmes soumis à des chargements de fatigue du contact.
Afin de quantifier l'effet de gradient de contraintes et l'effet de taille, des essais ont été effectués sur une machine de fatigue munis de deux vérins verticaux à l'université de Brasilia. Les essais ont été menés de sorte que les gradients de contraintes, puis les volumes contraints, soient différents. Une étude post-mortem des surfaces de rupture a été effectuée à l'aide d'un microscope confocal.
Durant cette thèse, il a été montré que, pour un alliage de Ti-6Al-4v, une approche non locale basée sur un champ de vitesse équivalent extrait à l'intérieur d'une zone prédéterminée autour de l'extrémité du contact amène des résultats encourageants pour la détermination de la durée de vie. L'influence de la force de fatigue sur la description des mécanismes d'initiation de fissures et leur propagation a également été déterminée et il est apparu que cette dernière ne pouvait pas être négligée lors de la définition de la frontière d'initiation des fissures. En effet, si, en fatigue du contact, environ 75% du mécanisme d'initiation des fissures est contrôlé par les contraintes de contact, i.e. les contraintes de cisaillement et de pression, la prise en compte de la contrainte normale permet d'obtenir des prédictions plus précises.
L'étude de l'effet de taille a été divisée en deux phases. Premièrement, l'influence de la taille du volume sous contrainte a été analysée. Pour cela, l'épaisseur des éprouvettes a été réduite tandis que le gradient de contraintes sous le contact ainsi que l'aire de la surface endommagée étaient maintenus constants. Dans un second temps, l'impact de la zone endommagée sur la résistance à la fatigue a été isolé en maintenant les paramètres expérimentaux, i.e. $\sigma_{B,max}/p_0$ et Q/fP, constants tandis que l'aire endommagée par le frottements était réduite. Les résultats expérimentaux ont été analysés à l'aide d'un critère de fatigue multiaxial, le Courbe de Wöhler Modifiée, conjointement avec l'application de la théorie de la distance critique. Il a été montré qu'aucun de ces deux paramètres n'influence significativement la durée de vie en fatigue, et ainsi le terme « effet de taille » généralement référencé dans la littérature comme un effet d'endommagement devrait seulement être adressé comme un effet de gradient.

Title : Study of the Stress Gradient Effect and the Size Effect in Fretting Fatigue.

Keywords : Fretting fatigue, Size effect, Gradient effect

Abstract: Fretting fatigue refers to the damage process localized at the frontier of the contact between two contacting bodies subjected to fatigue loadings. The prediction of this phenomenon is of major importance in determining, for instance, the lifetime of fan's disk. In the vicinity of the contact front, the stress field inherited from the contact loads is maximal at the surface and displays a strong gradient under the contact. The difference of scale between the laboratory's experiments and the industrials' system motivated the study of the impact of the size effect for the determination of the lifetimes.
To quantify the effect of the stress gradient and of the size effect, tests were carried out on a two vertical-actuators fretting-fatigue rig at the University of Brasilia, with experimental conditions ensuring different stress gradient and later different volume solicited under the contact. Damage mechanisms were studied using post-mortem analysis with a confocal microscope on some contact elements tested.
It was shown on this thesis, for a Ti-6Al-4V alloy, that a nonlocal approach, based on equivalent velocity field on a determined area around the contact, leads to good expectation for the determination of fretting fatigue lives. The influence of the bulk stress for the description of the fretting fatigue crack initiation and propagation was also determined and it appears that it could not be neglected for the determination of the crack initiation boundary. As a matter of fact, if around 75% of the crack initiation mechanism in fretting fatigue is controlled by the contact stresses, i.e. shear and contact stresses, the consideration of the normal stress allows to obtain more realistic prediction.
The study of the size effect was divided into two phases. First the influence of the volume stressed was investigated by reducing the width of the contact but maintaining the stress gradient under the contact and the damaged area within the slip zone constant. Then, the influence of the damaged area within the slip zone was isolated by maintaining the experimental parameters, i.e. $\sigma_{B,max}/p_0$ and Q/fP, constant while the damaged area under the slip zone was reduced. The experimental results were analysed by applying a fatigue criterion, the Modified Wöhler Curve Method, in conjunction with the Theory of the Critical Distance. It was found that none of these two parameters influences significantly the fretting fatigue lifetimes, and so the term 'size effect' usually referenced in the literature as a damaging effect should refer only to the gradient effect.

Université Paris-Saclay
Espace Technologique / Immeuble Discovery
Route de l'Orme aux Merisiers RD 128 / 91190 Saint-Aubin, France